

Alma Mater Studiorum – Università di Bologna

DOTTORATO DI RICERCA IN

Meccanica e Scienze Avanzate dell'ingegneria:
progetto N 1 "Disegno e Metodi dell'Ingegneria
Industriale e Scienze Aerospaziali

Ciclo XXV

Settore Concorsuale di afferenza: 09/A1

Settore Scientifico disciplinare: ING-IND/04

TITOLO TESI

FATIGUE CRACK PROPAGATION IN PRESSURIZED METELLIC FUSELAGES

Presentata da: Gianluca Molinari

Coordinatore Dottorato

Prof. Vincenzo Parenti Castelli

Relatore

Prof. Enrico Troiani

Esame finale anno 2013

Acknowledgements

A hug with love to my parents, my sister and my nephews which are my life.

A heartfelt greetings to my beloved grandparents watching me from somewhere beyond the belt of orion

A heartfelt thank you goes to Enrico Troiani, Ivan Meneghin and Andrea Cimarelli for all the support given to me. A special thanks to Lorenzo Donati, Paolo Proli and Andrea Rizzo for the efforts to keep the MaSTeR Lab alive. Last but not list, many thanks to AIRBUS in the persons of Marco Pacchione, Domenico Furfari, Mauro Biasizzo and Nikolaus Ohrloff of AIRBUS for all the useful advices and the priceless experimental test data used during my work.

1. Introduction

Fatigue and Damage Tolerance (F&DT) requirements drive the design of wide areas of the modern transport aircraft structures. Airworthiness regulations concerning F&DT, e.g. the American Federal Aviation Regulations FAR 25.571[1], require that Principal Structural Elements¹(PSEs) must be able to withstand design limit loads even in the presence of damages, permitting their repair during the scheduled inspections.

¹ PSE - An element that contributes significantly to the carrying of flight, ground, or pressurization loads, and whose integrity is essential in maintaining the overall structural integrity of the airplane [2].

Airframes are mainly composed by thin panels (skins) reinforced with longitudinal and transverse stiffeners (such as stringers, doublers, frames and tear straps, sketched in **Error! Reference source not found.**) and, therefore, their DT performances are entrusted mainly by these types of structures. Incidentally, stiffened panels have been employed from 1930 due to their high load-bearing capacity combined with low weight, and substantially remained unchanged ever since. After the Comet disasters in 1954, when the aeronautical fatigue began to be studied systematically by means of fracture mechanics, stiffened panels have also been proved to have

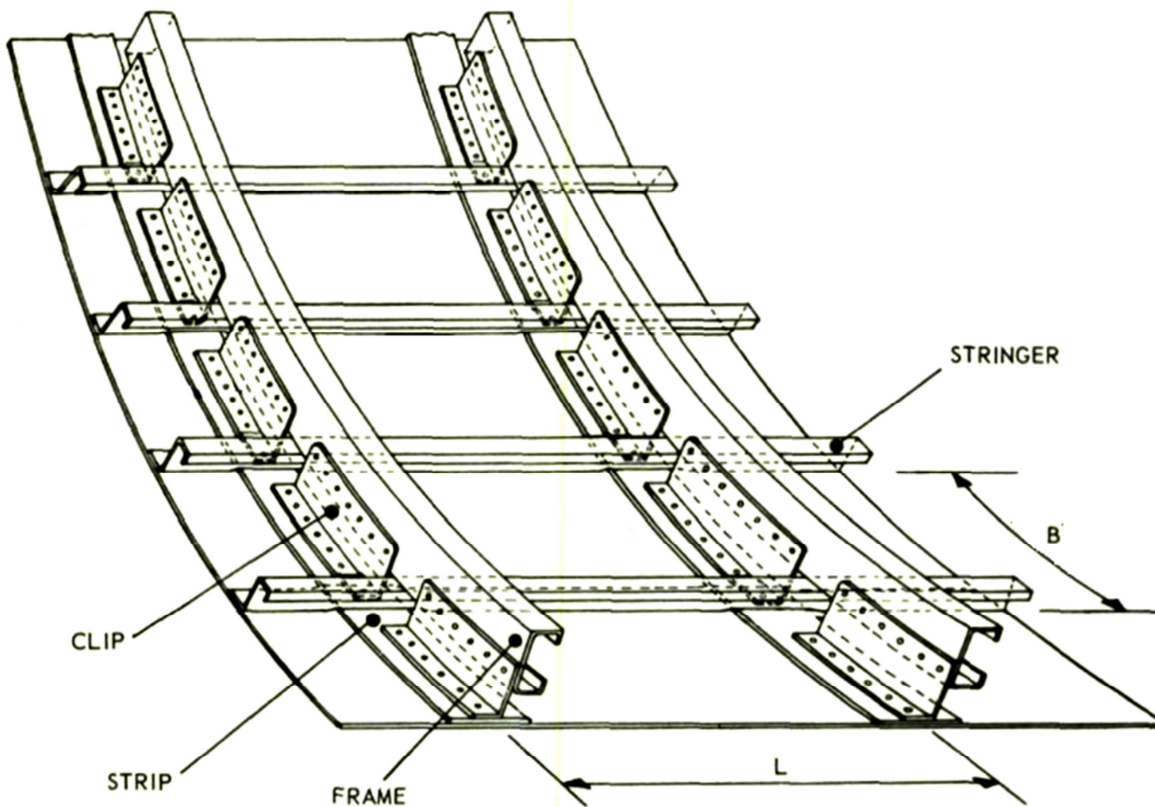


Figure 1.1. Typical stiffening arrangement of a fuselage panel.

intrinsic DT capabilities.

A careful F&DT analysis of the airframe is, therefore, needed to reduce the *fatigue crack propagation* (FCP) periods and to increase the static *residual strength* (RS) in the presence of damages in order to combine low weight with high structural reliability.

The linear elastic (fracture mechanics) *stress-intensity factor* (SIF), usually referred to as K and which describes the state of stress near the crack tip, proved to be effective to assess the *F&DT* capabilities of thin-walled stiffened structures [3]. Although the strict hypothesis on which the SIF is based, the only allowed plastic zone is confined in a small area around the fatigue propagating crack tip, it was largely and successfully used for *F&DT* design since the 1960's [4].

Poe [5][6], in the 1969, developed a method to evaluate the SIF of a fatigue through crack propagating in a thin flat skin stiffened by identical and equally spaced riveted stiffeners. This model was extended by Swift to account the rivets flexibility [4] and to model also adhesively bonded stiffeners [7]

These methodologies were used and extended by this author to develop a software tool, named LEAF (Linear Elastic Analysis of Fracture), for the prediction of the *fatigue crack propagation* (FCP) in pressurized metallic fuselage panels characterized by a generic fastening system and various damage scenarios. Analytical tools are indeed preferred over the time-consuming numerical methods (i.e. finite element modelling, FEM) especially during the preliminary design phases, because extensive parametric analyses are required to establish the initial best structural configurations. LEAF [8] was validated by means of an extensive experimental tests investigated by Meneghin [9]

In the present work, a parametric analysis of the FCP in stiffened panels was performed using LEAF, figuring out which parameters drive the *F&DT* capabilities and weaknesses of different stiffening configurations. The effects of riveted, integral and adhesively bonded stringers on the FCP performances were investigated as well as the effect of bonded doublers placed in the middle of the stringers bays. Moreover, the likely presence of a debonding at the interface between the cracked skin and the doublers, close to the skin crack, was taken into account.

The works of Poe and Swift were extended by the authors in order to take into account the crack retarder contribution of the additional straps, usually named doublers, placed on the skin between

the main stiffening elements. The effect of the biaxial stress on the cracked skin was considered as well.

References

- [1] Anonymous. *Damage tolerance and fatigue evaluation of structure*, FAR Part 25 Sect. 571, Federal Aviation Administration, 1997.
- [2] Anonymous. *Damage tolerance and fatigue evaluation of structure*, FAR 25.571-1D, Federal Aviation Administration, 2011.
- [3] U. Zerbst, M. Heinemann, C. Dalle Donne, D. Steglich. *Fracture and damage mechanics modelling of thin-walled structures - An overview*, Engineering Fracture Mechanics, Volume 76, Issue1, pp 5-43, 2009.
- [4] T. Swift. *The application of fracture mechanics in the development of the DC-10 fuselage*, In *Fracture Mechanics of Aircraft Structures*, AGARD-AG-176, H.Liebowitz, Ed. AGARD Advisory Group for Aerospace Research and Development, pp 226- 287, 1974.
- [5] C.C. Poe. *Stress-Intensity Factor for a cracked sheet with riveted and uniformly spaced stringers*, NASA TR R-358, NASA Technical Report, Langley Research Center, 1971.
- [6] C.C. Poe. *The effect of broken stringers on the Stress-Intensity Factor for a uniformly stiffened sheet containing a crack*, NASA TM X-71947, NASA Technical Memorandum, Langley Research Center, 1973.
- [7] T. Swift. *Fracture Analysis of Adhesively Bonded Cracked Panels*, Journal of Engineering Materials and Technology, Vol. 100, pp 10-15, 1978.
- [8] G. Molinari, I. Meneghin, M. Melega, E. Troiani. *Parametric damage tolerance design of metallic aeronautical stiffened panels*, The Aeronautical Journal, Vol. 116, 2012.
- [9] I. Meneghin and M. Pacchione. *Investigation on the design of bonded structures for increased damage tolerance*, in Proceedings of the 25th Symposium of the International Committee on Aeronautical Fatigue, 2009.

2. Fatigue & Damage Tolerance of pressurized fuselages

2.1. Introduction

Since the 1800 several structural failures of bridges and railway components was ascribed to cyclic or fluctuating applied loads, phenomenon nowadays known as *fatigue*. Over the next century, the subsequent technological advancements pushed to a massive use of high-strength metallic materials in machinery manufacturing leading to an exponential increase of failures due to fatigue. The first studies proposed to investigate failures by fatigue were introduced by the rail engineer August Wöhler in the second half of the 1800. Wohler showed that fatigue occurs by crack growth from surface defects until the structural component cannot longer sustain the applied load and introducing, moreover, the concept of S-N curve (still used in mechanical engineering) which relates the applied stress to the number of load cycles necessary to reach the component failure (Figure 2.1).

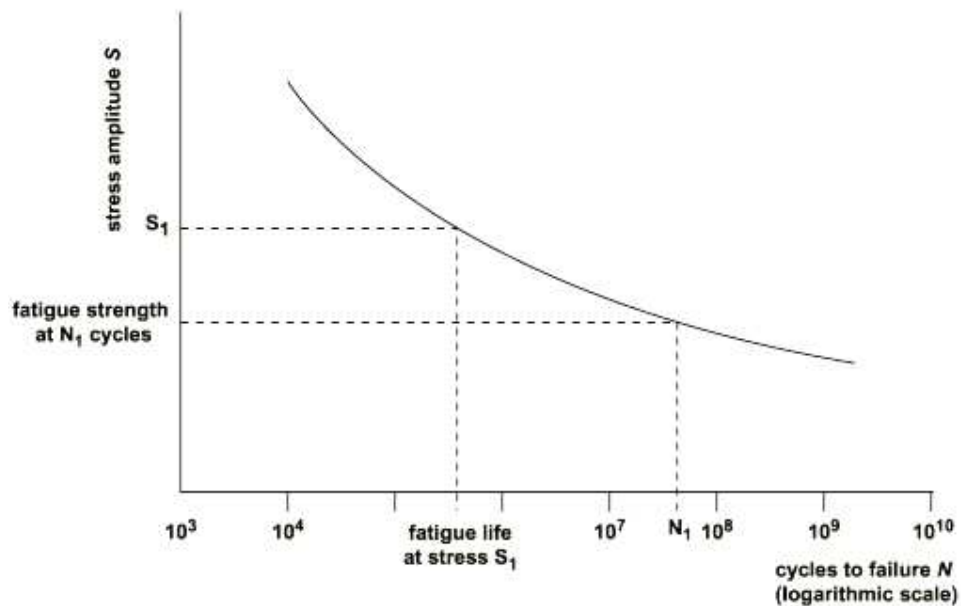


Figure 2.1. Generic S-N curve.

Aeronautics is one of the engineering fields in which fatigue has always been particularly critical. A notorious example was the first powered flight of history (Figure 2.2) that was delayed by two days due to fatigue failure of the propeller shaft; Orville Wright left Kitty Hawk for Dayton to build a new one. Furthermore, during World War II more than 200 civil aircraft fatal accidents were due to fatigue failures.

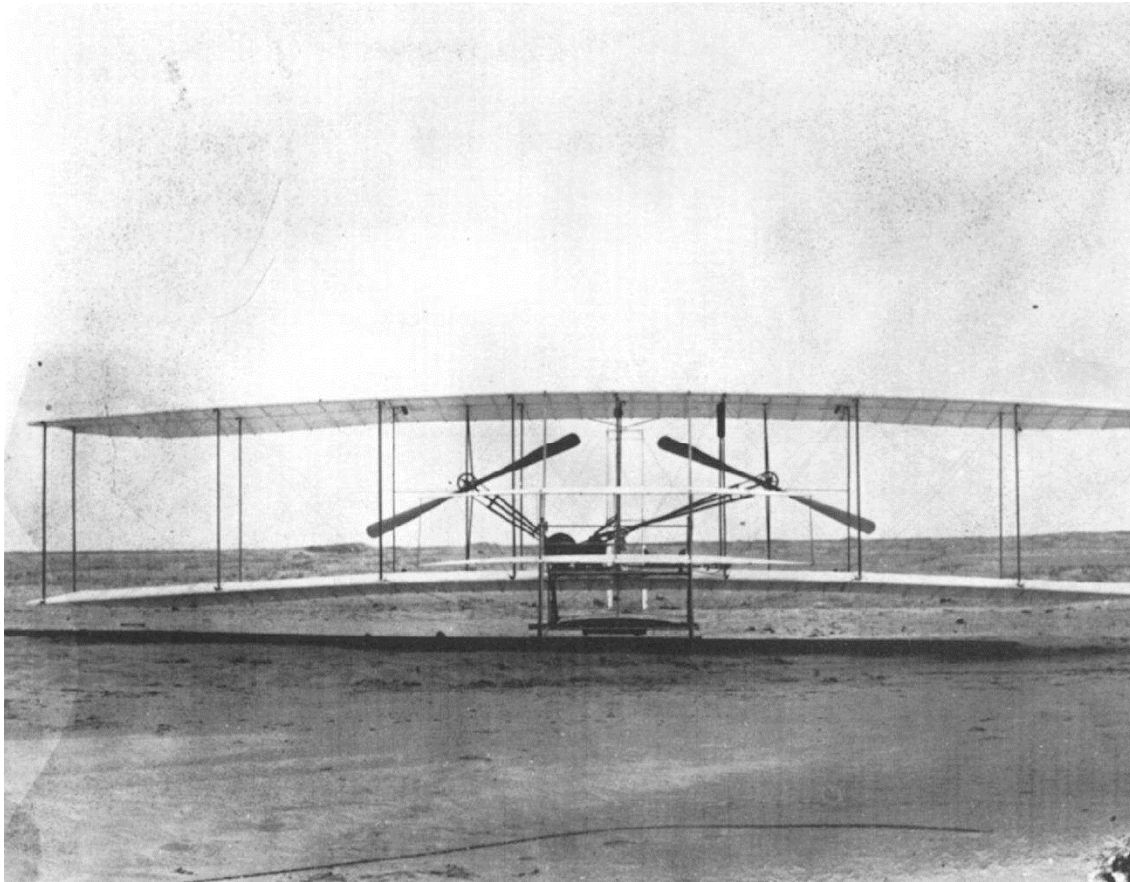


Figure 2.2. The Wright Flyer I (1903).

The real wake-up call, however, was the case of Comet 1 (Figure 2.3). The de Havilland DH 106 Comet, a project born in 1946, was at its time a futuristic aircraft with a cabin pressure of 8.25 psi (570 hPa), almost the double of any pressurized aircraft designed until then. This characteristic, together with not very judicious design choices were the base of the tragic events that followed: the Comet named G-ALYP experienced an explosive decompression during a flight at an altitude of about 30.000 ft and crashed in the sea near the Elba Island on 10 January 1954. At the time of the accident, the airplane had done only 3680 hours of flight, corresponding to

1286 pressurized flights. The fleet of Comet was grounded after a similar accident happened near Naples on 18 April 1954 to the aircraft named Yoke Yoke. When a large portion of the G-ALYP fuselage was recovered from the Mediterranean sea (Figure 2.4), a series of extensive (and intensive) investigations were made on the wreckage adducing both the accidents to a fatigue crack, nucleated in the right corner of the rear window (for the automatic direction fi der, ADF, antenna location, Figure 2.5), which caused the explosive decompression of both the fuselages.



Figure 2.3. De Havilland Comet I.

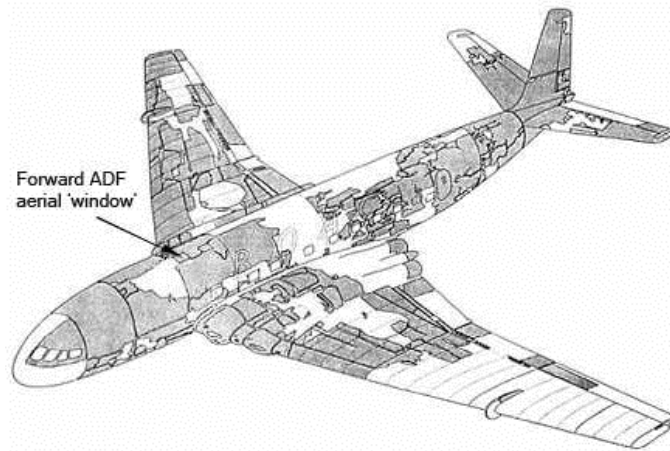


Figure 2.4. G-ALYP wreckage recovered from the Mediterranean Sea.

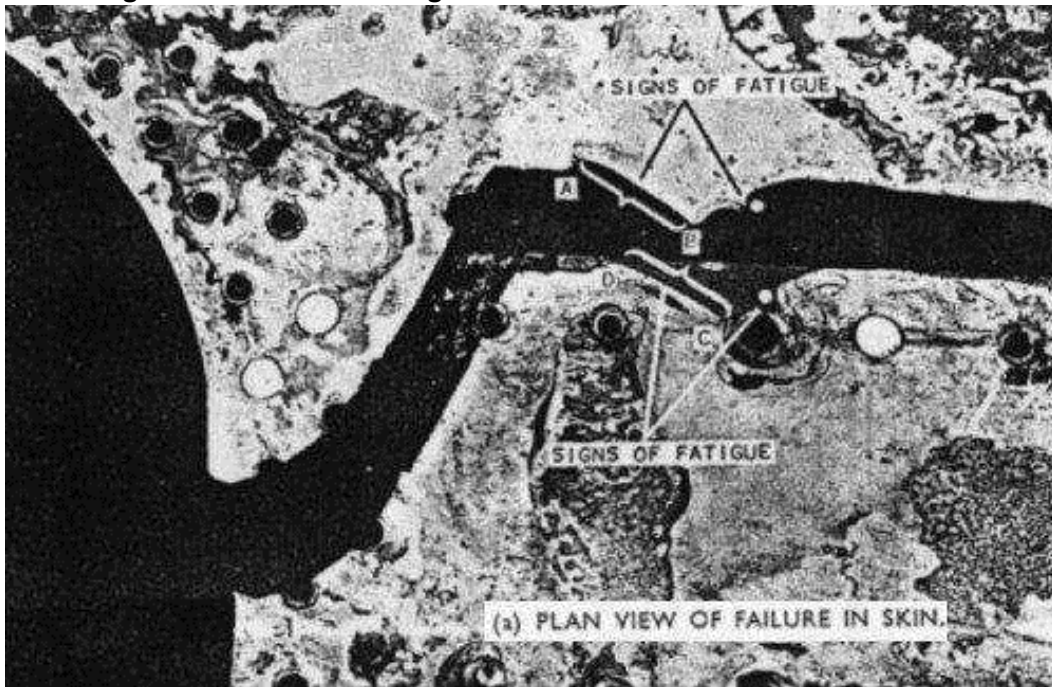


Figure 2.5. Detail of the crack (highlighted in black colour) nucleated at the ADF cut-out.

Before the Comet accidents, the airworthiness regulations then in force, the Civil Air Regulations (CAR), fatigue was only briefly mentioned into the CAR 4b.216 in relation to the pressurization of the cabin, and which stated:

"The airplane structure shall have sufficient strength to withstand the pressure differential loads corresponding with maximum relief valve setting multiplied by a factor of 1.33 to provide for such effects as fatigue and stress concentration. It shall to be accepted to omit all other loads."

On February 1956 it was introduced the new section CAR 4b.270 that includes more specific rules for the assessment of fatigue damage, pointing out two criteria for certification:

1. The criterion of fatigue strength (safe-life approach) where the integrity of the structure must be ensured (through analysis and experimental tests) for all the cyclic loads of variable amplitude which are provided in the operational life of the aircraft.
2. The criterion of intrinsic safety (fail-safe approach) where the integrity of the structure must be ensured (through analysis and experimental tests) even in the presence of a partial collapse of a principal structural element (PSE), and also any structural deformations (caused by the damage) shall not affect the behavior of the aircraft during the flight. The allowable loads in the presence of damage are the 80% of the limit loads multiplied by a dynamic coefficient of 1.15.

FAR / EASA 25.571, the currently in force airworthiness regulations, substantially maintained the previous form, but formally introducing the need to ensure damage tolerance (DT) as a "sine qua non" for the airworthiness of an airplane.

2.2. Damage Tolerance Philosophy

Both structure and materials commonly used in aeronautics are subject to a natural degradation during its operational lifetime. Cracks may be nucleate by fatigue in the most stressed structural elements and propagate under the application of variable loads. The presence of phenomena such as corrosion can aggravate and accelerate the structural degradation. Damages can also be caused by accidental impact or introduced as a result of deficient processes of production and assembly, deducing that also new aircraft entered into service may not be free of defects.

The static resistance of an airplane is noticeably affected by the presence of a generic damage, obviously the more it is extended and the more the resistance will be reduced. The amount of static strength that has damaged the structure is defined by the residual strength (RS) which takes into account the effect of the damage during its propagation. Due to the continuous application of the service loads and

exposure to contaminants, a generic defect / cracks / damage will tend to grow reducing the RS of the defected/cracked/damaged structure (Figure 2.6b).

As already mentioned, the regulatory requirements related to F&DT are described in section 571 part 25 of the European Aviation Safety Agency (EASA) and the American Federal Aviation Regulation (FAR) [1] They require that all PSE in a structure must be identified and designed accordingly to the damage tolerance design criterion.

The DT design philosophy asks two fundamental questions: how the resistance of a structure is affected by the presence of the damage (RS), and how long the damage takes to propagate due to fatigue (fatigue crack propagation, FCP). It is clear that the damage need to be detected and repaired before it reaches such dimensions (a_{cr}) where the RS is lower than L_L (Figure 2.6), thereby making a catastrophic failure highly likely (if not certain). In Figure 2.6a a_{det} represents the minimum size of damage detectable by non-destructive testing.

The safety of the airplane is thus entrusted by the possibility to detect a damage before it reaches its critical dimensions: using the DT philosophy an inspection plan must be defined for each PSE such as a generic defect nucleated due to fatigue, corrosion, accidental damage or introduced by deficient manufacturing processes must be identified and repaired before it causes a catastrophic failure. If the PSE cannot be (easily) inspected, and therefore it is not possible to define a inspection plan, it should be designed using the safe-life approach, ensuring that the structural element must be free of defects during the whole its expected operating life (Safe-Life range in Figure 2.6), after which it have to be replaced even if there are no visible damages.

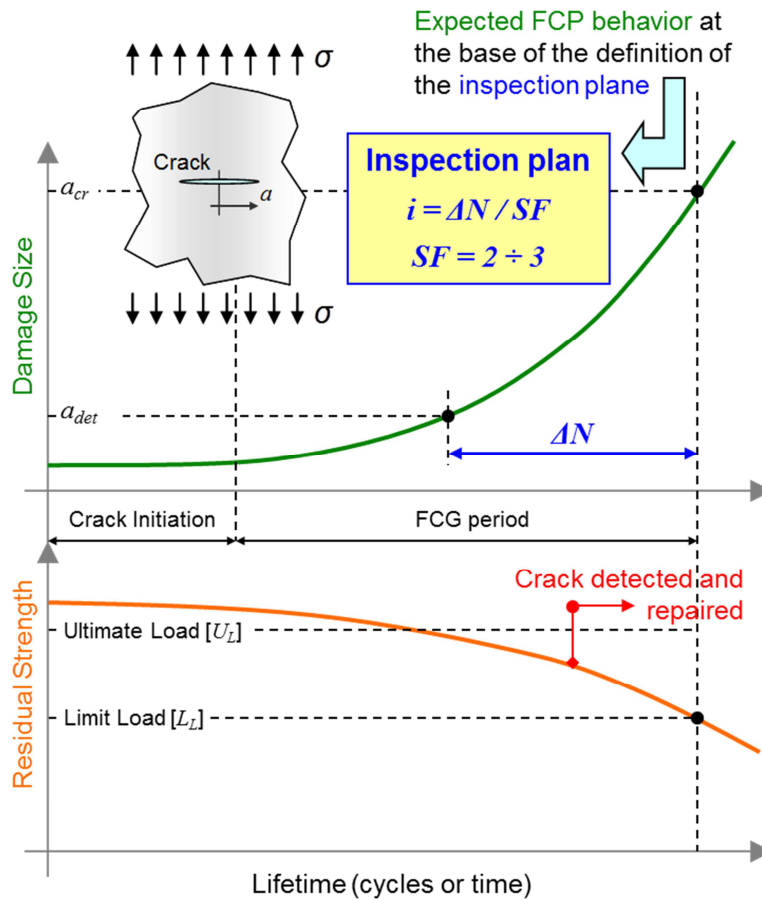


Figure 2.6. Evolution of the FCP(a) and the corresponding RS(b) during the aircraft operational life.

The disadvantage in terms of cost of such a methodology is obvious, but there is a second serious disadvantage: as a consequence of the uncertainty that characterizes the phenomenon of fatigue, the deviations between theoretical and practical results (scatter factors) are very high (typically equal to five). Therefore, to ensure the integrity of the PSE high reserve factors must be applied, increasing the structural weight. Two examples of safe-life criteria in civil aircraft structures are landing gears and engine mounts. In helicopters, however, many structural components are still designed with the safe-life philosophy, due to the impracticality of any other design criterion.

2.3. Linear Elastic Fracture Mechanics

In the previous section was showed that DT philosophy asks basically two questions:

1. What is the *residual strength* of the damaged structure?
2. How long takes a crack to propagate until it reach a critical value?

Fracture mechanics was developed, since from the 1940's, in order to answer at these two questions. Assuming the existence of damage, the fracture mechanics studies the evolution and the effects of damages on a structure.

As part of fracture mechanics, the linear elastic fracture mechanics (LEFM) limits his study to those materials which have a linear elastic relationship between stresses and strains during the crack propagation, or the fatigue failure must occur before the intact part of the material become plastic.

In LEFM the fracture analysis can be carried out just by means of stress-intensity factor (K) which describe the local stress state near the crack tip, as sketched in Figure 2.7, by the well-known equation [2]

$$\sigma_{ij}(r, \theta) = \frac{K}{\sqrt{2\pi r}} f_{ij}(r, \theta) \quad (2.1)$$

Where:

- (r, θ) are the system of polar coordinates with the origin placed on the crack tip (see Figure 2.7);
- σ_{ij} is the stress tensor near the crack tip;
- f_{ij} is a trigonometric tensor function [2].

In this work will not dwell on the theoretical aspects of the LEFM, limiting the discussion to the simple observation that in engineering practice the SIF can be expressed as

$$K = \beta \sigma \sqrt{2\pi a} \quad (2.2)$$

Where:

- β is the geometric correction factor;

- σ is the applied remote stress;
- a is the crack half-length.

The geometric correction factor β is a coefficient used in the engineering practice to take into account of several effects such as stiffeners, fuselage radius, and so on.

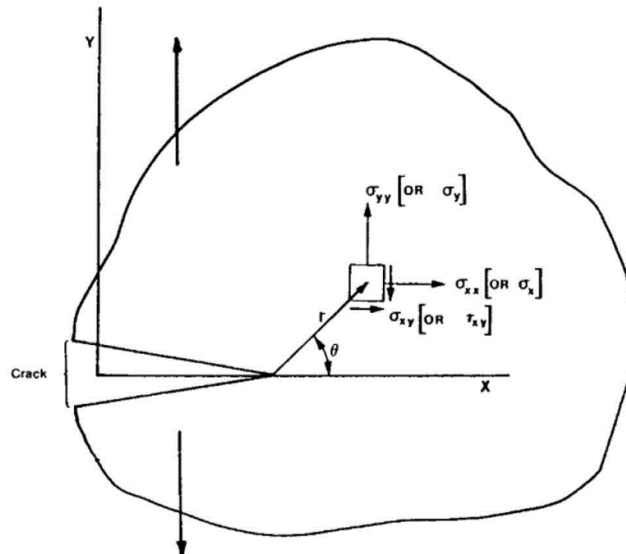


Figure 2.7. Generic body with a generic crack and subjected to a generic load.

2.3.1. Fracture toughness

The failure of a body occurs when the stress near the crack tip becomes too big to be borne by the non-cracked material. Since the crack-tip stress state is associated with the value assumed by K , it is possible to state that the failure occurs when this parameter exceeds a value called toughness and referred to as K_c .

Like any other engineering parameter, such as the elastic modulus E or the yield stress F_{ty} , the toughness must be obtained from experimental tests. For flat panels (with through cracks) it was seen that the K_c depends almost on the thickness and the width of the body, and obviously on the material from which it is made.

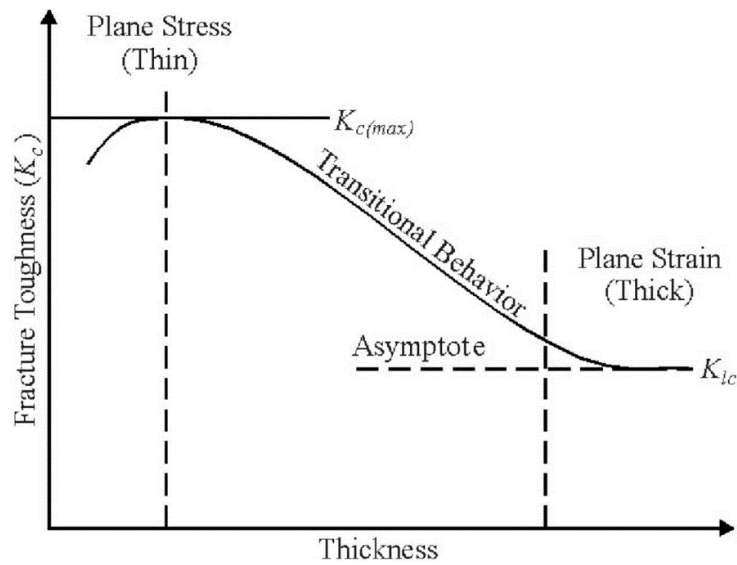


Figure 2.8. Dependency of K_c on the panel thickness.

In Figure 2.8 can be observed three zones: in the first one K_c increases with the thickness until it reaches a maximum, in the second one K_c slowly decreases until it reaches a minimum value, in the third one K_c remains constant for any value of thickness. This behaviour follows directly from the equation (2.1) which has a singularity near the crack tip ($r \rightarrow 0$ and $\theta \rightarrow 0$, see Figure 2.7) bringing the stress state σ_{ij} to infinity. Obviously a real material cannot withstand an infinite stress, but reached the yield the stress tends to remains almost constant and equal to F_{ly} . As a consequence of the high crack tip stress, a small plastic area take places around the crack tip (Figure 2.9) which being subjected to a residual stress tends to deform.

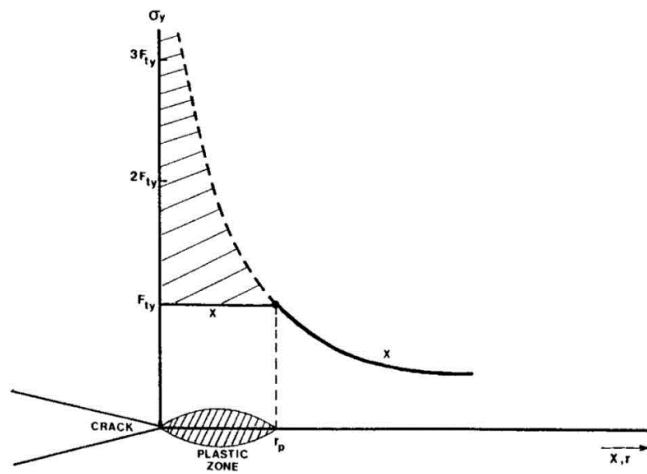


Figure 2.9. Plastic zone around the crack tip.

The plastic material is surrounded by the material remained elastic and, thus, deformations are possible only on the free surfaces of the panel. As sketched in Figure 2.10, thicker is the panel lower is the deformation because there is a higher amount surrounding elastic material which restrains the deformations, and vice versa.

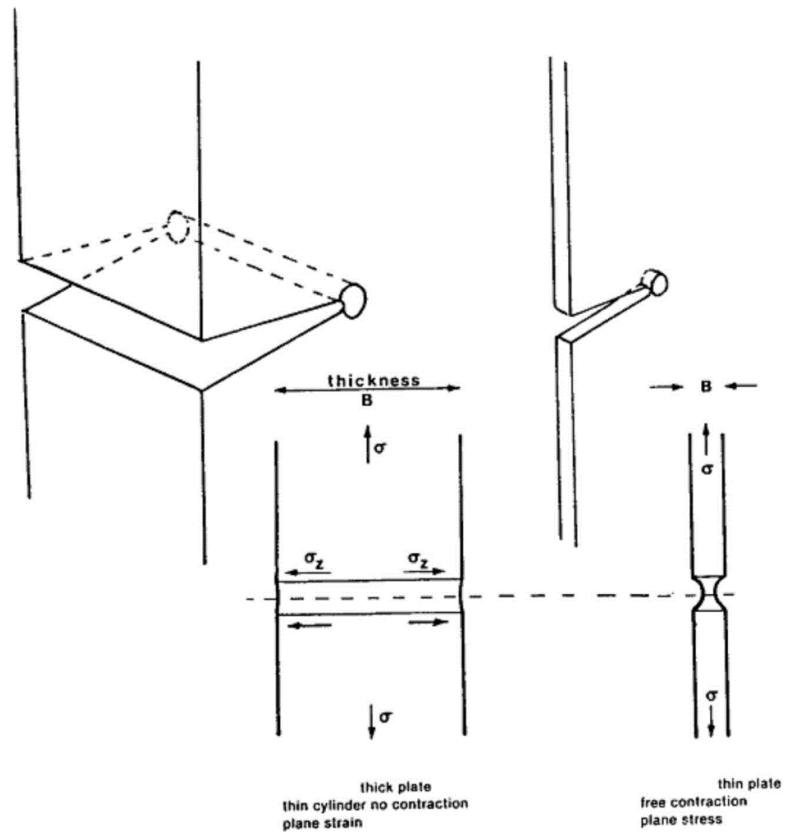


Figure 2.10. Deformation of the plastic zone for thick and thin panels.

For high values of the thickness the panel is subject to a plane strain state in the neighborhood of the crack, where along the thickness a stress σ_{zz} develops. Otherwise, for low values of the thickness the panel is subject to a state of plane stress, where σ_{zz} is zero and thus is easier to sustain. It follows that for a thin cracked panel the fracture toughness is much higher compared to a thick panel.

2.3.2. Fracture resistance and Residual Strength

In the previous section was showed as the fracture of a generic body could be referred to the fracture toughness K_c which can be found experimentally [3].

Therefore, for a given crack length $2a$, if K_c is known then possible to assess the stress σ_c at which failure occurs for any structural configuration of which is known also the value of β by reversing the (2.2)

$$\sigma_c = \frac{K_c}{\beta \sqrt{2\pi a}} \quad (2.3)$$

The above equation, depicted in Figure 2.11, represents the residual strength (RS) that has been discussed in section 2.2.

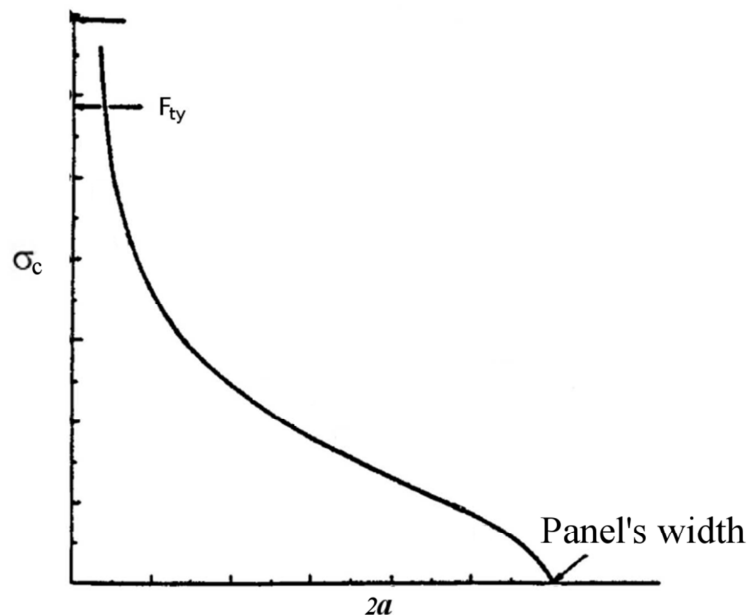


Figure 2.11. Residual static strength vs. crack length a .

This approach to the calculation of the residual strength cannot however be applied easily to thin panels, since K_c varies strongly with the thickness and cannot be considered as a material property.

A more general approach to the problem of RS is based on the (strain) *energy conservation principle*, which in the case of a cracked body can be written as

$$\frac{d}{da}(F - U) = \frac{dW}{da} \quad (2.4)$$

where F is the work done by the loads acting on the body, U is the energy of elastic deformation and W is the energy absorbed by the crack to propagate. It can be shown [2] that in the case of LEFM must apply the relationship

$$\frac{dU}{da} = \frac{dW}{da} \quad (2.5)$$

that is, the fracture can take place only if a sufficient amount of elastic energy is made available to the crack to propagate a quantity da . The left side of (2.5) is commonly named *crack driving force* and is indicated with the letter G . The right side is referred to as *fracture resistance* and is indicated with the letter R . The crack driving force is obtainable by theoretically and for infinitely extended flat panel of infinite extension is

$$G = \frac{\sigma^2 \pi a}{E} = \frac{K^2}{E} \quad (2.6)$$

which is linear in a . The trend of R is a property of the material obtainable experimentally [4]: in the case of plane strain is a horizontal straight line, while in the case of plane stress is a function increasing with the length of the crack, as shown Figure 2.12. The (2.5) expresses a condition of equilibrium, it follows that if the condition $G > R$ occurs the fracture would be unstable and would lead to the failure of the structure.

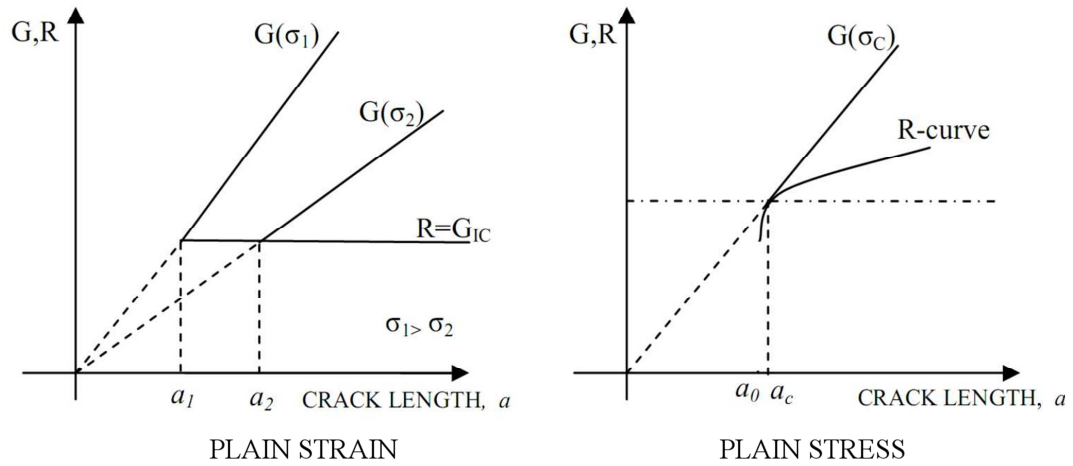


Figure 2.12. Crack driving force and fracture resistance.

Observing the trend of both the curves in Figure 2.12, the condition of instability becomes a condition of tangency, that is

$$\frac{dG}{da} \geq \frac{dR}{da} \quad (2.7)$$

For each value of the crack length is possible to identify single value of a for which G is always larger than R , the value of this stress is exactly the residual strength (for the given crack length).

2.3.3. Fatigue crack propagation

A mechanism that promotes fatigue crack propagation (FCP) is depicted in Figure 2.13 (from Ref. [2]). A plastic deformation is a sliding of the atomic planes of the material due to a shear stress (Figure 2.13, phase B). The progress of the sliding over complementary planes produces a rounded crack tip (Figure 2.13, phases B to D). The first sliding step produces a small increase Δa of the crack. During the relaxation phase (or phase of compression) the crack tip returns sharp. In the later stage, the loading process is repeated causing the advancement Δa of the crack.

Many theories were developed to describe the fatigue crack propagation rate (FCPR, also known as fatigue crack growth rate, FCGR) in mechanical components [5][6] but almost all are based on the linear elastic fracture mechanics (LEFM) *stress intensity factor* (SIF, commonly labelled as K).

In the case of cyclic loading with constant amplitude (Figure 2.14) has been found experimentally [2] that the parameters which drive the FCPR are the load range $\Delta\sigma = \sigma_{\max} - \sigma_{\min}$ and the load ratio $R = \sigma_{\min} / \sigma_{\max}$. In Figure 2.15 is depicted the time evolution of the SIF due to $\Delta\sigma$. Obviously, recalling the equation (2.2), the (direct) relationship between the SIF and $\Delta\sigma$ can be simply expressed as

$$\Delta K = \beta \Delta\sigma \sqrt{2\pi a} \quad (2.8)$$

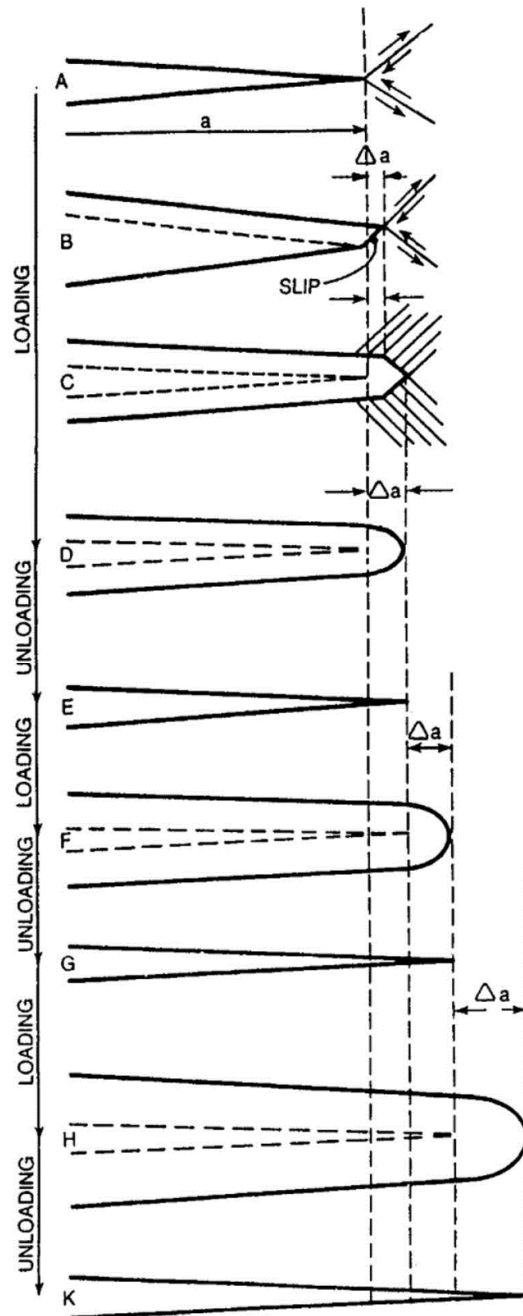


Figure 2.13. Crack propagation mechanism [2].

Should be noted that a constant amplitude load $\Delta\sigma$ produces a SIF ΔK which increases with time (see Figure 2.15); this is due to the crack half-length (a) inside the square root in the equation (2.8) which grows with time (i.e. the applied load cycles).

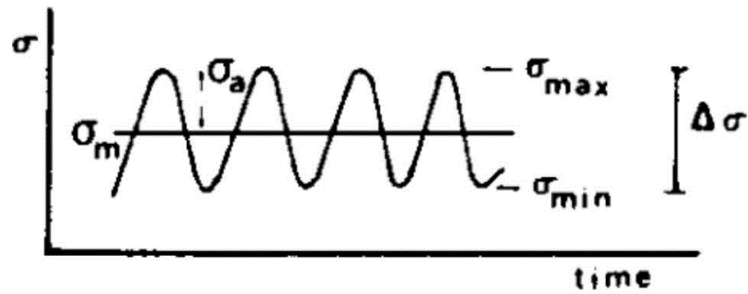


Figure 2.14. Constant amplitude cyclic load.

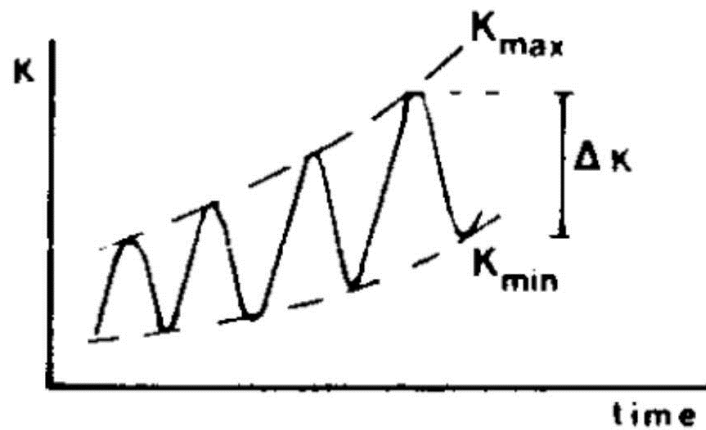


Figure 2.15. SIF vs. time.

Generally FCPR is measured in [mm / cycle] and can be expressed as

$$\frac{da}{dN} = f(\Delta K, R) \quad (2.9)$$

a typical trend of the is shown in Figure 2.16. There are three distinct regions:

- in the first region exists a threshold value ΔK_{th} below which there is only a propagation at microscopic (atomic) scale;
- in the second region the crack growth rate is defined and there is a linear relationship with ΔK (on a double logarithmic scale);
- in the last one the FCPR grows steeply until it reaches a vertical asymptote where the SIF equals the value of fracture toughness K_c .

There are currently no analytical formulations to describe the FCPR but several empirical relations were developed, and the most notable are: the law of Paris which considers just the linear region

$$\frac{da}{dN} = C_P(\Delta K)^{np} \quad (2.10)$$

and the Forman's law which includes also the behaviour of the third zone

$$\frac{da}{dN} = \frac{C_F(\Delta K)^{nf}}{(1-R)K_C - \Delta K} \quad (2.11)$$

The parameters C_P , C_F , np , nf must be obtained through experimental tests.

The number of load cycles N that a fatigue crack takes to propagate from an initial crack length a_o to a certain crack length a_i can be made integrating the reciprocal of the crack growth rate per unit cycle (da/dN).

$$N = \int_{a_o}^{a_i} \left(\frac{1}{\frac{da}{dN}} \right) da \quad (2.12)$$

Integrating with the (2.12) relationships such as (2.10) and (2.11) between the minimum detectable crack length (a_{det}) and the critical crack length (a_{cr}) the number of cycles required to reach the failure N_{cr} can be obtained. With N_{cr} an inspection plan can be established, answering to the second question asked by the DT design philosophy.

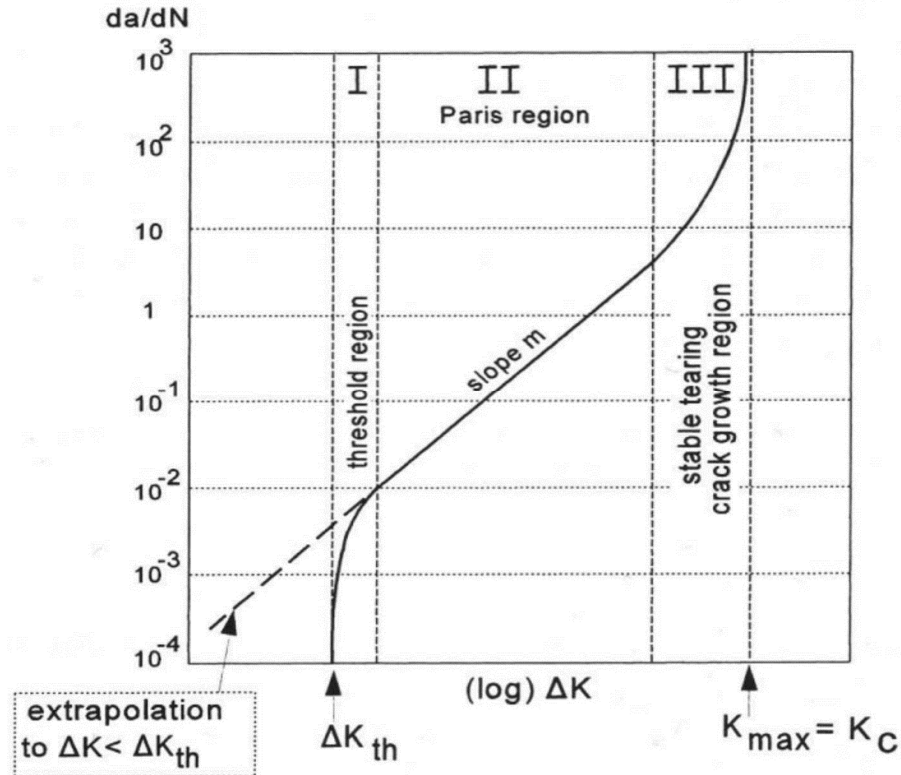


Figure 2.16. Fatigue crack propagation rate vs. SIF (double-logarithmic scale).

2.4. Fuselage stiffened panels

The stiffeners create secondary load paths which, in the presence of a crack, reduce the state of stress in the cracked skin and consequently the SIF.

For example, consider the panel (of elastic modulus E and thick t) sketched in Figure 2.17: with mechanically fastened (riveted, bolted or adhesively bonded) stringers (of elastic modulus E_s and cross-section A_s), subject to a remote stress σ and severed along the stiffeners bay (of width b) by a crack of length $2a$. In a stiffened panel the crack tip stress is transferred from the skin to the stiffeners and then back to the skin again (Figure 2.17). Therefore, under the same crack length ($2a$) and the same remote stress σ , a stiffened panel has a SIF lower than an unstiffened panel.

The effect of the stiffeners on the SIF is commonly expressed as a pure geometric effect by the geometric β correction factor, defined in this case as

$$\beta_s = \frac{K_{stiff}}{K_{unstiff}} \quad (2.13)$$

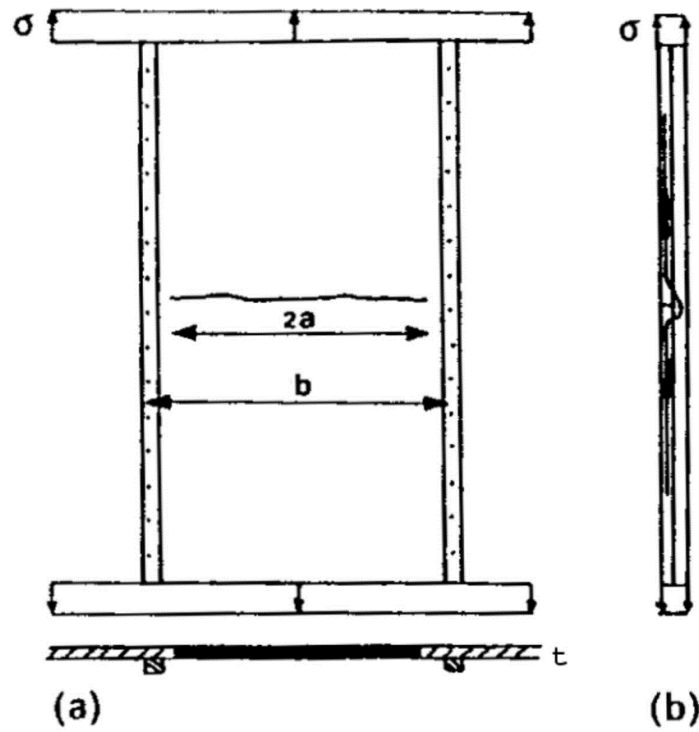


Figure 2.17. Stress distribution between skin and stiffeners.

Where K_{stiff} and $K_{unstiff}$ are the SIF of the stiffened and the unstiffened panel, respectively.

As a drawback, the load transfer which reduces the SIF in the cracked skin increases considerably the stress of the stiffeners, in particular when the crack is close to them. This effect can be expressed with the stiffeners *load concentration factor* L_s

$$L_s = \frac{F}{\sigma_s A_s} \quad (2.14)$$

Where F is the resulting force reacted by the stiffener and σ_s is the remote stress applied to the stiffener. The stiffer is the reinforcement the lower is β_s (i.e. the SIF) and hence the higher is L_s .

The stiffness of a fuselage panel increase increasing the section and the elastic modulus of the reinforcements, and is characterized by the parameter μ (relative stiffness) defined as the ratio between the stiffness of the reinforcement and the total stiffness of the fuselage bay

In Figure 2.18c is depicted the behaviour of β_s as a function of μ

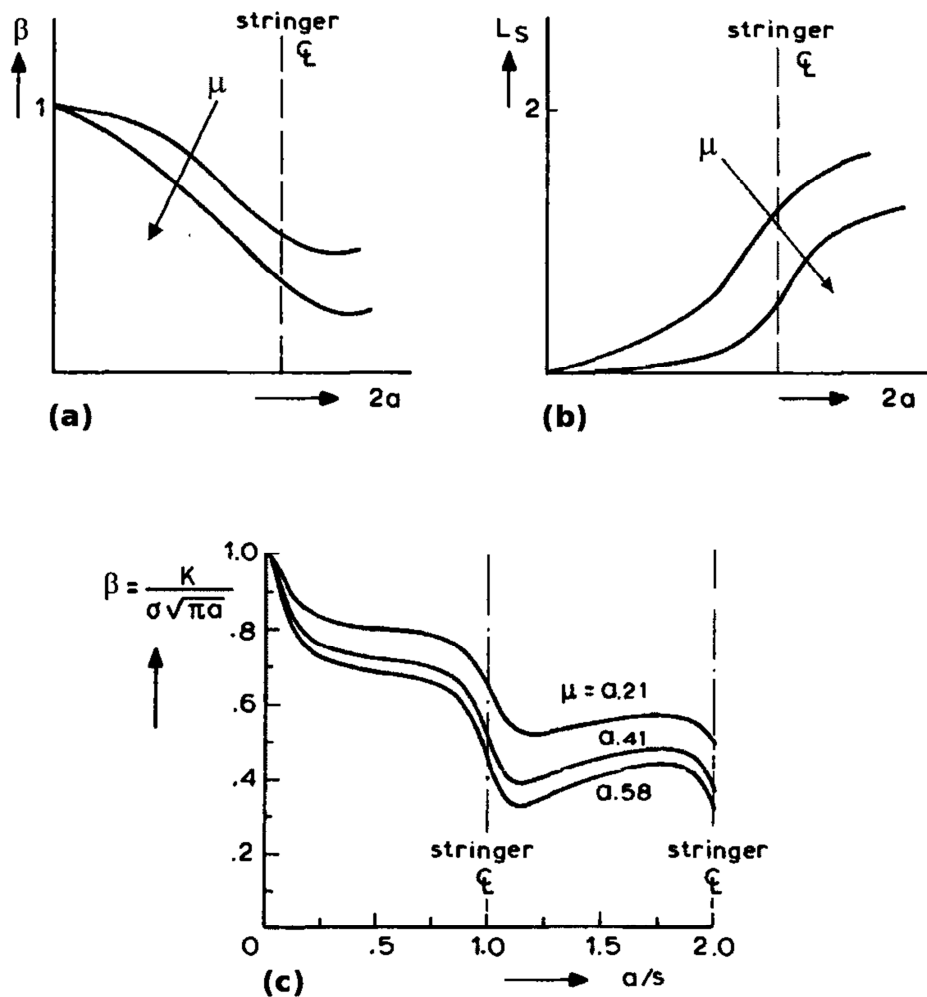


Figure 2.18. Effect of the relative stiffness μ on β and L_s .

2.4.1. Fatigue crack propagation on stiffened panels

Recalling the section 2.3.3, once is known the geometric factor due to the stiffeners (β_s) it is possible to evaluate the FCP in stiffened panels using again the Equations (2.8), (2.10), (2.11) and (2.12).

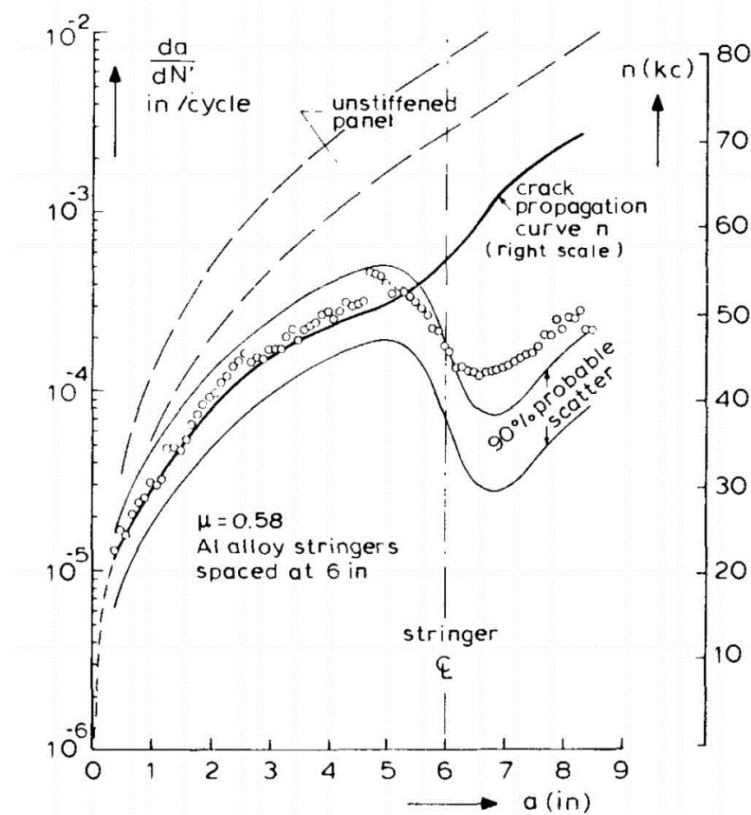


Figure 2.19. FCPR in a stiffened panel.

The reduction of β showed in Figure 2.18 indicates the reduction of the SIF in proximity of a stiffener ($a/b \cong 1$) which produces a slowdown of the crack propagation rate. The stiffener starts to lose its influence on the crack when the crack tip cross it, then the propagation rate rises again until the damage approaches the next stiffener ($a/b \cong 2$) inducing a further crack growth slowdown. This behavior is verified experimentally [7], as can be seen in figure Figure 2.19 where the FCPR is plotted together with the FCP curves (dashed lines represent the velocity of propagation in the case of a non-stiffened panel).

2.4.2. Fuselage loads

Under normal level flight conditions (1 g) a fuselage is subjected principally to pressurization and bending stresses around the airplane pitch axis (y-axis), as depicted in Figure 2.20. Pressurization stresses, acting on circumferential (σ_ϕ) and longitudinal (σ_x) direction, can be approximated by the well-known boiler formulas [8]

$$\sigma_\phi = \frac{\Delta p \cdot R_f}{t_f}, \quad \sigma_x = \frac{\sigma_\phi}{2}$$

Where Δp is the differential (inside-outside) cabin pressure, R_f is the fuselage radius and t_f is the fuselage skin thickness. The uniform stress distribution expressed by the 0 is exact only for unstiffened pressure vessels but is heavily influenced by the presence of reinforcements such as frames and longerons. A better approximation can be obtained using the stress expression developed by Flugge [9]

$$\sigma_\phi = \frac{t_x N_\phi + v(t_\phi - t_f) N_x}{(1 - v^2)t_x t_\phi + v^2 t_f (t_x + t_\phi - t_f)} \quad (2.15)$$

$$\sigma_x = \frac{t_\phi N_x + v(t_x - t_f) N_\phi}{(1 - v^2)t_x t_\phi + v^2 t_f (t_x + t_\phi - t_f)} \quad (2.16)$$

Where:

- $N_\phi = \Delta p \cdot R_f$ is the circumferential membrane stress
- $N_x = N_\phi/2$ is the longitudinal membrane stress
- $t_\phi = t_f + \frac{A_R}{l}$ is the effective circumferential skin thickness
- $t_x = t_f + \frac{A_L}{b}$ is the effective longitudinal skin thickness

And:

- A_R is the frame cross-section area
- l is the frame spacing
- A_{RL} is the longeron cross-section area
- b is the longeron spacing

The bending stress contribution originates from the superposition of the distributed weight of the airframe with the vertical accelerations due to gust and manoeuvring, as schematically depicted in Figure 2.20.

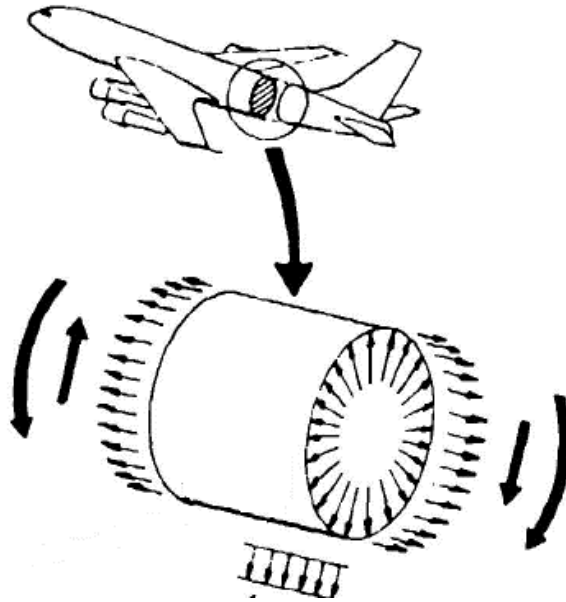


Figure 2.20. Fuselage stress components. Hoop + Bending.

Bending stress acts in the longitudinal direction with the classical beam “butterfly distribution”, decreasing linearly from the fuselage crown (subjected to tension) to the belly (subjected to compression).

Pressurization stress can be considered constant over the overall fuselage length, whereas bending stress reaches its maximum at the wing attachments to the main frames, where wing lift loads are reacted by the fuselage.

2.4.3. Crack bulging

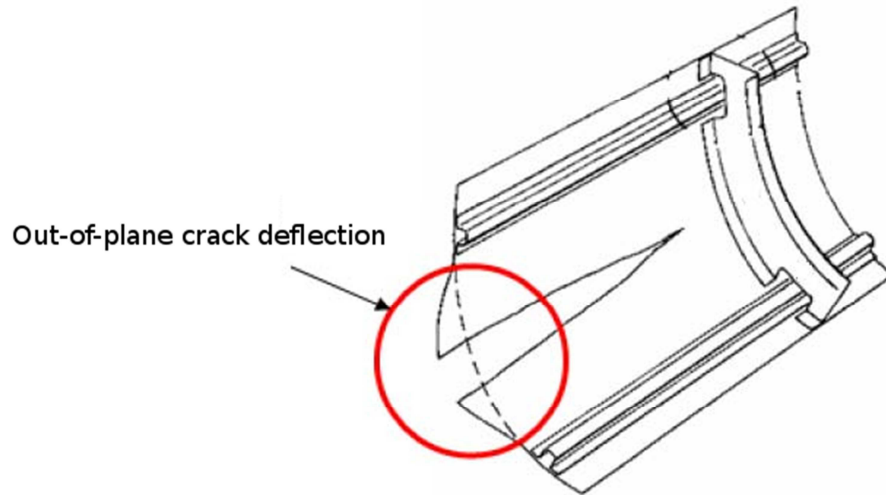


Figure 2.21. Sketch of the crack bulging phenomenon.

As reported in the previous subsection, fuselages are subjected mainly to the pressurization load which is more or less constant along the radius and the longitudinal (flight) direction. Other than the complicated biaxial stress state, pressurization has another drawback: when a crack nucleates into the skin and propagates along either the longitudinal or circumferential direction, the intern cabin pressure tends to bulge outwards the crack edges, as depicted in **Error! Reference source not found.**. This additional crack displacement, called exactly “*crack bulging*” [10], influences the crack tip stress state, and thus the SIF, affecting strongly both the FCP and the RS. The bulging effect is always detrimental because, due to the out-of plane deflection, the crack opening displacement (COD), i.e. the geometrical counterpart of the SIF to which is related by

$$COD(x) = \frac{2 \cdot K(a)}{G \cdot (1 - \nu)} \sqrt{\frac{a-x}{2\pi}} \quad (2.17)$$

is evidently increased by the outward rotation of the crack edges (**Error! Reference source not found.**).

The bulging phenomenon is rather complex and will be discussed more in detail in the last chapter.

2.4.4. Typical fuselage damage scenarios

Current airworthiness regulations [11] require that an aircraft must be able to withstand limit loads in the presence of:

- I. the complete failure of a single PSE , or
- II. partial failure between damage containment features that significantly retard or arrest a crack.

These two sentences are known as Structural Damage Capability (SDC) requirements. Actually the SDC criterion is not so clear, and was interpreted in the past as the capability of the fuselage to sustain a crack propagating in the skin between two longitudinal or circumferential stiffeners, i.e. the so-called one-bay crack damage scenario. This is because the fuselage bay included between two frames and two stringers is actually a PSE.

Assessments DT of a structure must, however, necessarily must referring to the most critical and likely damage scenarios that may occur during the operational life of the aircraft (Design Service Goal, DSG), since the residual strength must be quantified in these conditions.

As noted by Swift [12] on fuselage panel tests of during the development of the DC-10, the nucleation of fatigue cracks were evidenced often at the following locations:

- 1) for longitudinal cracks
 - a. along the most external rivet line in longitudinal lap joints;
 - b. on the rivet closest to the shear-clip cut out needed for the stringers housing;
- 2) for circumferential cracks
 - a. at the skin-to-shear clip attachments in midway between the stringers;
 - b. at the attachments between frame and stringer due to the stringer failure caused by the high bending moments, as described in [12].

Therefore, the two-bay crack damage scenario, with a crack propagating on both the side of a main intact or broken stiffeners (Figure 2.22), should be seriously considered to assess the F&DT capabilities of an airframe.

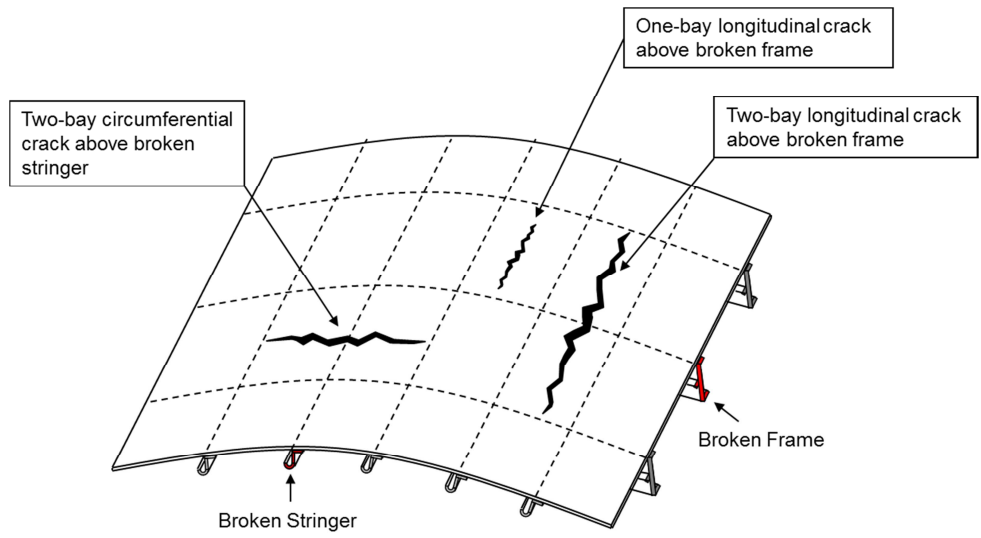


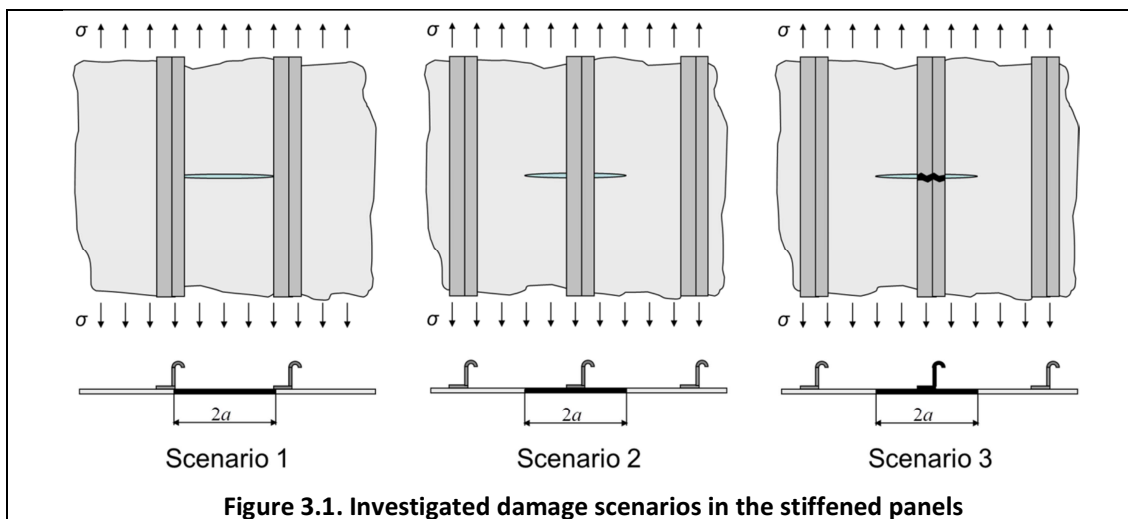
Figure 2.22. Fuselage damage scenarios to be considered during F&DT design.

References

- [1] Anonymous. *Damage tolerance and fatigue evaluation of structure*, FAR Part 25 Sect. 571, Federal Aviation Administration, 1997.
- [2] D. Broek, *The Practical Use of Fracture Mechanics*, Springer, 1989.
- [3] Anonymous. *ASTM E1820 - 11e1 Standard Test Method for Measurement of Fracture Toughness*, ASTM International.
- [4] Anonymous. *ASTM E561-10e1 Standard Test Method for K-R Curve Determination*, ASTM International
- [5] Paris, P.C., Gomez, M.P. and Anderson, W.E. *A rational analytic theory of fatigue*, *The Trend in Engineering*, January, 1961, 13, pp 9-14.
- [6] HRR
- [7] C.C. Jr. Poe. *Fatigue crack propagation in stiffened panels*, *Damage Tolerance in Aircraft Structures*, ASTM STP 486, pp 79-97, 1971.
- [8] S. Timoshenko. *The theory of plates and shells*, McGraw-Hill, 1964.
- [9] W. Flugge. *Stress problems in pressurized cabins*, NACA-TN-2612, 1952.
- [10] D. Chen. *Bulging of Fatigue Cracks in a Pressurized Aircraft Fuselage*, TU-Delft Report LR-647, 1990
- [11] Anonymous. *Damage tolerance and fatigue evaluation of structure*, FAR 25.571-1D, Federal Aviation Administration, 2011.
- [12] T. Swift. *The application of fracture mechanics in the development of the DC-10 fuselage*, *In Fracture Mechanics of Aircraft Structures*, AGARD-AG-176, H.Liebowitz, Ed. AGARD Advisory Group for Aerospace Research and Development, pp 226- 287, 1974.

3. Fatigue crack propagation in stiffened panels

In the present chapter, a parametric analysis of the FCP in stiffened panels was performed using LEAF for three damage scenarios (depicted in Figure 3.1), figuring out which parameters drive the DT capabilities and weaknesses of different stiffening configurations. The effects of riveted, integral and adhesively bonded stringers on the FCP performances were investigated as well as the effect of bonded doublers placed in the middle of the stringers bays. Moreover, the likely presence of a debonding at the interface between the cracked skin and the doublers, close to the skin crack, was taken into account.



1.1. Flat Stiffened panels

Airframes are mainly built with thin-walled stiffened panels, thin plates (skins) reinforced with longitudinal and transverse stiffeners, and thus DT performances are entrusted mainly by these types of structures.

Stiffened panels proven to have intrinsic DT capabilities. Stiffening elements, such as stringers, frames and tear straps (sketched in Figure 3.2), could indeed act as skin crack retarders, reducing the fatigue crack growth rate, and stoppers, arresting unstable fast

crack propagations. At the basis of the crack restrain mechanism lies the load transfer established between the cracked skin and the stiffeners, which slow-down the crack growth by reducing the tensile stresses around the crack tip.

The effectiveness of the stiffeners as crack retarders and stoppers has been shown by several authors in the past. In 1970 Poe [1] has compared the skin Fatigue Crack Propagation Rate (FCPR) in flat wide panels with bolted and integral stiffeners subjected to a constant amplitude fatigue load. Bolted panels have shown lower rates than the corresponding unstiffened skin, resulting in an increased Fatigue Crack Propagation (FCP) life, whereas integral panels don't have provided any significant benefits. This occurred because integral stiffeners are severed concurrently with the skin during the crack propagation, resulting in a totally lack of crack arresting capability. Due to this limitation, welded and machined stiffened panels find application where the design is driven mainly by static requirements, like upper wings and lower fuselage panels that are subjected essentially to compression loads during the flight.

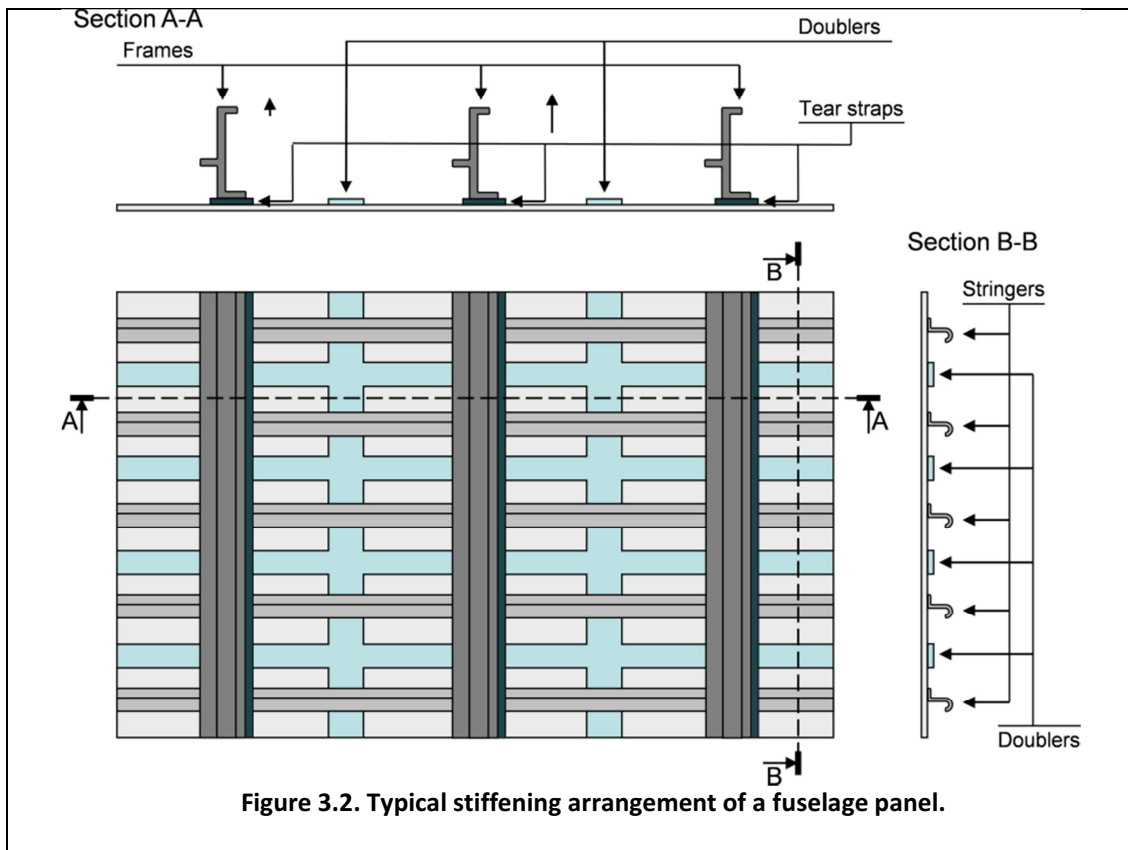


Figure 3.2. Typical stiffening arrangement of a fuselage panel.

On the other hand, mechanically fastened joints, riveted or bolted, still remain the most commonly used in primary metallic structures, like wing spar and fuselage lap joints, where reliability and safety are fundamentals. A third joining system currently used in airframe manufacturing is the adhesive bonding. Structural bonding was employed in aeronautics since the 1945, but until the early '70s was not so popular [2][3] because of some issues related to corrosion and durability, which was solved improving the bonding processes and the surface pre-treatments. Nowadays, it is widely used in wings and fuselage secondary structures, e.g. for bonding stringers and cut-out reinforcements, thanks to the high static and fatigue strength of adhesive joints. As for integral stiffeners, bonded stiffeners provide weight benefits, due to the absence of the fasteners, and longer crack nucleation periods, due to the absence of the fastener holes that act as stress risers, but unlike integral stiffeners they provide crack arresting capabilities thanks to the physical separation between the adherents.

An early experimental investigation of the crack growth behaviour in panels reinforced with adhesively bonded straps was reported by Schijve [4]. Tests were performed also using riveted and integral straps. Both the riveted and bonded reinforcements were made of different materials: aluminium alloys (2024-T4 Alclad and 7075-T6 Clad), titanium alloys (Ti-6Al-4V) and ARALL (7075-T6 aluminium laminates reinforced with aramid fibres). Adhesive bonding have shown to be even more effective than riveting, from about 15% to above 40% in terms of FCP life. Bonded aluminium straps, being made of a fatigue-critical material, provide the shortest FCP lives because they failed while the crack propagated underneath them. The best performances were achieved by titanium and ARALL straps despite the tensile residual stresses developed during the hot-bonding process, as a result of the thermal expansion coefficients mismatch between the skin and reinforcements.

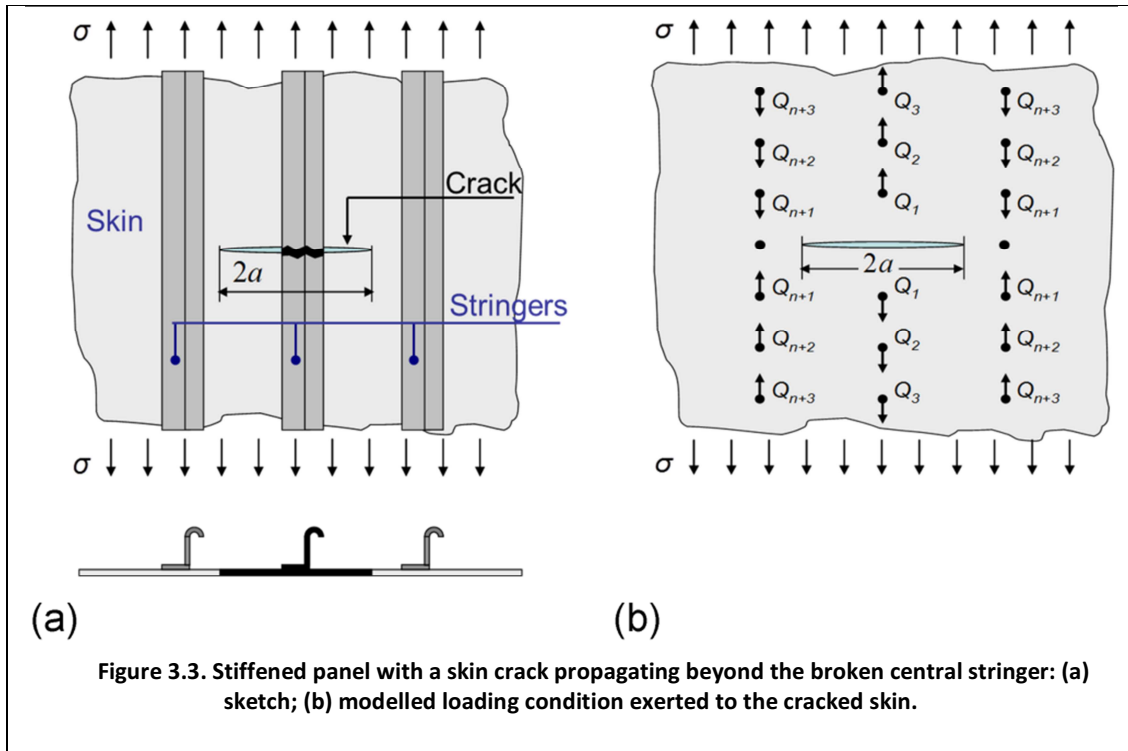
The high restraint effect that a bonded stiffener exerts on a crack is the result of the high loads transferred through the adhesive joint, even more than in a riveted joint, already when the crack is close to the stiffener edge. As a drawback, the high shear stresses induced in the adhesive could cause its failure (debonding), reducing significantly the crack retarding and arresting capability of a bonded stiffener, as highlighted in Ref. [4].

In a more recent work, Heinemann *et al* [6] have extended the experimental investigation to straps made either of glass (GLARE®) or carbon Fibre-reinforced Metal Laminates (FMLs) bonded on thick-gauges aluminium plates (from 6.35mm to 12.70mm) subjected to constant amplitude and spectrum fatigue loads. The aim of the work was to demonstrate the effectiveness of bonded reinforcement also on thick panels, typical of inner and outer lower wing covers of long range transport aircraft, in which the stresses transmitted through the adhesive are more intense because of the plane strain condition [7]. Bonded panels have shown FCP lives increased by a factor of 2 to 4 and, moreover, an increased residual strength up to 40% when compared to equal weight unstiffened panels. Auxiliary tests were also performed on integrally machined stiffened panels reinforced with aluminium (7085-T7651) straps, achieving FCP lives increased by 50% in respect with the unreinforced panel counterparts. However, as pointed out also in Ref. [4], some aluminium straps broke during the tests causing the premature failure of the panels, and thus evidencing the need of fatigue insensitive straps materials.

Starting from this consideration, Zhang *et al* [8] developed a numerical Finite Element (FE) model to evaluate the effect of straps made of high (static and) fatigue strength materials bonded on integrally stiffened panels. The model was validated through experimental tests on narrow panels reinforced with titanium (Ti-6Al-4V), CFRP or Glass Fibre Reinforced Polymers (GFRP) bonded straps, taking also into account the detrimental effects of adhesive debonding and residual stresses induced by the hot-bonding process. Numerical simulations performed on welded and machined wide stiffened panels [9] proved the effectiveness of bonded reinforcements to improve the fatigue crack growth life significantly, reconsidering the possibility to employ reinforced integral panels also where the F&DT requirements are critical.

Further study on the beneficial DT effects of bonded reinforcements was made by Meneghin [10] by means of an extensive experimental campaign performed by Airbus, in the framework of EU project DIALFAST. Aluminium, Titanium and glass FML straps, located between and under the main stiffeners, have shown how the wise use of these reinforcements make possible to achieve longer propagation lives or, correspondingly, higher allowable stress levels with a minor weight increase.

1.1. Analytical approach

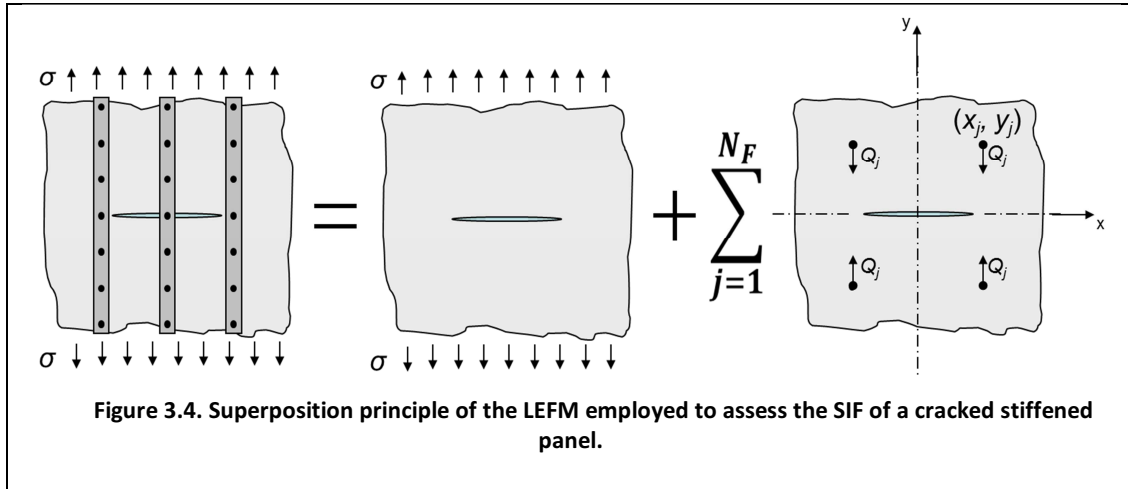


For a through-the-thickness skin crack propagating under fatigue loads along a stiffened panel, with the applied remote stress acting parallel to the stiffeners as depicted in Figure 3.3a, the SIF can be divided into two components invoking the superposition principle: the SIF due to the remote stress applied to the cracked sheet, and the SIF due to the load carried by the stiffeners. Modelling each stiffener as a series of concentrated forces Q_j located at its centre line, as sketched in Figure 3.3b, the complete solution is thus obtained by the sum of the elementary solutions represented mathematically in Equation (1)(3.1), depicted in Figure 3.4, and listed below:

	$K_{stiff} = K_{unstiff} + \sum_{j=1}^{N_F} K_j Q_j$	(3.1)
--	--	-------

1. The SIF associated to a through-the thickness-crack (semi-crack length a) in an unstiffened infinite flat panel remotely loaded by a nominal stress (σ).

2. The SIF associated to a through-the-thickness-crack in an unstiffened infinite flat panel due to a set of four concentrated forces (Q_j), symmetrically arranged around the crack origin.



In both Equation (3.1) and Figure 3.4, N_F is the number of sets of concentrated forces needed to model the whole system of forces Q_j , which describe the load transfer from the cracked skin to the stiffeners through the fastening system.

For a stiffened panel with a crack propagating along a straight line orthogonal to the stiffeners (and to the remote stress) both the analytical expressions of K are available in literature

	$K_{unstiff} = \sigma \cdot \sqrt{\pi a}$	
	$K_j = \frac{1}{2 \cdot t \cdot \sqrt{\pi a}} \left[\frac{1 + \nu}{4} \operatorname{Im} \left(\frac{a \cdot (\bar{z}_j - z_j)}{(\bar{z}_j - a) \sqrt{\bar{z}_j^2 - a^2}} \right) - \operatorname{Im} \left(\frac{a + z_j}{\sqrt{z_j^2 - a^2}} \right) \right]$	(3.2)

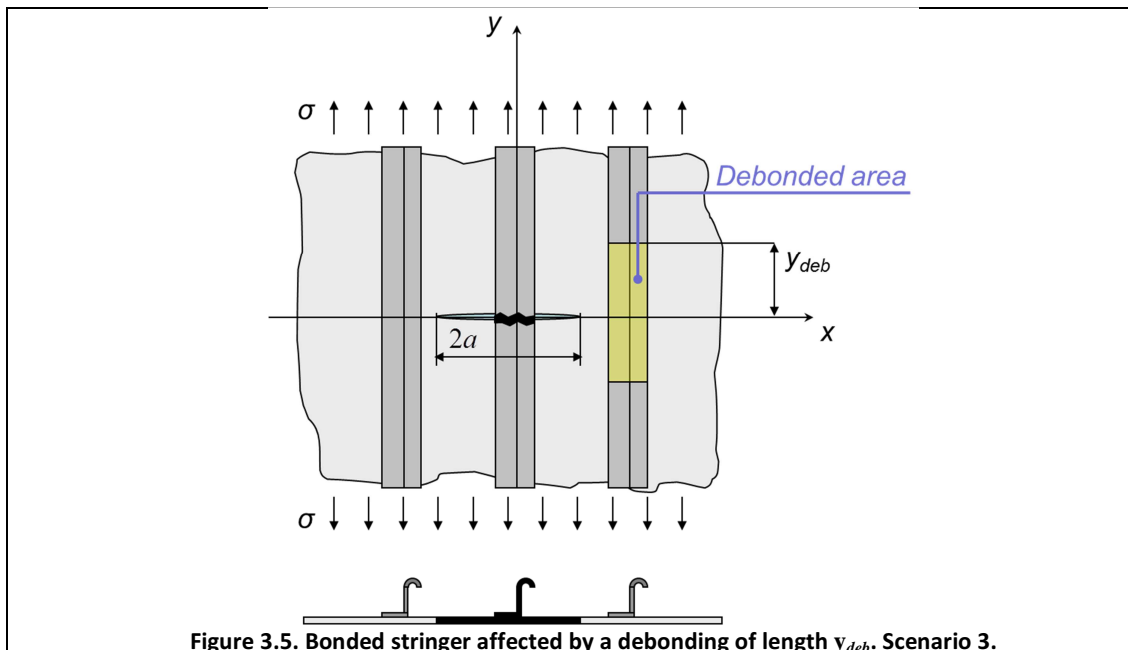
Where:

- t is the panel thickness;
- ν is the Poisson's ratio of the panel material;
- $z_j = x_j + i y_j$ ($\bar{z}_j = x_j - i y_j$) is the location of the force Q_j

To calculate the SIF for the stiffened panel the force reacted by the stiffeners must be known.

2.1. Displacement Compatibility Method

To evaluate the magnitude of the concentrated forces Q_j in equations (3.1)(3.2) , a pseudo-analytical method was developed by Poe[11][12] observing that the displacement field of the cracked skin must be compatible (congruent) with the displacements of the stiffeners evaluated at the same locations (x_i, y_i) . Accordingly to any compatibility methods (also known as force methods) [Ref to any book of structures], the displacements of both skin and stiffeners can be expressed by means of compliance coefficients which represents the displacements per applied unit force or stress.



The compliance matrix A_{ij} of a general elastic body can be defined as the displacement (per unit force) of the point (x_i, y_i) due to a force Q_j located at (x_j, y_j) ; in the same way the displacement of the point (x_i, y_i) per unit of applied remote stress can be represented by the compliance vector B_i .

Therefore, invoking again the superposition principle, the displacement field in the cracked skin (v^{skin}) can be expressed as the sum of the part due to the concentrated forces with the part due to the remote skin stress:

	$v_i^{skin} = - \sum_{j=1}^{N_F} A_{ij}^{skin} \cdot Q_j + B_i^{skin} \cdot \sigma$	(3.3)
--	---	-------

Similarly, the displacement *at the same locations* of the stiffeners (v^{stiff}) can be written as:

	$v_i^{stiff} = \sum_{j=1}^{N_F} A_{ij}^{stiff} \cdot Q_j + B_i^{stiff} \cdot \sigma_s$	(3.4)
--	--	-------

where σ_s is the stress applied remotely to the stiffeners which, for the strain compatibility between skin and stiffeners far away from the crack ($\varepsilon = \varepsilon_s$), is $\sigma E_s / E$. (E and E_s are the skin and the stiffeners elastic modulus, respectively). Imposing the displacement compatibility between the skin and the stiffeners, Eq. (3.5), the problem is reduced to a system of linear equations in the force unknown.

	$v_i^{skin} = v_i^{stiff}$	
	$(A_{ij}^{skin} + A_{ij}^{stiff}) \cdot Q_j = B_i^{skin} \cdot \sigma - B_i^{stiff} \cdot \sigma_s$	(3.5)

To account also the effect of the jointing system flexibility, Swift modified the (3.5) by adding an additional compliance matrix A_{ij}^{joint} of the jointing system (riveted or adhesively bonded) as follow:

	$(A_{ij}^{skin} + A_{ij}^{stiff} + A_{ij}^{joint}) \cdot Q_j = B_i^{skin} \cdot \sigma - B_i^{stiff} \cdot \sigma_s$	(3.6)
--	--	-------

The explicit expressions of the compliance coefficients are reported in [11].

The choice of suitable arrangement of concentrated forces permits to investigate different types of fastening systems: both integral and adhesively bonded stringers are modelled using a dense distribution of concentrated forces. The effect of the joint flexibility of the rivet or the adhesive layer is taken into account, but is not considered in the case of integral stiffeners; furthermore, the effect of the adhesive debonding is modelled imposing the extension of the debonded area (y_{deb}), i.e. the distance (from the crack path) where the concentrated forces begin to act (see Figure 3.5).

2.2. Effect of a stiffener on the SIF

The load transfer from the skin to an intact stiffener increases its stress and thus the forces acting along the y-axis positive direction as sketched in Figure 3.6a. As a consequence, to satisfy the equilibrium, the forces reacted on the cracked skin are directed in the y-axis negative direction (Figure 3.6b) reducing the magnitude of the stress field in front of the crack tip. Therefore, the SIF contributions associated to an intact stiffener are negative (i.e. $K_j Q_j < 0$) and so, in accordance with Equation (3.1), intact stiffeners act as crack retarders.

On the contrary, a broken stiffener, which is subjected to the remote stress $\sigma E_s/E$, exerts a tension on the skin crack surfaces, and thus the system of concentrated forces is opposed in respect with an intact stiffener as depicted in figures (Figure 3.6c). Therefore, the SIF contributions associated to a broken stiffener are positive (i.e. $K_j Q_j > 0$) increasing the crack opening displacement, and thus the related SIF, i.e. a broken stiffener accelerates the crack growth.

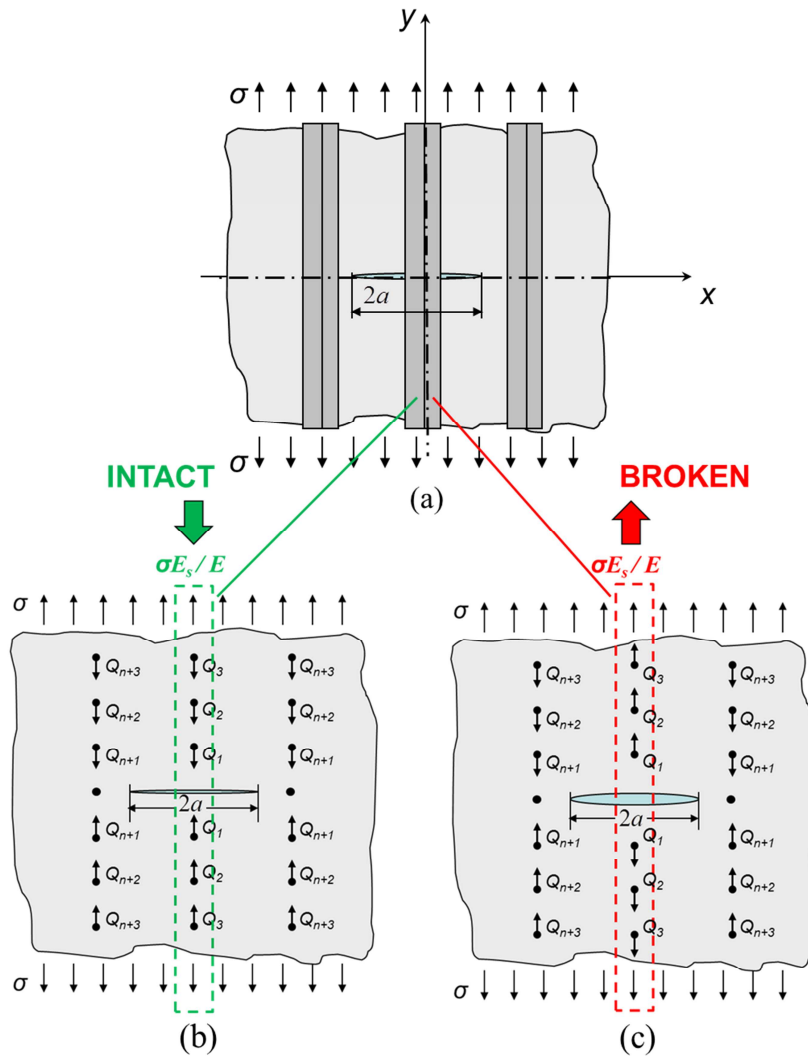


Figure 3.6. Reaction forces direction for intact and broken stiffeners.

Since the effect of the stiffeners on the SIF is commonly considered just like a geometric effect, is usual to express it in the term of the geometric correction factor β , as aforementioned in chapt. 2, which from the (3.1) can be expressed as

$$\beta_s = \frac{K_{stiff}}{K_{unstiff}} = 1 + \frac{\sum_{j=1}^{N_F} \bar{K}_j Q_j}{\sigma \sqrt{\pi a}} \quad (3.7)$$

Figure 3.7. β_s correction factor for intact and broken central stiffener. Scenario 3.

2.2.1. Additional crack retarders between and under the main stiffeners

In the common practice, additional crack retarders, usually named *doublers* or *tear straps*, can be placed between and under the main stiffeners (Figure 3.8) to slow down sub-critic crack growth or to stop fast unstable fracture of the skin. These additional stiffening elements are simply flat and thin straps that can be made of different materials: typically aluminium, titanium or fibre metal laminates¹.

To model the effect of the doublers between the stiffeners it is sufficient to use the appropriate compliance coefficients A_{ij}^{stiff} which are function of the cross-sections and the elastic modulus of the straps (see [11]).

If the doubler is placed under a stiffener, its effect can be accounted considering an equivalent stiffening element with equivalent total cross-section area and elastic modulus. The equivalent area A_{eq} is equal to the sum of each cross-section area

$$A_{eq} = A_d + A_s \quad (3.8)$$

Where A_d and A_s are the cross-section areas of doublers and main stiffeners, respectively. The equivalent elastic modulus E_{eq} is equal to the area weighted average of all the modulus

$$E_{eq} = \frac{A_d E_d + A_s E_s}{A_d + A_s} \quad (3.9)$$

¹A Fibre Metal Laminate (or FML) is one of a class of metallic materials consisting of a laminate of several thin metal layers bonded with layers of composite material, typically glass fibres.

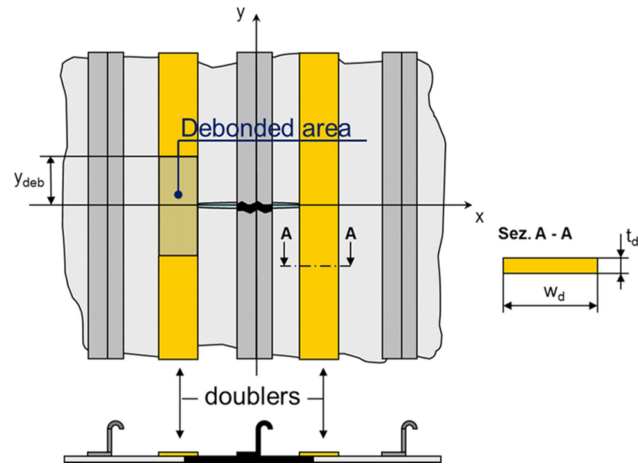


Figure 3.8. Doublers in the middle of the stringers bay. Damage scenario 3.

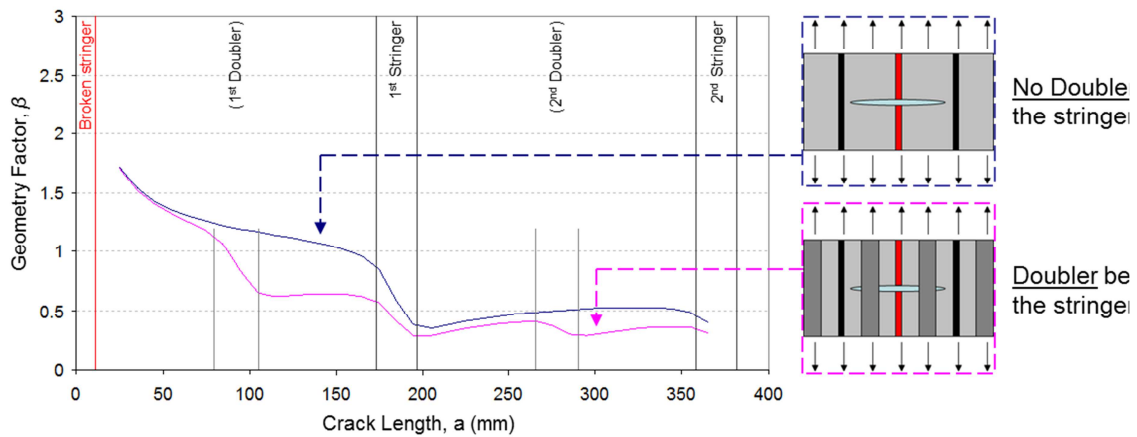


Figure 3.9. Effect of doublers bonded in the middle of the stiffeners bay. Damage scenario 3.

1.1.1. Test – analytical result correlation

As anticipated in the introduction, LEAF was validated through an extensive experimental campaign, provided by Airbus focused on the FCP behaviour of wide “seven-stringer” panels with different geometries and materials of skin, stringers and crack retarders from [10]. In Figure 3.10 and Figure 3.11 are reported the comparison of analytical and experimental results for the panels configuration summarized in Table 3.1.

.Additionally to prove the tool validity, in Figure 3.12 is provided a comparison between LEAF results, showed as dashed and solid lines, and literature experimental data, showed as round and square markers, in terms of geometric correction factor β .

Ref. [10]	Aluminum doubler	Titanium doubler
Skin		
Material	2024-T3 Alclad	2024-T3 Alclad
Young's modulus	MPa	MPa
Thickness	mm	mm
Paris' Law [C, n]	-	-
Aluminum Stringer		
Material	7349-T76511	7349-T76511
Young's modulus	72000 MPa	72000 MPa
Stringer pitch	185mm	185mm
Cross-sectional area	139mm ²	139mm ²
Doublers		
Material	2024-T3 Alclad	Ti 6Al-4Va
Young's modulus	73100 MPa	114000 Mpa
Position	Middle bay	Middle bay
Cross-sectional area	21mm ²	21mm ²
Joint		
	Epoxy adhesive FM73	Epoxy adhesive FM73
Shear modulus	500 MPa	500 MPa
Thickness	0.2 mm	0.2 mm
Gross stress	86 MPa	86 MPa

Table 3.1. Characteristics of the modelled panels from Ref. [10].

Ref. [4]	Bonded	Integral
Skin		
Material	2024-T3 Alclad	2024-T3
Young's modulus	68500 MPa	73100 MPa
Thickness	1 mm	1 mm
Paris' Law [C, n]	-	-
Straps		
Material	2024-T3 Alclad	2024-T3
Young's modulus	68500 MPa	73100 Mpa
Stringer pitch	105 mm	105 mm
Cross-sectional area	100 mm ²	100 mm ²
Joint		
	Epoxy adhesive FM123-5	Chemical milling
Shear modulus	138 MPa	-
Thickness	0.2 mm	-
Gross stress	117.7 MPa	117.7 MPa

Table 3.2. REF_Ref350719703 \h Figure 3.12 shows the results regarding the adhesively bonded and integral stiffened panel from the “test series 2” reported by Schijve [4]. The data used for the analysis are listed in Table 3.2. For the bonded case, it should be noted that the best agreement between experimental and calculated data was achieved considering a skin-stiffener debond size (y_{deb}) of 8mm. However, this prediction

was verified only qualitatively because the measured size of the debonded region wasn't reported in Ref. [4].

Ref. [1].	t = 1.86 mm	t = 9.53 mm
Skin		
Material	2024-T3	2024-T3
Young's modulus	73100 MPa	73100 MPa
Thickness	2.29 mm	2.29 mm
Paris' Law [C, n]	$1.16 \times 10^{-13} \frac{\text{mm}}{(\text{MPa}\sqrt{\text{mm}})^n}, 3.89$	$1.16 \times 10^{-13} \frac{\text{mm}}{(\text{MPa}\sqrt{\text{mm}})^n}, 3.89$
Straps		
Material	2024-T3	2024-T4
Young's modulus	73100 MPa	73100 MPa
Stringer pitch	152 mm	152 mm
Cross-sectional area	91.8 mm ²	486 mm ²
Joint		
	Lock-bolts d = 6.4 mm	Lock-bolts d = 6.4 mm
Young's modulus	71000	71000
Fastener pitch	25 mm	25 mm
Gross stress	103 MPa	103 MPa

Table 3.3. Characteristics of the modelled panels from Ref. [1].

REF_Ref350719703 \h Figure 3.12 shows the results regarding two of the bolted panels tested by Poe in [1], specifically the panels with 1.80mm and 9.53mm thick aluminium stringers (see Table 3.3). The experimental values of β , not available in the original work, were obtained evaluating K_{max} from the experimental FCPR data by reversing the Paris' law. The appropriate Paris' coefficients were derived from the FCPR data of the tested unstiffened panels, always reported in Ref. [1].

A good agreement between experimental data and LEAF prediction was found, evidencing the tool reliability.

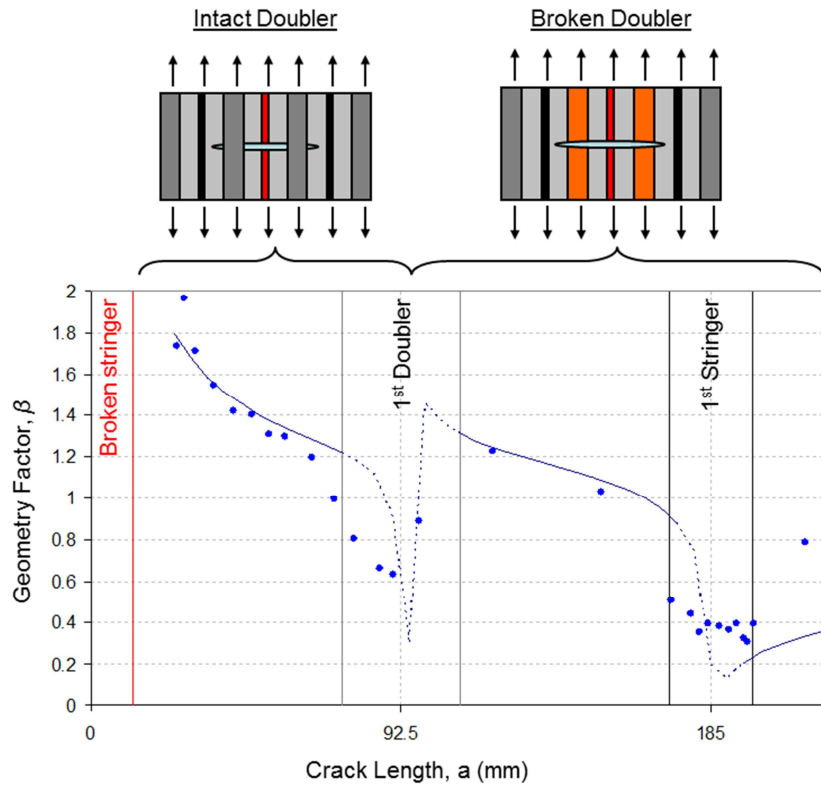


Figure 3.10. 7-Stringer panel with aluminium doublers bonded in the middle of the stiffeners bay from Ref. [10]. Damage scenario 3.

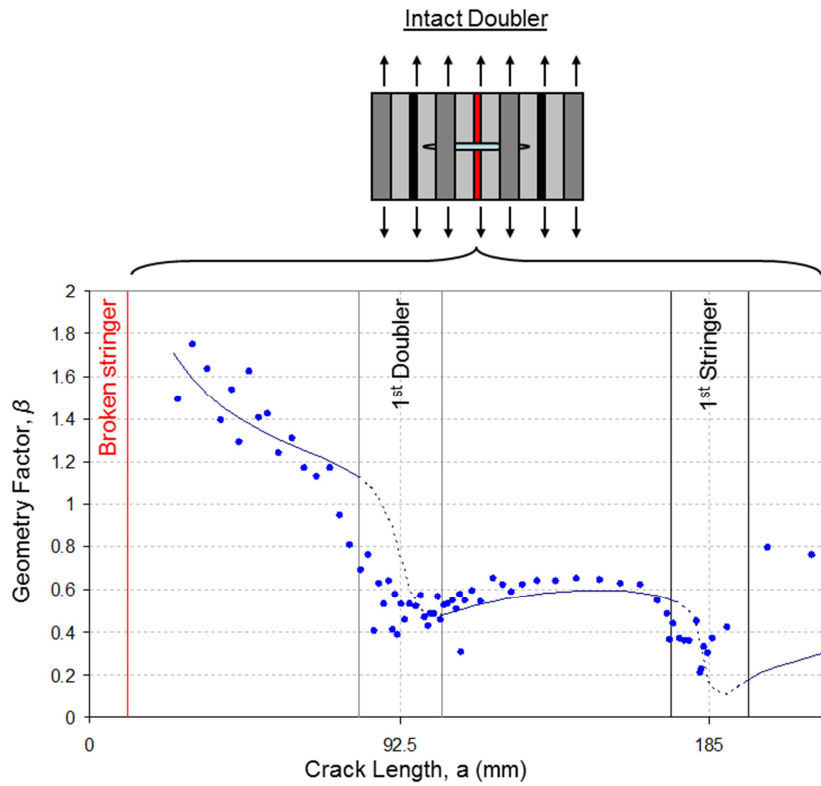


Figure 3.11. 7-Stringer panel with titanium doublers bonded in the middle of the stiffeners bay from Ref. [10]. Damage scenario 3.

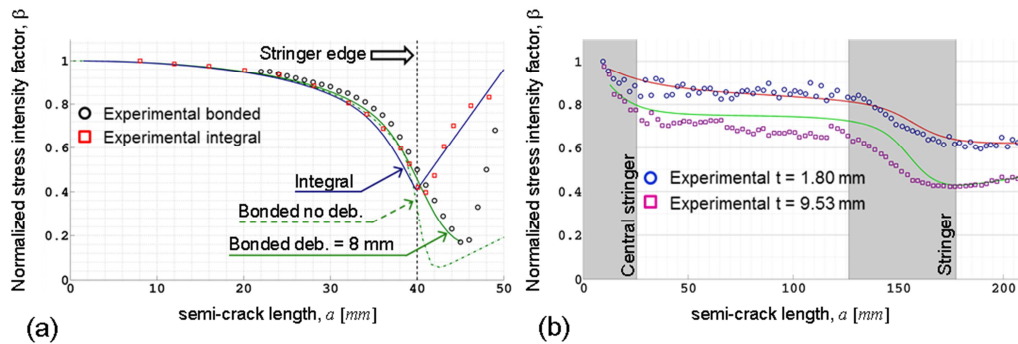


Figure 3.12. Normalized stress intensity factor (β) vs. the crack half-length (a): (a) “test series 2” from Ref.[4], (b) bolted panels with aluminium stiffeners from Ref. [1].

1.2. Parametrical DT analysis

The fatigue crack propagation performances of stiffened flat panels, representative of conventional aircraft constructions, were assessed using the LEAF. The modelled panels

consisted in a flat skin stiffened by evenly spaced “Z-shaped” stringers, parallel to the loading direction and orthogonal to the propagation of a through-the-thickness skin crack, as illustrated in Figure 3.3a. Configurations, dimensions, loading conditions of the modelled cracked panels are typical of a pressurized fuselage shell with a circumferential crack propagating by fatigue. The main characteristics of the modelled panels were reported in Table 3.4. The fatigue crack propagation performances were calculated in the cases of riveted, adhesively bonded and integral stringers in order to assess the effect of the adopted stringer fastening system.

In the case of riveted stringers, the effects of rivet pitch and rivet diameter were expressed by the rivet pitch to diameter ratio p/d , to reduce the numbers of sensitive analysis parameters as used by Poe [11]. Furthermore, in the case of the riveted panel, three meaningful types of damage scenarios were investigated, as sketched in Figure 3.1

1. Scenario 1: the one-bay crack scenario, with a crack propagating from a point midway between two stringers;
2. Scenario 2: the two-bay crack scenario, with a crack propagating on both sides of an intact stringer;
3. Scenario 3: the two-bay crack with a broken central stringer scenario, with a crack propagating on both sides of a broken stringer.

The crack retarding contribution obtained by the use of adhesively bonded doublers on the cracked skin between the bonded stringers in the case of the damage scenario 3, as sketched in Figure 3.8, was investigated as well. The effects of materials and dimensions (i.e. both the width w_d and thickness t_d) on the doubler crack retarder capability were analysed. The characteristics of the modelled doublers were reported in Table 3.5 where the dimensions were expressed in terms of width-to-thickness aspect ratios (w_d/t_d). The aspect ratios were chosen to maintain the same cross-sectional area A_d , assumed to be one third of the stringer area ($A_s/A_d = 3$).

The detrimental effect of the likely adhesive failure on the FCGR was quantified for different size of the debonded area (y_{deb}), expressed in millimetres, and listed in Table 3.5.

Skin	
Material	Al alloy sheet
Young's modulus	73100 MPa
Thickness	1.6 mm
Paris' Law [C, n]	$2.13 \times 10^{-12} \frac{\text{mm}}{(\text{MPa}\sqrt{\text{mm}})^n}, 3.24$
Plain stress fracture toughness	100 MPa $\sqrt{\text{m}}$
Stringers	
Material	Extruded Al alloy
Young's modulus	71700 MPa
Stringer pitch	185 mm
Cross-sectional area	89 mm ²
Ultimate tensile strength	576 MPa
Riveted joints	
Young's modulus	71000
p/d	2.5, 3.75, 5
Bonded joints	
Shear modulus	500 MPa
Thickness	0.2 mm
Applied load	
Maximum gross stress	90 MPa
Stress ratio	0.1

Table 3.4. Characteristics of the modelled panels.

Aluminum doublers	
Material	Bare Al alloy
Young's modulus	73100 MPa
A_s/A_d	3
w_d/t_d	23.5, 32, 41.8
Ultimate tensile strength	440 MPa
Titanium doublers	
Material	Ti-6Al-4V
Young's modulus	113800 MPa
A_s/A_d	3
w_d/t_d	41.8
Ultimate tensile strength	980 MPa
Doublers debonding	10, 20, 30, 40 mm

Table 3.5. Characteristics of the additional bonded doublers. [A_s/A_d] = Stringer to doubler cross-sectional area ratio, [w_d/t_d] = Doubler width to thickness ratio.

1.3. Effects of damage scenarios

The calculated fatigue skin crack propagation through the riveted stiffened panel in the case of both one-bay crack (scenario 1) and two-bay crack (scenario 2) was plotted for different rivet pitch to diameter ratios p/d in Figure 3.14 and in Figure 3.15, respectively. No doublers were considered in these analyses.

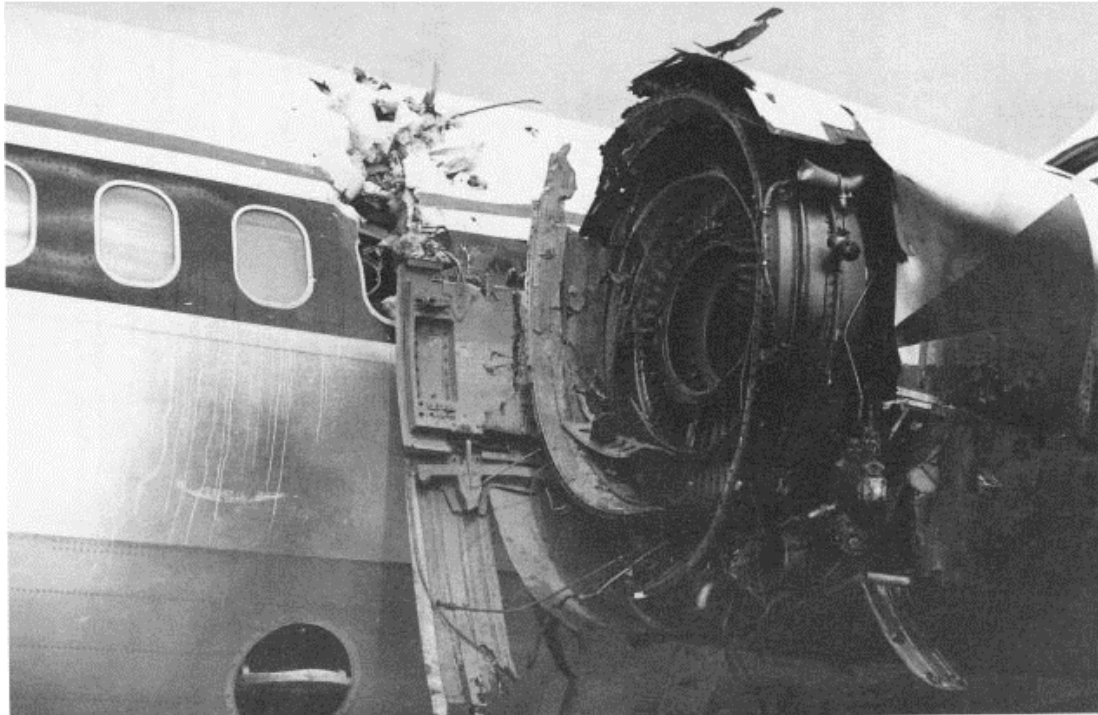


Figure 3.13. Discrete source damage, uncontained engine failure (Delta Airlines MD-88, 6 July 1996).

It is easy to see that a lower rivet pitch led to a lower fatigue skin crack propagation rate and, as an obvious consequence, to a longer crack growth period (in terms of load cycles). In the case of the one-bay crack scenario, it is possible to note that crack propagation was unaffected by the p/d ratio until the crack has reached the stringer, whereas, on the contrary, the two-bay crack scenario showed a strong dependence on this parameter from the earliest stages of the crack propagation. Under the same conditions, i.e. the same p/d ratio, the one-bay crack damage scenario showed to be more critical than the two-bay over intact stringer scenario. In fact, as a consequence of the faster growth rates, after 1.6×10^4 cycles the one-bay crack has reached the entire bay length ($2a = b$), while the two-bay crack has propagated only to a small fraction of the same bay length. For this reason the one-bay crack damage scenario is the sizing criterion

of the damage tolerance design philosophy of aircraft structures. This is also justified by the highest tensile stresses that act in the portion of skin located in the middle of the stringer bay, which is then a likely point of crack nucleation.

Nevertheless, a stringer failure due to fatigue or to accidental impacts (indicated by airworthiness regulation as discrete-damage sources, e.g. the uncontained engine failure showed in Figure 3.13) could happen during a flight [13]. For this reason, a damage scenario with a crack propagating on both sides of a broken stringer (scenario 3) was investigated in Figure 3.15, evidencing the detrimental effect of the broken stringer on the crack propagation.

As in the case of the two-bay crack with a central intact stringer, the broken stringer scenario showed the dependence between the crack growth (rate) and the rivet pitch. Lower values of p/d led to slightly higher crack propagation rates in the proximity of the broken stringer. This is because a reduced rivet pitch produces a higher load transfer from the cracked skin to the stiffeners and, once they fail, the gross stress carried by them is released completely to the cracked skin; the resulting skin overload promotes the crack propagation. This behaviour is reversed when the crack propagates after the first intact stringer (see the intersection point in Figure 3.15). A direct comparison between the fatigue crack propagation of the two-bay crack with a broken central stringer scenario and the one-bay crack scenario, shows that the former represents the worst case: in fact after 6×10^3 cycles the two-bay crack has covered the whole two bay length ($2a = 2b$), while the one-bay crack has only reached a very small fraction of one bay length (about the 9% of b).

At the present, only the one-bay crack damage scenario is envisaged by the airworthiness regulations. But, as suggested by Swift [13][14] and in accordance with the data presented here, a two-bay crack with a broken central stiffener sizing criterion should be adopted where a stiffener failure is probable to occur, due to fatigue or accidental damages.

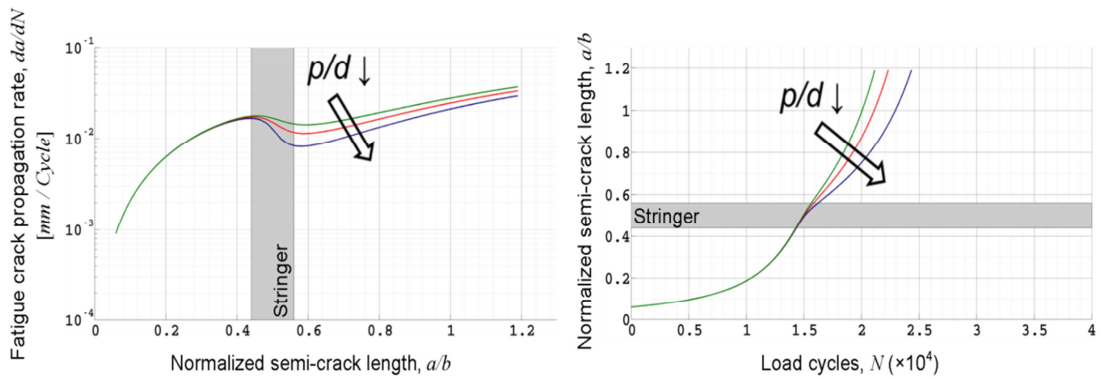


Figure 3.14. Fatigue crack growth rate (da/dN) and fatigue crack propagation life (a vs. N) through the riveted panel as a function of the rivet-pitch to rivet-diameter ratio p/d . Riveted panel, scenario 1.

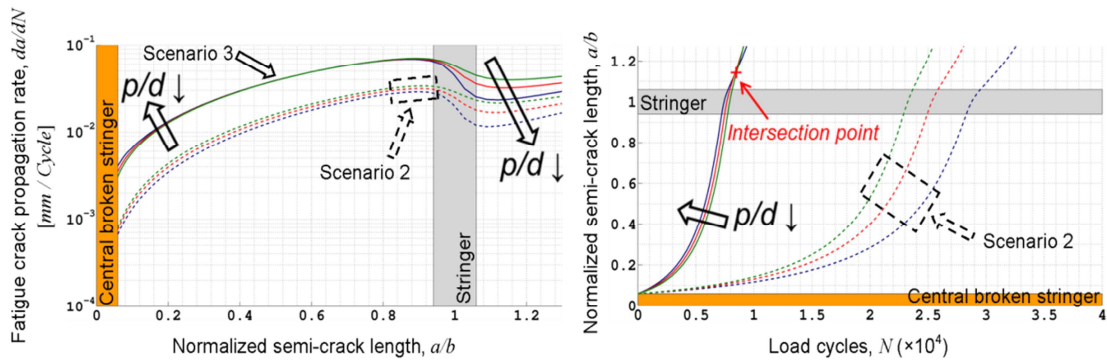


Figure 3.15. Fatigue crack growth rate (da/dN) and fatigue crack propagation life (a vs. N) through the riveted panel as a function of the rivet-pitch to rivet-diameter ratio p/d . Riveted panel, comparison between scenarios 2 and 3.

1.4. Effects of fastening system

In Figure 3.16 the effects of riveted, adhesively bonded and integral stringers on the skin crack propagation were reported. The one-bay crack scenario (scenario 1) was chosen as a representative case to put in evidence only the effect of the fastening method, excluding the influence of an intact or broken central stringer.

Riveted joints showed to be less effective than both adhesively bonded and integral joints, due to the highest FCGR. The slowest crack propagation was observed in presence

of the intact integral stringer, as showed in the graph with a dashed line and triangle markers, at least up to the inner stringer edge.

In fact, after the stringer edge, the skin crack propagates through the stringer due to the material continuity of the integral fastening system. The progressive loss of the stringer integrity causes the overloading of the cracked skin, with a consequent rise of the crack propagation rate. The realistic behaviour of the integral stringer was indicated by the solid line with triangle markers: it can be noted that the crack propagation rate grows rapidly, going well beyond the values achieved by the riveted joints. This issue does not affect the adhesively bonded joints, as a consequence of the physical separation between the stiffeners and the skin. Therefore, the bonded joints provide the best crack retarding properties, as given in literature [2][4]. The detrimental effect of the adhesive debonding was considered imposing a size of 10mm of the debonded area (y_{deb}): despite the increased FCGR, the bonded stringer remained the most effective in retarding the crack growth.

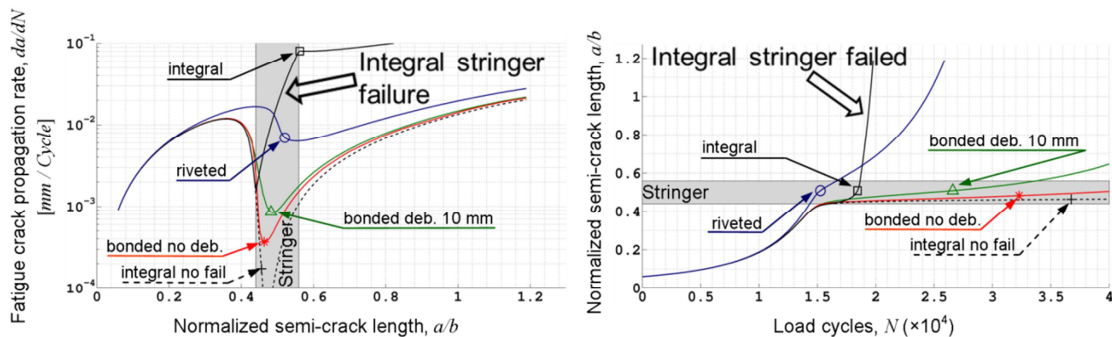


Figure 3.16. Fatigue crack growth rate (da/dN) and fatigue crack propagation life (a vs. N) through a panel with riveted, bonded or integral stringers. Scenario 1.

1.5. Effects of additional doublers

In order to increase the DT properties of stiffened panels, aircraft manufactures are usual to bond additional thin strap crack retarders, named doublers, between and under the stringers. The effects of adhesively bonded aluminium doublers placed between the stringers were depicted in Figure 3.17. Different doubler geometries were compared at

constant cross-sectional area $w_d \times t_d$, as reported in Table 3.5. Doublers with highest aspect ratios w_d/t_d , i.e. widest and thinnest doublers, showed the better crack retarding effects in the term of FCGR reduction.

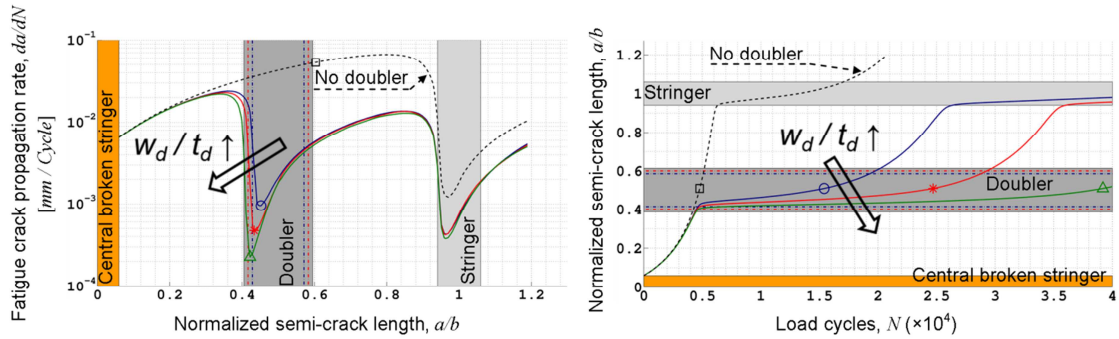


Figure 3.17. Fatigue crack growth rate (da/dN) and fatigue crack propagation life (a vs. N) through a bonded panel with additional doublers as a function of the doubler width-to-thickness aspect ratio w_d/t_d . Scenario 3.

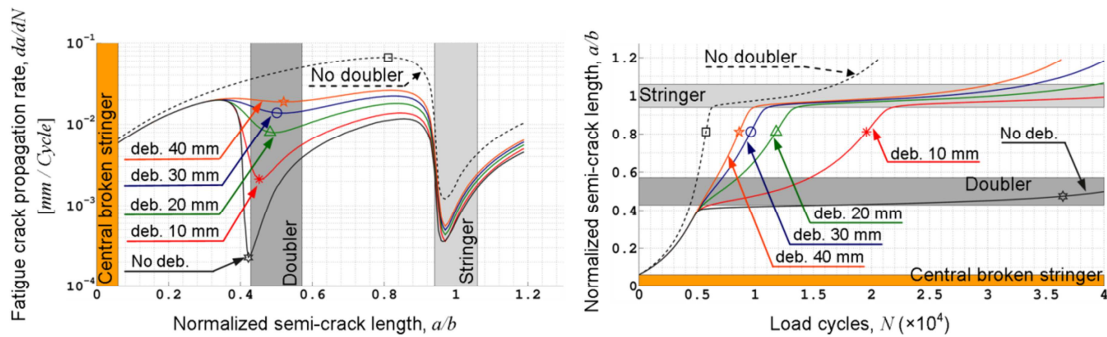


Figure 3.18. Fatigue crack growth rate (da/dN) and fatigue crack propagation life (a vs. N) through a bonded panel with additional doublers as a function of the doubler adhesive delamination. Doublers width-to-thickness aspect ratio $w_d/t_d = 41.8$. Scenario 3.

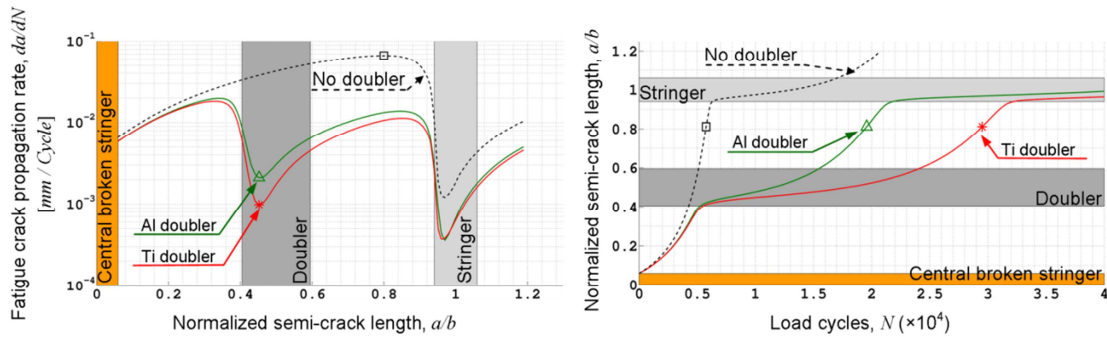
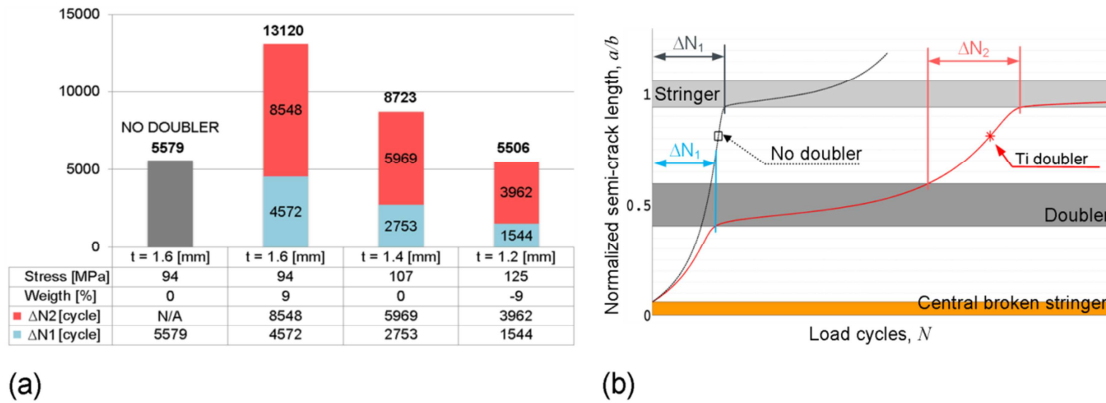


Figure 3.19. Fatigue crack growth rate (da/dN) and fatigue crack propagation life (a vs. N) through a bonded panel with both aluminium and titanium doublers. Doublers width-to-thickness aspect ratio $w_d/t_d = 41.8$. Scenario 3..

Another important aspect that affects the doublers behaviour is the presence of delamination in the adhesive layer around the advancing crack tip, caused either by static or fatigue failure of the adhesive. Figure 3.18 shows both the FCGR and the crack growth for different sizes of adhesive debonding. The effectiveness of doublers to restrain the crack propagation is reduced by the extension of the debonding, as a consequence of the skin-to-doubler load transfer breakdown. Despite debonding, the adoption of additional doublers provides a great beneficial effect on the DT properties of stiffened panels.

Aluminium doublers, however, are extremely sensitive to fatigue damages as evinced by experience [4][6][10], in fact they fail when a crack propagates underneath them. Once the doubler fails the FCGR begins to grow rapidly, as seen in the case of a broken stringer. The adoption of high fatigue strength materials, like titanium, is then recommended. A comparison between aluminium and titanium doublers with the same aspect ratio ($w_d/t_d=41.8$) was illustrated in Figure 3.19. Titanium doublers have proven to be more effective than aluminium ones, as an obvious consequence of their higher elastic modulus [2][4][8][10]. The increased FCP life can then be exploited in terms of reduced operative costs by relaxing the inspection plans but with the penalty of an increased structural weight. This issue can be partially avoided using lightweight and fatigue resistant reinforcements made of FML, GFRP or CFRP (paying attention to galvanic corrosion) instead of titanium alloys [6][8][10]. Otherwise, another feasible option is to increase the allowable stresses by reducing, for example, the stiffener dimensions or the skin

thickness, and thus the structural weight, within the constraints of static and residual strength.



(a) (b) **Figure 3.20. Effect of titanium doublers on the DT properties of bonded stiffened panels: (a) fatigue crack propagation life and structural weight as a function of the skin thickness, (b) crack propagation periods between the bonded stiffeners. Scenario 3.**

Panel	σ_{max} [MPa]	$1.33 \times (K_{max})_{max}$ [MPa m ^{1/2}]	σ_s max [MPa]	σ_d max [MPa]
Baseline	94	81	347	N/A
t = 1.6 mm	94	58	247	717
t = 1.4 mm	107	67	268	777
t = 1.2 mm	125	79	295	853

Table 3.6. Stresses in the skin, in the stringer, in the titanium doubler and stress intensity factors of the panels presented in Fig. 14, as a function of the skin thickness.

In the bar chart in Figure 3.20a was illustrated an example of the effect of the skin thickness on both the FCP life and the structural weight of a stiffened panel reinforced with a titanium doublers. Three skin thicknesses were considered: 1.6mm, 1.4mm and 1.2mm; in addition, a panel without doublers and with a 1.6mm thick skin was used for comparison (baseline). The weight per unit (of panel) length and per number of bays was expressed as a percentage of the baseline. The baseline maximum skin stress (σ_{max}) was imposed to 94MPa; this value was increased in the three case studies by the same proportion as the skin thickness reduction (see Table 3.6 and Figure 3.20a), as happens with the hoop stress that is inversely proportional to the thickness. The likely presence of adhesive debonding was taken into account performing the analyses with an imposed size of the debonded area equal to 10mm, for both doublers and stringers.

Obviously, the panel with the thickest skin achieved the longest FCP life, 135% greater than the baseline, but with a weight penalty of 9%. Reducing the thickness from 1.6mm to 1.4mm the FCP life was increased (+56%) without increase the weight, and moreover, a further reduction to 1.2mm led to a weight saving of 9% maintaining the FCP life almost unchanged (-1.3%), if compared to the baseline. FCP lives were evaluated up to a crack length of two bays considering only the number of applied load cycles that the skin crack takes to propagate between the stiffeners, as depicted in Figure 3.20b, because, to be conservative, the propagation periods underneath the bonded stiffeners are currently not considered during the design phases [15].

It should be noted that the skin thickness cannot be reduced without considering the effects on the residual strength of the panel, perhaps a thorough analysis in this regard goes beyond the scope of this paper. However, a simplified analysis was performed to make this example more realistic. Instead of the R-curve approach, which is the suitable choice for thin shell panel, the simpler (but less accurate) static failure criterion of LEFM ($K_{max} = K_C$) was used to verify the skin resistance. A reasonable value of 100MPavm was chosen for the (plain stress) fracture toughness K_C , although higher values can be found in literature for the materials usually employed in fatigue critical areas. The maximum SIFs K_{max} were calculated multiplying the (maximum) stress in the skins by a safety factor of 1.33; for the sake of conciseness, only the overall maximum $(K_{max})_{max}$ for each case studies was reported in Table 3.6. K_{max} was found to be always less than K_C , ensuring the integrity of the skin.

In addition, the likely failure of the stiffeners was checked, because in the event of a failure the calculated SIFs would be incorrect. For this reason, in Table 3.6 were also listed the maximum stresses reached in the doubler ($\sigma_{d max}$) and in the stringer ($\sigma_{s max}$) during the crack propagation. The computed stress levels remained under the stiffeners ultimate strengths (see the Table 3.4 and Table 3.5) ensuring also the integrity of both doublers and stringers.

1.6. Fatigue crack propagation above bonded stiffeners

Was seen in the previous section how the long crack propagation period through the skin above a bonded stringer (between ΔN_1 and ΔN_2 in Figure 3.20) is currently

disregarded). Therefore, significant benefits in terms of structural weights, reliability and maintenance costs could be achieved by taking into account this FCP period during the design of the adhesive bonded stiffened panels.

Therefore, a deep investigation of the phenomena involved during this propagation phase is fundamental, as well as the analysis of the mechanisms that can drive the stringer to failure while the skin crack is still in the stringer covered area. In accordance with the effective crack restrain capability of intact stiffeners and the detrimental crack opening action of the failed ones, the latter is indeed a fundamental aspect that drives the FCP through the stiffened panel.

Displacement compatibility method showed its reliability in predicting the SIF when the skin crack tip is outside the stiffener covered areas, whereas it proved to be unsuitable when the skin crack tip is propagating above the bonded stiffeners. Figure 3 shows the prediction of the normalized SIF (i.e. the geometry factor β) plotted as a function of the crack half-length a for together with the relative experimental data, confirming the previous conclusion.

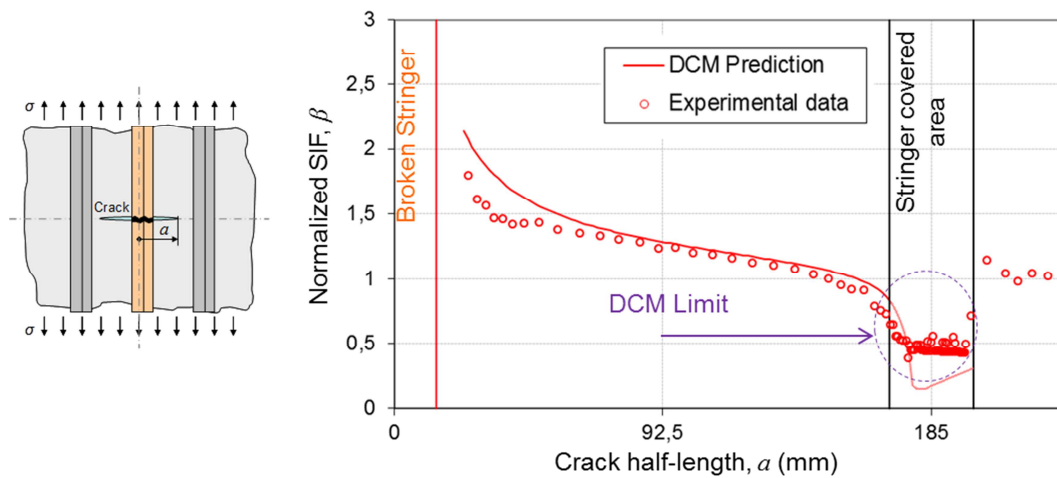


Figure 3.21. FCP above a bonded stiffener: comparison between DCM and experimental data . Scenario 3.

The reason of the discrepancy when the crack propagates above the stringer covered area is the inadequacy of the DCM to capture the real mechanisms which drive the skin crack propagation above the adhesively bonded stiffener.

During this crack propagation phase, the most effective stringer hindering action on the crack propagation is the restraint on the crack opening due to the bonded reinforcement. This mechanism, known as crack-bridging, acts along the crack faces above the stringer, as shown in Figure 3.22; the predicted skin crack opening displacement (COD) of a crack approaching the stringer ($a \approx b$) and a crack extended through the whole bonded stringer covered area ($b < a < c$) are herein plotted.

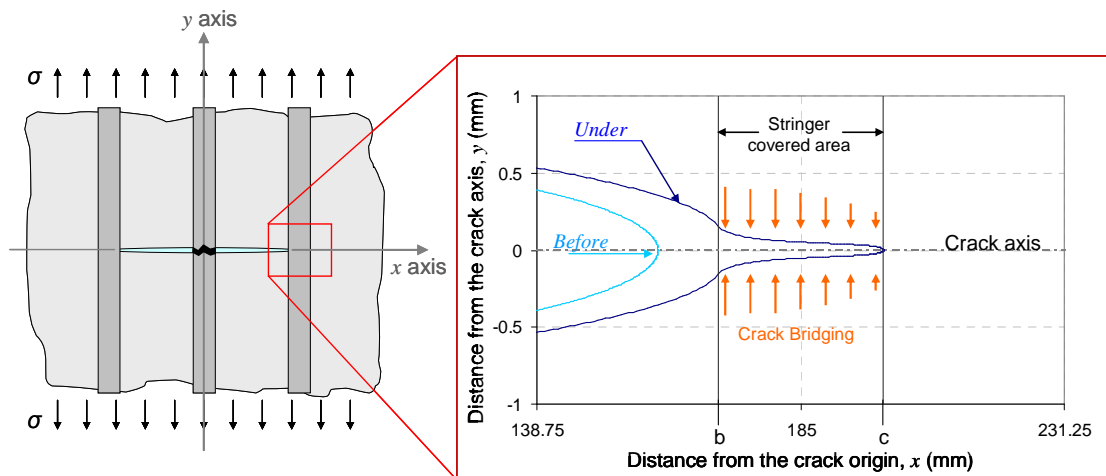


Figure 3.22. Predicted COD of a skin crack approaching the bonded stringer edge ($a \approx b$) and of a skin crack with the crack tip at the end of the bonded stringer covered area ($b < a < c$). CODs. Scenario 3.

COD predictions in Figure 3.22 are the result of a crack-bridging model proposed by L.R.F. Rose [21] on the basis of the F. Erdogan work [22], that was implemented in LEAF to describe analytically the skin crack propagation above the bonded stringers.

The basic simplification proposed by L.R.F. Rose is that the restraining action exerted by the crack-bridging mechanism can be modelled by the crack-closure effect of a continuous distribution of linear springs acting between the crack faces above the bonded stringers, as sketched in Figure 3.23.

The restrained COD above the stringer ($2v(x)$) is indeed driven by the local stress field relief due to the crack-bridging stress induced by the springs σ_b , as depicted by the

	$v(x) = f(\sigma_0 - \sigma_b) = f(\sigma_0 - k \cdot E \cdot v(x))$	(3.10)
--	--	--------

Where σ_0 is the local skin stress due to the redistribution of the remote stress σ_∞ between the skin and stringer. σ_0 can be obtained from the one-dimensional theory of bonded joints in accordance with the skin/stringer stiffness ratio.

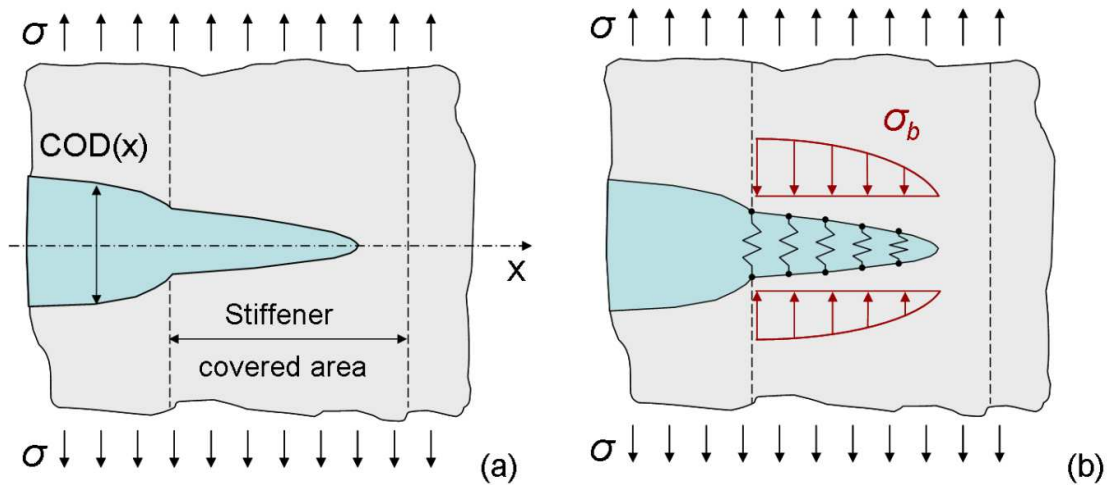


Figure 3.23. Crack-bridging mechanism of the bonded reinforcement modelled by a continuous distribution of springs acting between the crack faces in the stringer covered area.

The linear behaviour of the springs acting between the crack faces is expressed by the last term of the equation (3.10), where k is the spring stiffness constant and E is the elastic modulus of the skin material. The k constant can be determined from a one-dimensional analysis of a single-strap joint representative of the load transfer from the cracked plate to the bonded stringer, as sketched in Figure 3.24.

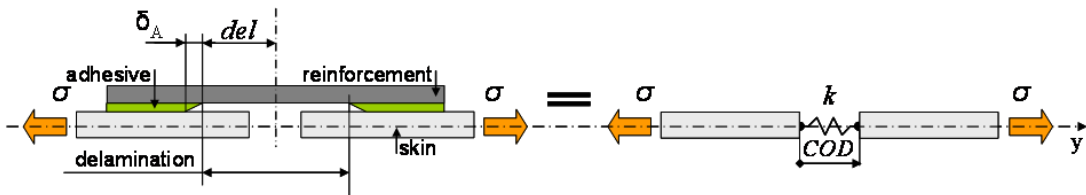


Figure 3.24. Single-strap joint representative of the load transfer from the cracked plate to the bonded stringer. Scenario 3.

In the case of perfectly bonded single-strap joint (i.e. no delamination), the remote stress determines an opening of the joint only due to the adhesive displacement contribution δ_A .

A delamination around the crack provides an additional displacement contribution induced by the deformation of the reinforcement over the delaminated area “ $2d$ ” wide $\varepsilon_r \cdot d$; ε_r is the linear deformation of the reinforcement. In accordance with the (3.11)[23], a delamination reduces the stiffness proprieties of the adhesive single-strap, and thus the magnitude of its spring stiffness constant k .

$$k = \frac{\sigma_\infty}{E \cdot u_p} = \frac{\sigma_\infty}{E \cdot (\delta_A + \varepsilon_R \cdot d)} \quad (3.11)$$

The solution of the skin crack propagation above the bonded stringer comes from the solution of the function in the (3.10). This function is described by means of the dislocation theory, transforming the (3.10) into an integral singular equation in the unknown $v(x)$, to be solved with the numerical solution as described by F. Erdogan.

Under the hypothesis of the LEFM, the relation between the crack-displacement $v(x)$ and K for the plane-stress condition is expressed reversing the (2.17) as:

$$K(a) = v(x) \frac{G(1-\nu)}{2} \sqrt{\frac{2\pi}{a-x}} \quad (3.12)$$

where G and ν are, respectively, the shear modulus and the Poisson’s ratio of the skin material.

The effect of no delamination and delaminations d extended among 10mm and 30mm on both sides of the advancing crack are considered. Furthermore, the effect of a delamination that likely extends during skin crack growth above the stringer is considered (“del $d=0 - 30\text{mm}$ ”); in absence of a suitable delamination growth law (and related data of the adhesive) a linear growth of the delamination with the number of the applied load cycles up to 30mm was assumed.

Longer is the crack extension through the stringer covered area and more effective is the crack-bridging mechanism which reduces monotonically the crack driving force, and thus the geometry factor β .

A delamination that can develop at the adhesive interface between the bonded stringer and the cracked skin around the advancing crack tip can significantly affect the effectiveness of the crack-bridging mechanism. As shown in Figure 3.25, where the COD of the skin crack propagated through the whole stringer covered area plotted for various delamination extensions, the delamination reduces the crack-opening restraint exerted by the bonded stringer.

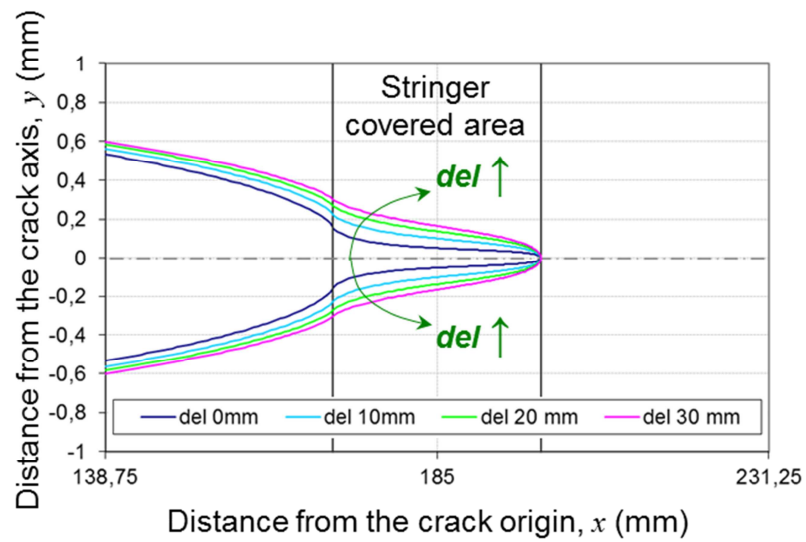


Figure 3.25. Predicted COD as a function of the delamination extension above the adhesive bonded stringer.

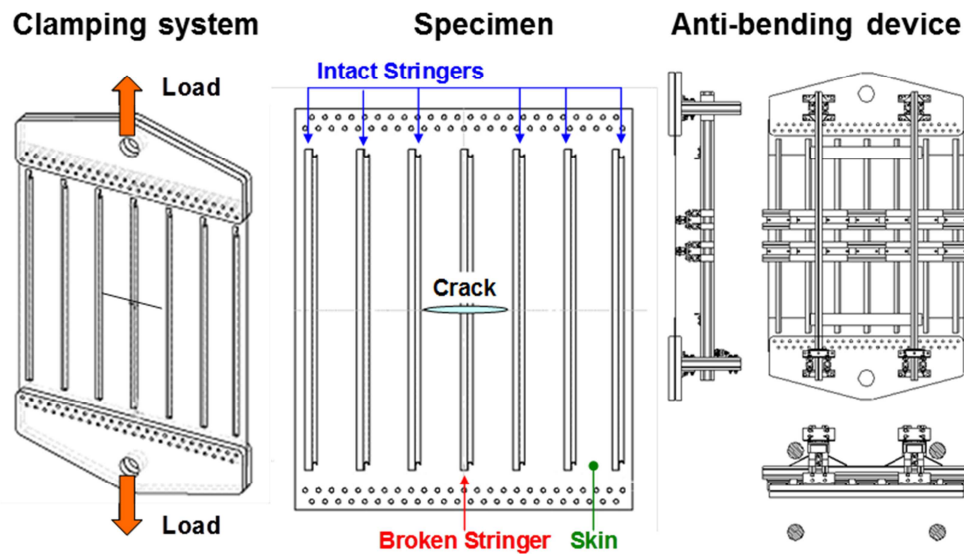


Figure 3.26. Sketch of the tested specimens, clamping system and anti-bending device.

1.6.1. Experimental investigation

The specimens under consideration were constituted by a wide flat skin with seven equally-spaced parallel stringers, as sketched in Figure 3.26, together with the clamping system and the anti-bending device employed during the FCP test.

The skin was a 1224mm wide, 1300mm long, 2524-T3, 1.6mm thick one-side clad sheet. Seven identical “Z-shaped” 7349-T76511 extruded stringers were adhesively bonded to the uncladded side of the skin of each panel with a stringer pitch of 185mm. The three investigated panels differed for the cross-sectional area of the bonded stringers: 89mm², 151mm² and 207mm² stringers were bonded, respectively, in the panel named A089, A151 and A207.

During the test a constant amplitude fatigue with a load ratio ($\sigma_{min}/\sigma_{max}$) $R = 0.1$ was applied to the skin through the clamping system. The FCP was driven by a merely tensile stretching of the panel thanks to the anti-bending device which prevented the out-of plane deflection of the stiffened panel induced by the load-path eccentricity inherent to the one-side bonded stringers.

1.6.2. Test – analytical result correlation

The predicted β for the all the tested panels (Figure 3.27, Figure 3.28, Figure 3.29) provide a good agreement with the experimental data, showing the reliability of the crack-bridging model to describe the fatigue crack propagation through the skin above bonded stiffeners.

Furthermore, the test-analytical results correlation suggests that the FCP above the bonded stiffener is coupled with the simultaneous fatigue growth of a delamination at the adhesive interface around the advancing crack tip. This conclusion is in accordance with the Alderliesten model [24] describing the delamination growth at the adhesive interface of fibre metal laminates around the through crack based on a Paris type relation, i.e. the delamination extension as a function of the applied load cycles (i.e. $\text{del} = f(N)$).

Smaller delaminations in comparison with the A207 panel are expected above the stringer of the A151 (“del d=0 - 15mm”) and A089 (“del d=0 - 10mm”) panels as a consequence of the shorter FCP through the skin above the stringer as shown in Figure 3.30.

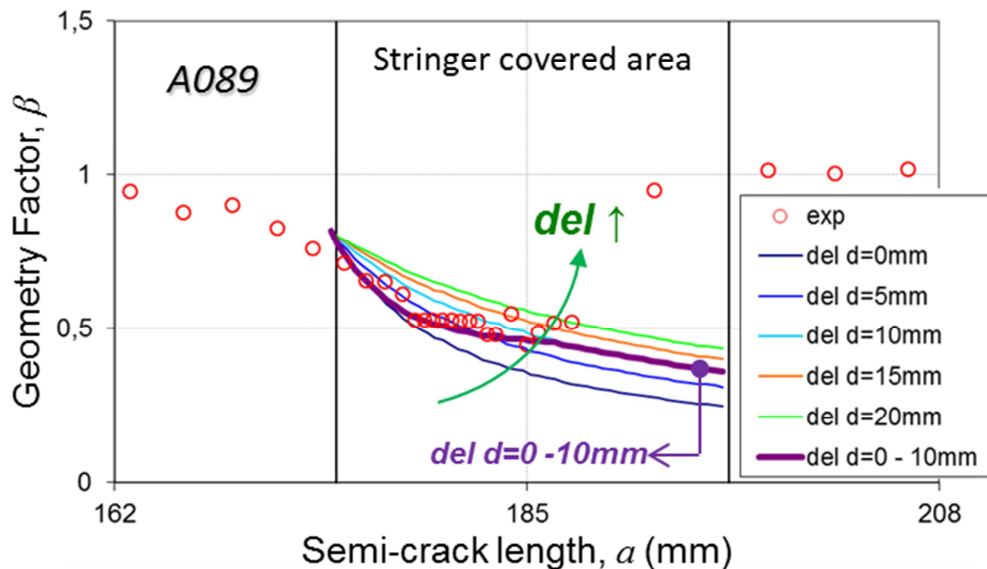


Figure 3.27. Geometrical factor predicted for several degrees of delamination extension d and experimental data of the A089 panel.

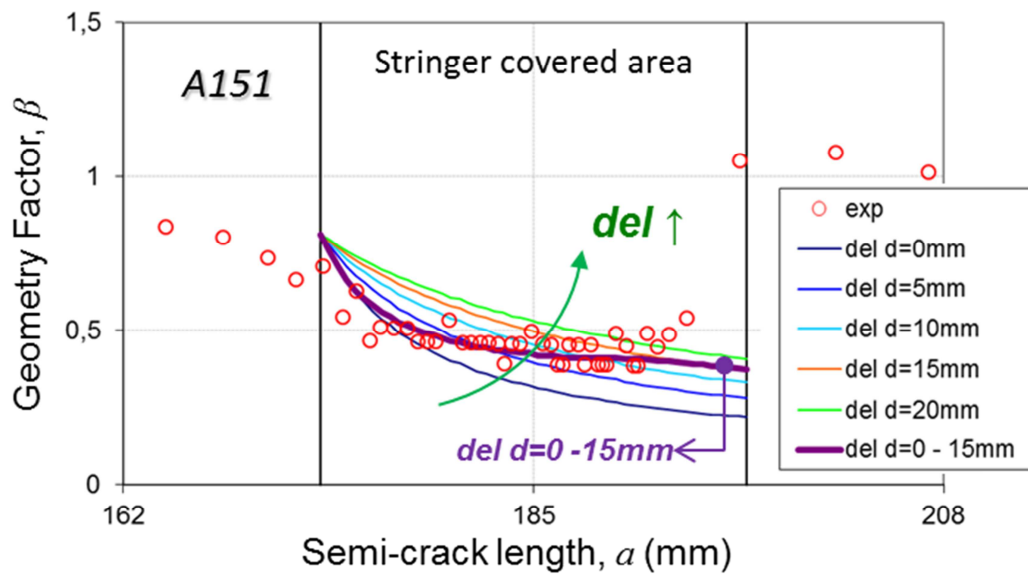


Figure 3.28. Geometrical factor predicted for several degrees of delamination extension d and experimental data of the A151 panel.

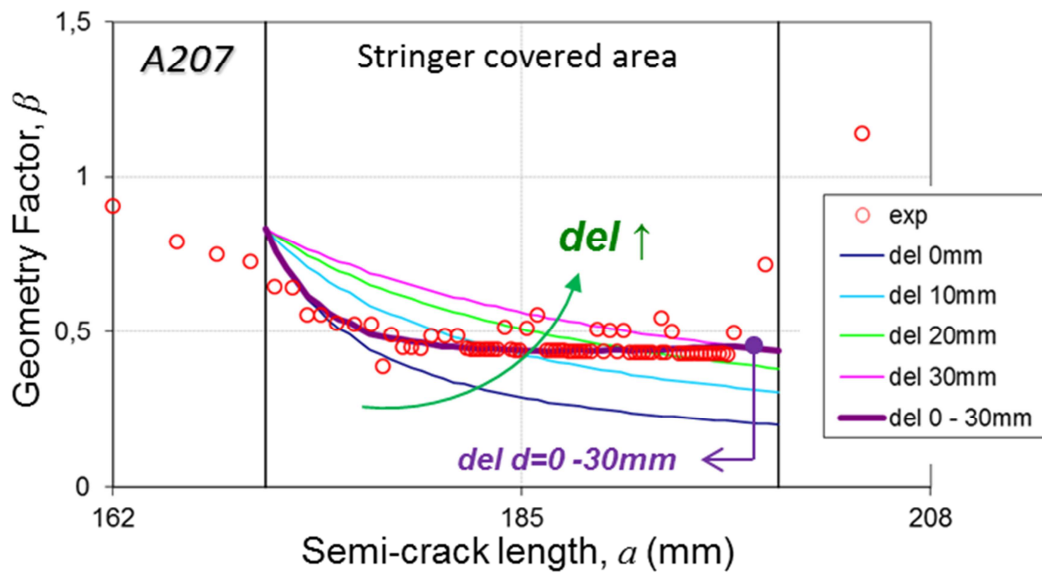


Figure 3.29. Geometrical factor predicted for several degrees of delamination extension d and experimental data of the A207 panel.

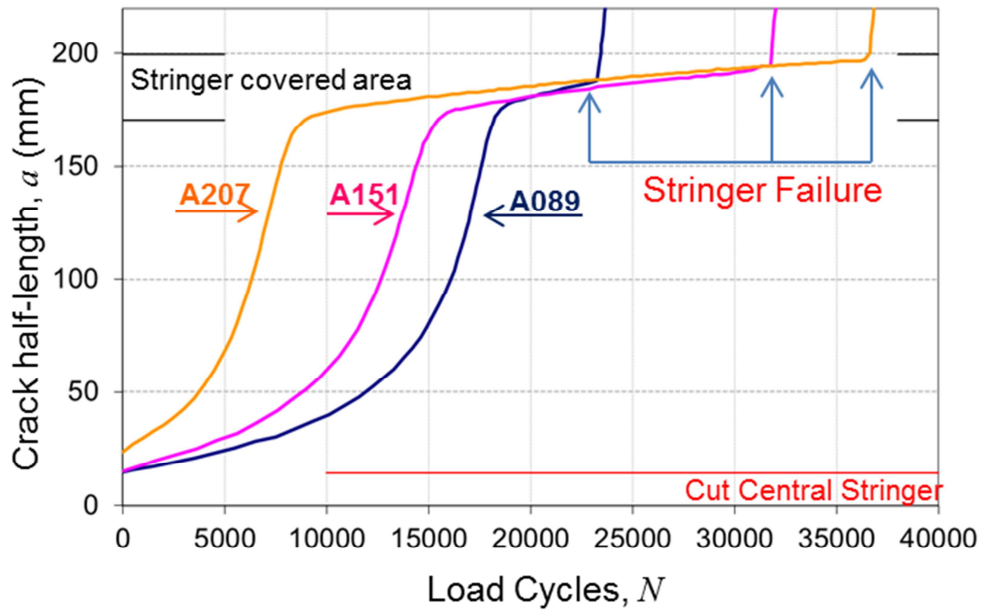


Figure 3.30. Experimental fatigue crack propagation within the first two stringer bays over the central broken stringer.

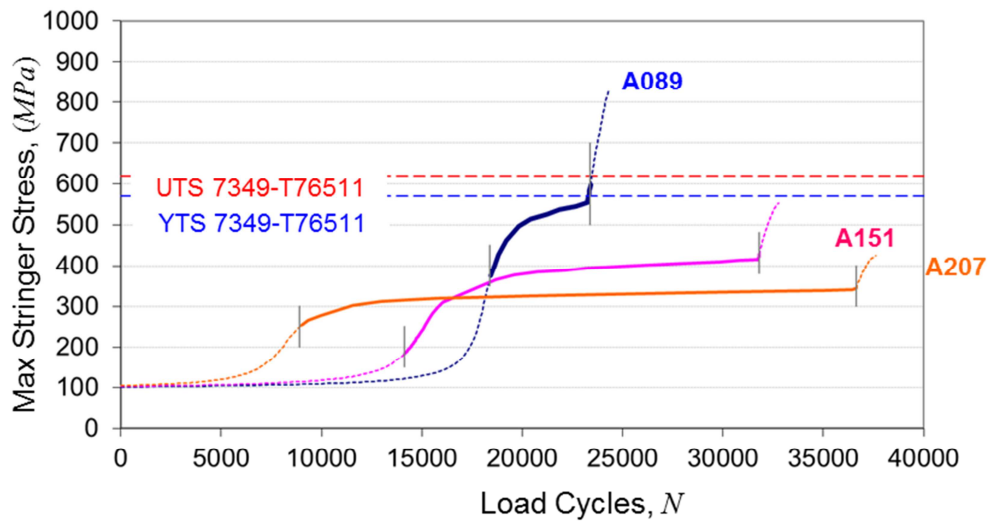


Figure 3.31. Maximum predicted tensile stress acting in the stringer foot as a function of the applied cycle loads during the FCP.

1.1.1. Stiffeners Failure

A sudden increase of the experimental geometry factor while the skin crack is still in the stringer covered area, not captured by the crack-bridging model, is shown in Figure 3.27, Figure 3.28 and Figure 3.29.

The failure of the bonded stringer, overloaded when the skin crack tip propagates above it, is the driver of the observed phenomenon. In Figure 3.30 the experimental FCP life of the three investigated panel are reported: as a consequence of the stringer failure, the crack-bridging mechanism cannot be exerted by the failed stringer which, on the contrary, promotes the FCP by means of traction forces exerted to the crack surfaces, thus increasing the crack propagation rates.

As a consequence of the significant effect of the stringer failure on the FCP performances, the development of a reliable stringer failure criterion is fundamental in order to exploit the FCP period under the bonded stringers. For this reason, it is important to get a deep insight into the mechanisms which drive the bonded stringer to failure when a skin crack fatigue propagates through the bonded stiffened panel.

The maximum stress acting in the stringer foot during the skin crack fatigue propagation was calculated LEAF and plotted in Figure 3.31 as a function of the number of applied load cycles N for the three investigated panels. The vertical lines, which intercept the predicted curves, represent the stringer edges reached after a different number of load cycles for the three panels. The stringer starts experiencing the most significant stresses when the skin crack enters in the stringer covered area. These stresses increase for thinner stringers. In accordance with a low-cycle fatigue failure mechanism, lower are the stresses applied at the stringer foot and longer is the fatigue life of the stringer itself. This behaviour determines the precocious failure of the thin stringer in the A089 panel after a few thousands of load cycles with the skin crack underneath it, and the long FCP period above the intact thick stringer in the A207 panel.

Table 3.7 reports the experimentally recorded FCP periods taken by the skin crack to reach the first stringer edge ("First bay" in Table 3.7) and to propagate through the stringer covered area ("Above" 1st Stringer in Table 3.7) for the three investigated panels.

The reported FCP periods are expressed as percentage of the total FCP period taken by the skin crack, for each panel, to pass beyond the stringer.

Specimen	FCP Performances	
	First Bay (Between the Stringers) [%]	Above the 1 st Stringer [%]
A089	78.7	21.3
A151	44.5	55.5
A207	24.3	75.7

Table 3.7. FCP periods recorded during the experimental tests taken to reach the first stringer edge (“bay”) and to propagate under the stringer (“under”). FCP periods expressed as percentage of the total period to pass beyond the first stringer.

It is interesting that in the case of a stringer with a cross-sectional of 207mm 75% of the total FCP was spent underneath the stringer. This period is completely neglected in the current sizing of the bonded stiffened panels.

References

- [1] C.C. Jr. Poe. *Fatigue crack propagation in stiffened panels*, Damage Tolerance in Aircraft Structures, ASTM STP 486, pp 79-97, 1971.
- [2] T. Swift. *The application of fracture mechanics in the development of the DC-10 fuselage*, In *Fracture Mechanics of Aircraft Structures*, AGARD-AG-176, H.Liebowitz, Ed. AGARD Advisory Group for Aerospace Research and Development, pp 226- 287, 1974.
- [3] M. Pacchione and J. Telgkamp. *Challenges of the metallic fuselage*, in Proceedings of the 25th International Congress of Aeronautical Sciences, 2006.
- [4] J. Schijve. *Crack stoppers and ARALL laminates*, TU Delft Tech. Report LR-589, 1989.
- [5] J.S. Przemieniecki. *Theory of matrix structural analysis*, Dover Publishing, 1985
- [6] M. Heinimann, R. Bucci, M. Kulak, M. Garratt. *Improving the damage tolerance of aircraft structures through the use of selective reinforcement*, in Proceedings of the 23th Symposium of the International Committee on Aeronautical Fatigue, 2005.
- [7] D. Broek, *The Practical Use of Fracture Mechanics*, Springer, 1989.
- [8] X. Zhang, M. Boscolo, D. Figueroa-Gordon, G. Allegri, P.E. Irving. *Fail-safe design of integral metallic aircraft structures reinforced by bonded crack retarders*, *Eng Fract Mech*, 76, (1), pp 114-133, 2009.
- [9] X. Zhang and Y. Li. *Damage tolerance and fire safety of welded aircraft wing panels*, *AIAA J*, 43, (7), 1613-1623, 2005.
- [10] I. Meneghin, M. Pacchione, P. Veermer. *Investigation on the design of bonded structures for increased damage tolerance*, in Proceedings of the 25th Symposium of the International Committee on Aeronautical Fatigue, 2009.
- [11] C.C. Jr. Poe. *Stress intensity factor for a cracked sheet with riveted and uniformly spaced stringers*, NASA TR-R-358, 1971.
- [12] C.C. Jr. Poe, *The Effect of Broken Stringers on the Stress Intensity Factor for a Uniformly Stiffened Sheet Containing a Crack*, NASA TM X-71947, 1973.
- [13] T. Swift. *Fail-Safe design requirements and features, regulatory requirements*, AIAA Paper 2003-2783, 2003.
- [14] T. Swift. *Damage tolerance capability*, *Int J Fatigue*, 16, (1), pp 75-94, 1994.

- [15] H.J. Schmidt. and B, Schmidt-Brandecker. *Damage tolerance design and analysis of current and future aircraft structure*, in AIAA/ICAS international air and space symposium and exposition, 2003.
- [16] Anonymous. *Damage tolerance and fatigue evaluation of structure*, FAR Part 25 Sect. 571, Federal Aviation Administration, 1997.
- [17] Anonymous. *Damage tolerance and fatigue evaluation of structure*, FAR 25.571-1D, Federal Aviation Administration, 2011.
- [18] U. Zerbst, M. Heinemann, C. Dalle Donne, D. Steglich. *Fracture and damage mechanics modelling of thin-walled structures - An overview*, Engineering Fracture Mechanics, Volume 76, Issue1, pp 5-43, 2009.
- [19] T. Swift. *Fracture Analysis of Adhesively Bonded Cracked Panels*, Journal of Engineering Materials and Technology, Vol. 100, pp 10-15, 1978.
- [20] G. Molinari, I. Meneghin, M. Melega, E. Troiani. *Parametric damage tolerance design of metallic aeronautical stiffened panels*, The Aeronautical Journal, Vol. 116, 2012.
- [21] L.R.F. Rose. *Theoretical analysis of crack patching*, Bonded repair of aircraft structures, Baker A.A. and Jones R. Ed., Chap. 5, pp. 77-105, 1988.
- [22] P.F. Joseph and F. Erdogan, *Plates and shells containing a surface crack under general loading conditions*, NASA Contractor Report 178328, 1987.
- [23] J-H Kim, S-G Hong, S-B Lee. *Evaluation of stress intensity factor for a partially patched crack using an approximate weight function*, KSME International Journal, Vol. 17, (11), pp. 1659-1664, 2003.
- [24] C.D. Rans and R. Alderliesten. *Damage tolerance philosophy for bonded aircraft structures*, in Proceedings of the 25th Symposium of the International Committee on Aeronautical Fatigue, 2009.

4. Fatigue crack propagation pressurized fuselages

In the previous chapter a parametrical study was performed on generic stiffened panels subjected to uniaxial loading. Although, were considered geometries and materials typical of fuselage constructions, the obtained results are completely general and could be also applied to wing stiffened panels. In this chapter will be discussed about the peculiarities which drive the FCP on pressurized fuselage (metallic) stiffened panels. The effect of the biaxial skin stress state, as well as the stiffeners' secondary bending and the crack bulging phenomenon will be discussed.

4.1. Biaxial skin stress effect

4.1.1. Introduction

The effect of a biaxial stress state on the SIF of a flat panel was already being studied in the past especially for unstiffened flat panels [1][2][3][4][5]. Both theoretically and experimentally was found that in the presence of a tensile stress applied parallel to the crack ($\sigma_{||} > 0$) the SIF is reduced leading to lower FCPR than the uniaxial loading condition, whereas under a compressive stress applied parallel to the crack ($\sigma_{||} < 0$) the SIF is increased (leading to higher FCPR). This behaviour can simply be explained with the Poisson's effect whereby the strain orthogonal to the crack ε_{\perp} is reduced proportionally to the Poisson's ratio as expressed by the well-known equation

$$\varepsilon_{\perp} = \frac{1}{E} (\sigma_{\perp} - \nu \cdot \sigma_{||}) \quad (4.1)$$

Where E and ν are the Elastic modulus and the Poisson's ratio of the panel material, respectively. A reduced strain produces a reduced COD and thus a reduced SIF.

On the other hand, very few studies has been conducted on biaxial-loaded stiffened panels [6][7][8] founding that the SIF is always increased for both tensile and compressive parallel loads. This controversial results, at least for $\sigma_{||} > 0$, was explained by Ratwani [8]

as the consequence of the reduction on load transfer induced also by the Poisson's ratio which reduce the stress carried remotely by the stiffeners.

Against this conclusion, Dowrick and Cartwright [9] made a displacement compatibility analysis including the effect of the parallel stress into the original DCM equations, showing that the biaxial-stress ratio ($\chi = \sigma_{||} / \sigma_{\perp}$) have no influence on the SIF when the stiffeners are intact relieving, on the other hand, the detrimental effect of a broken stiffener.

The explanation of these so different conclusions was given also in [9], noting that in the experimental work of Swift [7] the SIF was expressed in terms of the *average* σ_{\perp} acting on the crack, which is dependent on the $\sigma_{||}$ applied to the stiffened panel. The controversial effect experimented by Swift is thus only apparent, and back to agree with [9] when the nominal σ_{\perp} is used to analyse the experimental data reported in [7]

The controversial results still remain, however, regarding the experimental work in [6] and the computational work in [8]. In this section the methodology used in [9] was implemented into LEAF producing the same results, including also an experimental validation (missing in [9]) using the FCP data obtained from a (1:1 scale) fuselage barrel test (courtesy of Airbus).

4.1.2. Extension of the Displacement Compatibility Method

Being the fuselage skin subjected to a biaxial stress state due to the pressurization load, the original DCM equations (see Chapt. 3, Sect. 2.1) must be modified to account the bi-dimensional skin displacement field. Invoking again the superposition principle it is possible to split the problem into two parts:

1. the effect of the skin stress acting orthogonally to the crack path σ_{\perp} (and so parallel to the stiffening elements);
2. the effect of the skin stress acting parallel to the crack path $\sigma_{||}$ (and so normal to the stiffening element).

The first part is the same already studied in Chapter 3, so it is sufficient to add the displacement equations the compliance coefficients related to the parallel stress $\sigma_{||}$. Recalling the equation (3.6) the new system to be solved is

$$(A_{ij}^{skin} + A_{ij}^{stiff} + A_{ij}^{joint}) \cdot Q_j = (B_i \cdot \sigma_{\perp} + B_{||i} \cdot \sigma_{||})^{skin} - B_i^{stiff} \cdot \sigma_s \quad (4.2)$$

where $B_{||i}$ are the additional skin compliance coefficients representing the orthogonal skin displacement per unit parallel stress.

The additional skin displacement due to the stress acting parallel to the crack ($\sigma_{||}$) can be calculated using the following complex function [9]

$$w(z) = u(z) + i \cdot v(z) = \frac{(1 + \nu)}{2E} \cdot \left(\frac{(1 - \nu)}{(1 + \nu)} \cdot z + \bar{z} \right) \cdot \sigma_{||} \quad (4.3)$$

Where:

- $w(z)$ is the complex skin displacement due to $\sigma_{||}$ and evaluated in $z = x + i \cdot y$;
- $u(z)$ is the (real) component of $w(z)$ parallel to the crack path evaluated in $z = x + i \cdot y$;
- $i \cdot v(z)$ is the (imaginary) component of $w(z)$ orthogonal to the crack path evaluated in $z = x + i \cdot y$;
- E and ν are the Elastic modulus and the Poisson's ratio of the skin material, respectively.

Considering just the effect of the main stiffeners placed orthogonally to the skin crack (stringers for circumferential cracks and frames for longitudinal cracks), as already been made in Chapter 3, the effect of $u(z)$ can be disregarded because it causes only the rigid translation of the stiffeners in the parallel direction, and so no reaction forces Q_j arise from it.

The only effect to account is, therefore, the orthogonal displacement $v(z)$ due to the parallel stress $\sigma_{||}$ which can be expressed extracting the imaginary parts from the (4.3)

$$v(z) = i \cdot w(z) = -\frac{\nu}{E} \cdot y \cdot \sigma_{||} \quad (4.4)$$

It can be noted that under a tensile parallel stress ($\sigma_{||} > 0$) the additional displacement is negative closing the crack ($v < 0$), whereas, under a compressive parallel stress ($\sigma_{||} < 0$) the crack is opened ($v > 0$), increasing the SIF in accordance with the literature.

Looking at the equation (4.4), the compliance coefficient to be added to the (4.2) can be easily obtained

$$B_{||i} = \frac{v(y_i)}{\sigma_{||}} = -\frac{v}{E} \cdot y_i \quad (4.5)$$

Substituting the (4.5) into the (4.2) and expressing the parallel stress in the terms of the biaxial stress ratio χ as $\sigma_{||} = \chi \cdot \sigma_{\perp}$, the new linear system to be solved become

$$(A_{ij}^{skin} + A_{ij}^{stiff} + A_{ij}^{joint}) \cdot Q_j = (B_i + B_{||i} \cdot \chi)^{skin} \cdot \sigma_{\perp} - B_i^{stiff} \cdot \sigma_s \quad (4.6)$$

4.1.3. Effect of biaxial stress on the stiffeners

Under a biaxial loading the remote stress acting on the stiffeners is no more $\sigma E_s/E$ as seen in Chapter 3. Due to the Poisson's effect, and considering again the stiffener like a beam stretched along its axis, the new strain compatibility condition between stiffeners and skin ($\varepsilon_s = \varepsilon$) far away from the crack becomes:

$$\frac{\sigma_s}{E_s} = \frac{1}{E} (\sigma_{\perp} - \nu \cdot \sigma_{||}) \quad (4.7)$$

And thus the remote stress applied on the stiffeners can be written as a function of the biaxial stress ratio χ

$$\sigma_s = \frac{E_s}{E} \cdot (\sigma_{\perp} - \nu \cdot \sigma_{||}) = \frac{E_s}{E} \cdot (1 - \nu \cdot \chi) \cdot \sigma_{\perp} \quad (4.8)$$

Substituting the (4.8) into the (4.2), and observing that for a uniaxial beam the displacement per unit of applied stress is simply $B_i^{stiff} = y_i/E_s$

$$\begin{aligned} & (A_{ij}^{skin} + A_{ij}^{stiff} + A_{ij}^{joint}) \cdot Q_j \\ &= \left(B_i^{skin} - \frac{\nu}{E} \cdot y_i \chi - \frac{y_i}{E} \cdot (1 - \nu \cdot \chi) \right) \cdot \sigma_{\perp} \end{aligned} \quad (4.9)$$

It is important to note that the alternating terms containing χ cancel each other, leaving the equation *unchanged* in respect with the original (3.6) and so independent by the biaxial-stress ratio χ . The results is different for a broken stiffener where the stress-free condition at the stiffener's cut requires that

$$\sigma_s = \frac{E_s}{E} \cdot (\sigma_{\perp} - \nu \cdot \sigma_{\parallel}) = \frac{E_s}{E} \cdot (1 - \nu \cdot \chi) \cdot \sigma_{\perp} = \sum_j Q_j \quad (4.10)$$

This condition also guarantee the equilibrium between the remote stress and the forces reacted by the broken stiffener. The (positive) detrimental concentrated forces (see the Chapt. 3 Sect. 2.2) are thus relieved by χ when it is positive (tension), reducing the SIF, and aggravated when it is negative (compression), increasing the SIF.

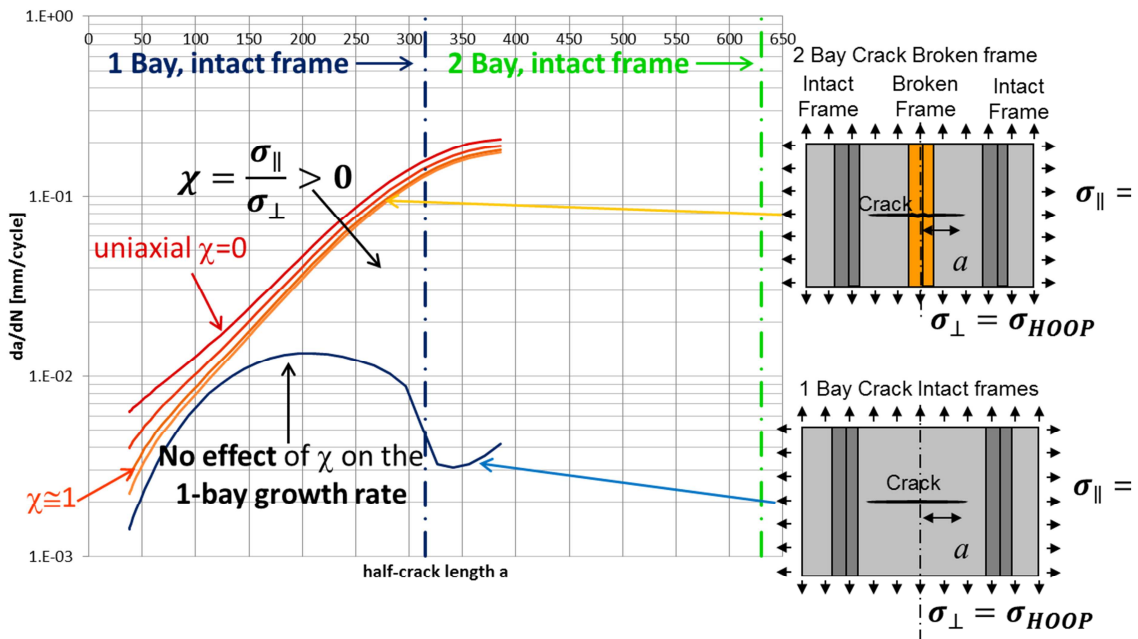


Figure 4.1. Effect of the biaxial stress ratio on the FCPR.

This behaviour is evidenced in Figure 4.1 where the FCPR for one-bay longitudinal cracks, propagating between intact frames, are compared with two-bay longitudinal cracks propagating above a broken frame for different values of χ . For longitudinal cracks the orthogonal stress is the hoop stress and the parallel stress is the longitudinal stress. The one-bay cracks are unaffected by χ (all the curves overlap) whereas the two-bay cracks show a strong dependence on χ in the very first stage of the crack growth (for short crack half-lengths). When the crack is far away from the frames, increasing χ the two-bay crack FCPR is reduced tending to the one-bay crack FCPR. In particular, for the panels in the fuselage crown where $\chi \approx 1$ the two-bay crack behaves very similarly to a one-bay crack. When the crack become longer, the divergence between one-bay and two-bay crack increases getting worst for the latter. This is because, for the same crack length, the two-bay crack is twice as far to the next intact frames in respect with the one-bay. Therefore, when the one-bay crack reach the next intact frame, slowing-down, the two-bay crack is still far away from intact frames so the FCPR grows steeply reaching the critical zone (see Chap. 2 Sect. 2.3.3).

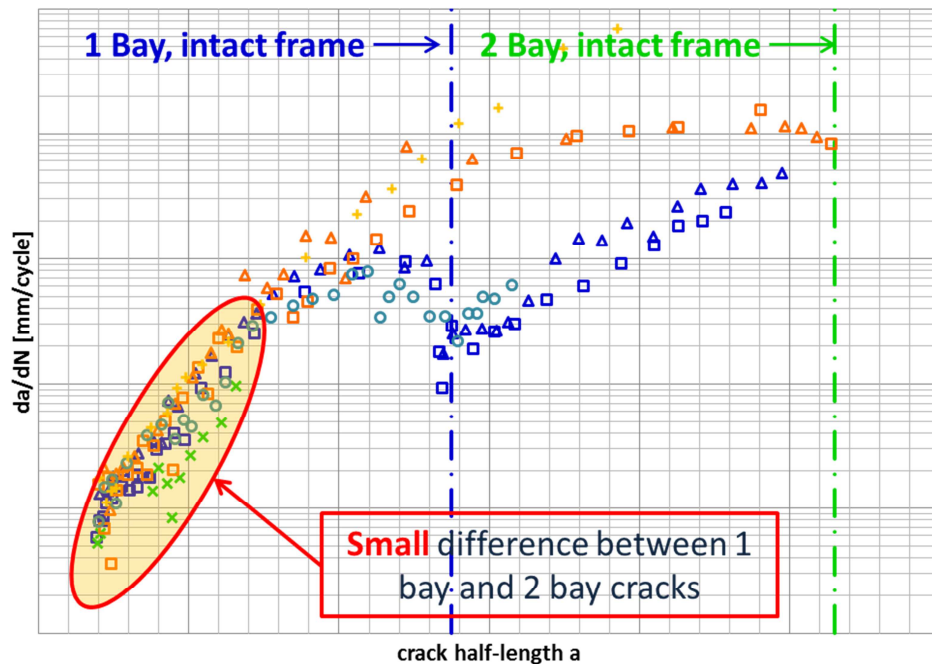


Figure 4.2. FCPR in the crown panels of a barrel test (1:1). Axis removed due to secrecy reasons.

These highly remarkable effects, especially the equivalence between one-bay and two-bay damages for short cracks, was evidenced in the FCPR data reported in Figure 4.2 obtained from a crown panels of a (1:1 scale) fuselage barrel. This demonstrate that χ has no influence on the crack behaviour when the stiffeners are intact, but heavily affect in a beneficial way a two-bay crack when it is positive for tensile parallel stresses. Should be moreover true, also if it was not investigated in this work, the detrimental effect of a compressive parallel stress applied remotely to the propagating crack.

4.2. Stiffeners' secondary bending effect

An important but controversial effect that could affect the fatigue crack propagation on a stiffened panel is the secondary bending due to the stiffeners eccentricity. As a skin crack propagates, the forces reacted by the stiffeners at the rivet/adhesive layer locations act at a distance z_0 from the neutral axis, as sketched in Figure 4.3, causing a bending stress which is superimposed to the stiffeners axial stress. This additional bending decreases the stiffeners' inner cap stress and increases both the stiffeners' outer cap and the adjacent skin stress. Obviously, an increased skin stress increases the SIF and, consequently, the crack growth rate.

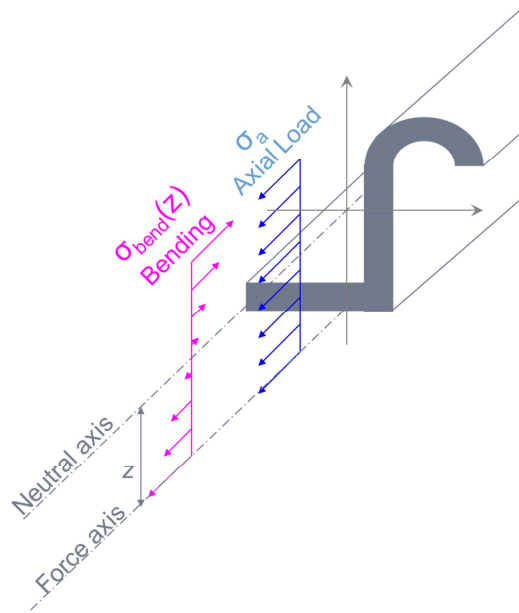


Figure 4.3. Effect of the stiffeners eccentricity.

The secondary bending effect is controversial because it is often disregarded [10] from the preliminary design of fuselage panels, whereas Tom Swift had repeatedly evidenced [11][12] the need to account it, especially dealing with the residual static strength of heavy stringers and frames which have high eccentricity.

Although this author agrees with the Swift opinion about the residual strength, there is no experimental evidence of the detrimental effect of the stiffeners bending at least during a one-bay or a two-bay crack propagation period.

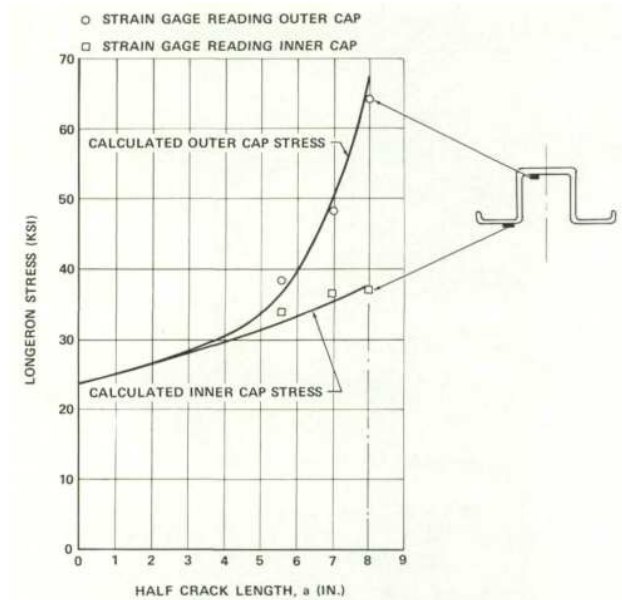


Figure 4.4. Stress in the next intact stringer during a 2-bay crack above central broken stringer, reported by [11].

The data presented by Swift about the stress level in the next intact stringer adjacent to a broken one, reported in Figure 4.4 and related to a circumferential two-bay crack propagating above a broken stringer (curved panel 16 ref. [11]), is comparable with experimental data obtained for the same damage scenario evolving in a seven-stringers flat panel with anti-bending device reported in Figure 4.5: the higher stress in the stringer outer cap is simply due to the high load transfer distributed locally on the stiffener cap close to the cracked skin, whereas the inner cap remains more or less at the same remote stress. The effect of the secondary bending appear to be evident only when the crack is well above the stringer where the stress in the inner cap start to decrease steeply (up to a quasi-compressive stress) while the inner cap stress is rising fast.

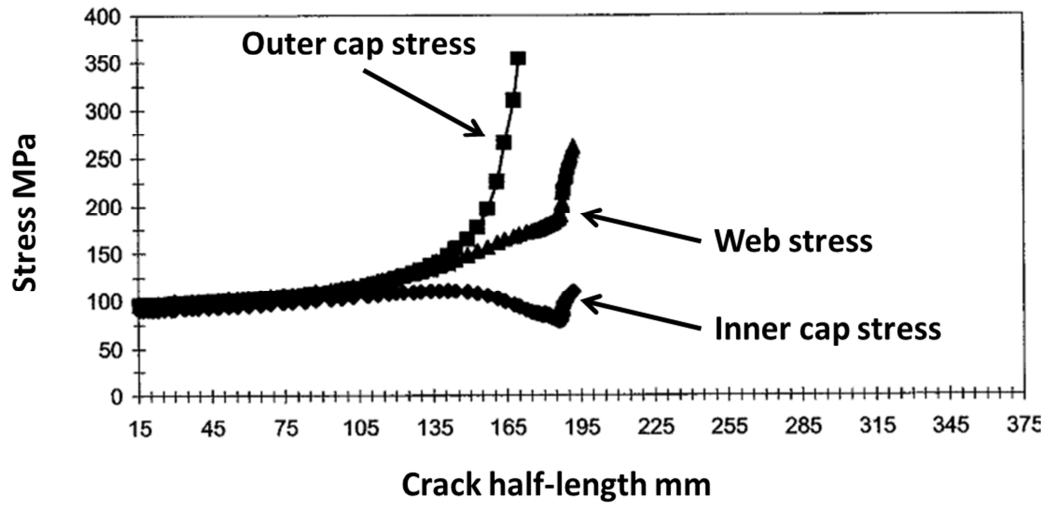


Figure 4.5. Stress in the next intact stringer during a 2-bay crack above central broken stringer, 7-stringer panel with anti-bending device.

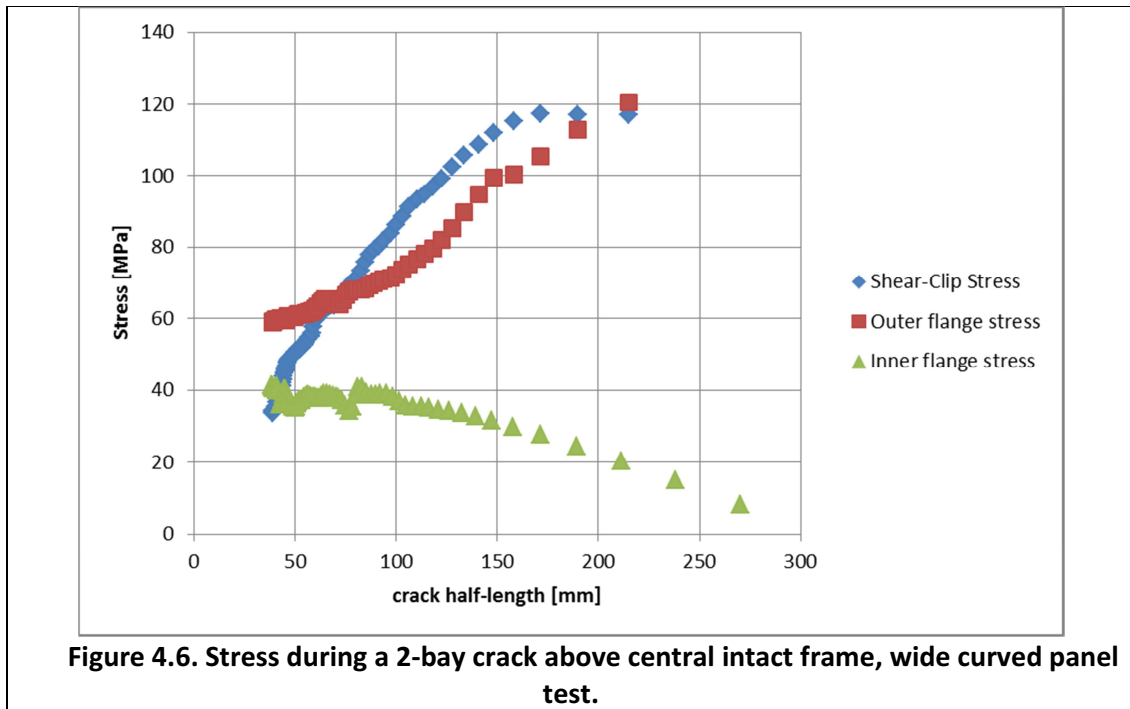


Figure 4.6. Stress during a 2-bay crack above central intact frame, wide curved panel test.

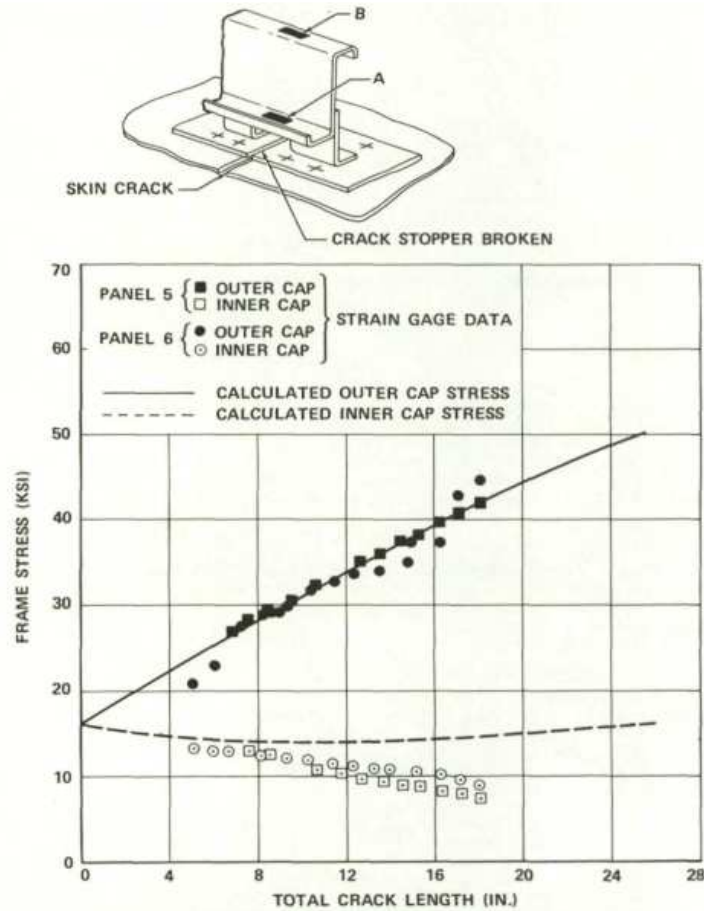


Figure 4.7. Stress in the intact frame during a 2-bay crack above intact frame, reported by [11].

Another evidence of the negligible effect of the stiffeners' secondary bending can be argued from the longitudinal two-bay crack propagation above an intact frame test performed on a wide curved panel, and reported in the Figure 4.5a and Figure 4.6b.

The former shows the stress versus the number of (constant amplitude) load cycles on the outer cap, the inner cap and the shear clip foot, measured on the intact frame centrally located above the propagating crack. The latter represent the same data expressed in term of the crack half-length. If compared with the data regarding a two-bay crack propagating above an intact frame (riveted on a broken titanium strap) presented in [11] and reported Figure 4.7, the similarity is clear. The very same result was obtained from several other wide curved shell tests not reported here for conciseness.

To avoid too conservative crack growth life predictions, for a one-bay or a two-bay crack propagation to neglect the secondary bending is thus recommended. On the other hand, for a residual strength analysis of the stiffened panel the secondary bending effect must be accounted for.

1. Modelling of the secondary bending effect

The choice to neglect the secondary bending effect during the crack propagation can be justified implementing into the DCM the bending formulation proposed by Swift [10]. Considering again the stiffener like a beam loaded along its axis, the additional stiffener displacement at the location (x_i, y_i) due to the bending stress, can be expressed (for an intact stiffener) as

$$v_i^{bend} = \frac{z_0}{EI_x} \sum_{k=1}^{k=i} M_k (y_k - y_{(k-1)}) \quad (4.11)$$

where:

- M_k moment applied at the location (x_k, y_k) .
- I_x stiffener's second moment of inertia along the x-axis (i.e. parallel to the crack path).
- y_k location of the k -th moment, and with $y_0=0$.

and with

The moment applied at each rivet/adhesive layer location derive from the correspondent reaction force applied at a distance z_0 from the stiffener neutral axis

$$M_k = z_0 \sum_{j=k}^{N_S} Q_j \quad (4.12)$$

where N_S is the number of concentrated forces chosen to represent the whole stiffener.

The Swift formulation assumes a stiffener with a constant axial cross-section shape with a constant neutral axis position (z_0), but can be easily extended to a generic changing shape considering appropriate z_0 and I_x at each k -th evaluation location.

Inserting the (4.12) into the (4.11), the stiffener displacement due to bending become

$$v_i^{bend} = \frac{z_0^2}{EI_x} \sum_{k=1}^{k=i} \sum_{j=k}^{N_S} Q_j (y_k - y_{(k-1)}) \quad (4.13)$$

The stiffener displacement is thus directly proportional to the square of z_0 and inversely proportional to the bending stiffness EI_x of the considered stiffening element.

From a displacement compatibility point of view the (4.13) is equivalent to a compliance matrix A^{bend}_{ij} to be summed to the axial compliance matrix A^{stiff}_{ij} already defined in the previous chapter, therefore, the total compliance of the stiffener is increased by the bending component resulting in an increased stiffener displacement under the same reaction force Q .

	A	I_x	Z_0	$1/(E A)$	$Z_0^2/(E I_x)$
Narrow	250	125000	45	5.5E-08	2.2E-07
Wide	450	750000	60	3.0E-08	6.6E-08
Ultrawide	630	1400000	76	2.2E-08	5.7E-08

Table 4.1. Geometries of typical fuselage frames (E=73000).

In Table 4.1 are reported geometrical cross-section data and the correspondent compliance coefficients for three frames typical for a narrow-body, a wide-body and an ultrawide-body aircraft. The total (axial plus bending) compliance for each configuration is higher than the simple axial compliance, and thus, the crack retarding effectiveness of all the three configurations is greatly reduced.

4.3. Crack bulging

Due to the fuselage loading conditions, longitudinal cracks are loaded by the hoop stress, whereas circumferential cracks are loaded by axial stresses resulting from the superposition of pressure and bending.

Due to the fuselage radius of curvature, pressurization affects heavily the SIF, and thus the crack propagation, inducing complex stress and displacement fields in which there is a strong coupling between membrane and bending stresses near the crack tip. This situation is sketched in Figure 4.8, where a pressure vessel of radius R and thickness t has been pressurised by the pressure p . In the presence of a crack of length $2a$, the pressure and coupling effects are forcing the crack edges to bulge out (Figure 4.9).

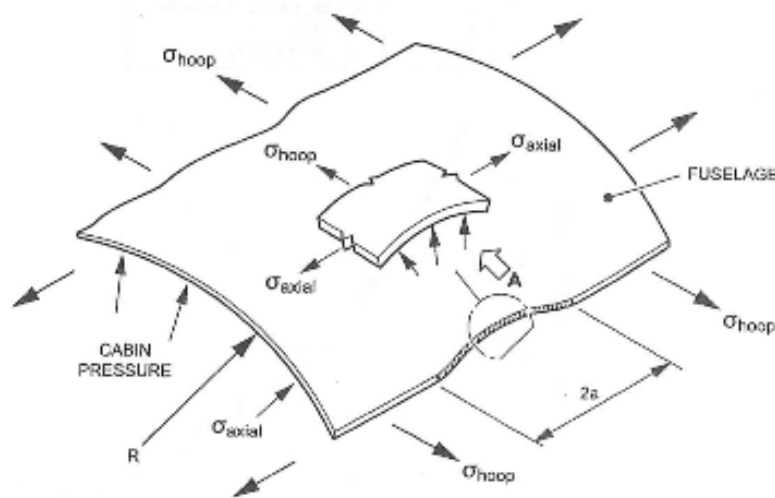


Figure 4.8. Membrane and bending stresses at the crack tip in a fuselage (cylindrical) panel.

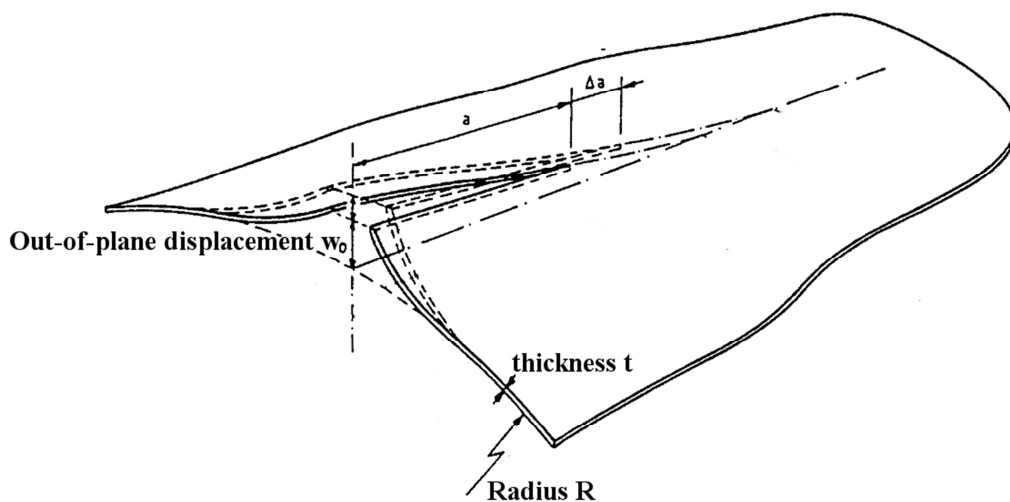


Figure 4.9. Out-of plane (bulging) displacement at the centre of the crack (w_0).

Experimentally was found [11][13][14] that crack bulging can significantly increase the stress-intensity factor (SIF) accelerating the crack growth rate and reducing the residual strength. This is commonly explained observing that, due to out-of-plane bulging sketched in Figure 4.8, the crack opening displacement (COD) is increased thus increasing the SIF.

An additional important effect is the stress stiffening caused by the longitudinal stress which can reduce the out-of-plane displacement of the skin as depicted in Figure 4.10

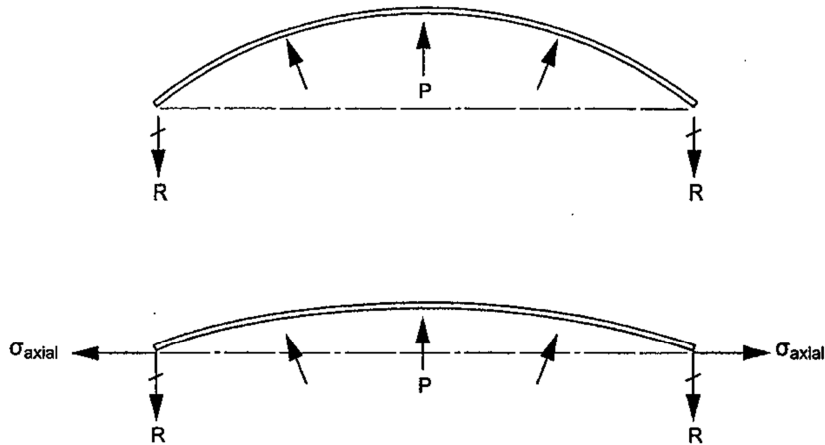


Figure 4.10. Effect of the axial load on the skin out-of-plane displacement.

Similarly to the stiffening elements effect to measure the magnitude of the bulging effect the bulging $\beta_{bulging}$ factor is defined as the ratio of the stress intensity factor of a curved shell (K_{curved}) to the stress-intensity factor of a flat panel (K_{flat}):

$$\beta_{bulging} = \frac{K_{curved}}{K_{flat}} \quad (4.14)$$

Several studies were made into the past to provide a direct formulation of $\beta_{bulging}$. The first equations were due to Peters and Kuhn [13] who proposed the simple formula

$$\beta_{bulging} = 1 + 4.6 \left(\frac{2a}{R} \right) \quad (4.15)$$

in which the bulging factor is linearly proportional to the crack length-to-fuselage radius ($2a/R$) by a constant of proportionality which experimentally was found to be 4.6. This expression resulted from a series of bursting strength tests made on capped unstiffened cylinders of 2024-T3 and 7075-T6 aluminium alloys containing slits (simulating cracks) of various lengths. From the (4.15), it is immediately evident how crack bulging has such a big effect on both FCP and RS, especially for longer cracks (in the order of the bay length): for example a fuselage of radius $R = 2000\text{mm}$ and bay length $L = 500\text{mm}$ with a crack length of $2a = 200\text{mm}$ (less than half the bay length) is affected by a bulging factor of 1.46, i.e. with a SIF that is 46% greater than the SIF in a flat plate under the same loading conditions.

Successively Kuhn [15] refined the analysis of the collected experimental data changing the proportionality coefficient to 5.0. Kuhn also noted that though this coefficient gives good experimental correlation with both the materials tested (2024-T3 and 7075-T6), it could not be applicable to other structural materials since the physical nature of phenomenon was unknown.

Starting from the experimental tests made by Peters and Kuhn, Anderson and Sullivan [14] made further investigations on the bursting strength of unstiffened cylinders at cryogenic temperature. They successfully applied the (4.15) to other materials changing the bulging coefficient, like titanium 5Al-2.5Sn, and concluding that the equation can be generalized as

$$\beta_{bulging} = 1 + C \left(\frac{2a}{R} \right) \quad (4.16)$$

founding also that C varies with the temperature. In Table 2 are summarized the coefficients for different materials at different temperatures resulted from the tests performed in [14].

Material/Temperature	20.4 K	77.6 K	Room
Al 2014-T6	2.86	3.46	6.51
Ti 5Al-2.5Sn	1.57	4.30	N/A
Al 2024-T3 & Al 7075-T6 (from ref. [13])	N/A	N/A	9.5

Table 2. Bulging coefficients for different materials at different temperatures, ref. [14].

The equation (4.16) was successively adopted by Swift [11] for the DT design of the DC-10 in the early 1967. He found, on the basis of an experimental comparison between curved and flat panels, that the coefficient proposed by Kuhn ($C=5.0$) was in good agreement with tests. However, he also found that the (4.16) is strictly valid when the crack tip is at least in the middle of the bay, i.e. far away from the stiffeners. This is because stiffeners affect the complex membrane-bending crack tip stress restraining also the out-of-plane crack bulging, especially when the crack is near the stiffeners. The contribution of frames and stringers on crack bulging phenomenon will be discussed hereinafter.

Although the Swift-Kuhn equation should be applicable only to geometries similar to a DC-10, i.e. wide-bodies aircraft (such as Airbus A330/340 and Boeing B767), this value is currently widely used in the common fuselage design practice.

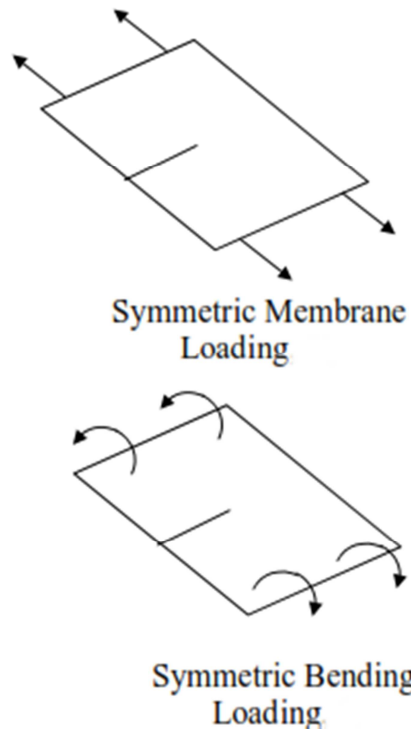


Figure 4.11. Membrane and bending loading of a cracked shell.

The first (approximated) theoretical approach, using the LFM and the linear shallow shell theory [16], to describe the crack behaviour in pressurized cylinder was developed by Folias [17][18], between the 1965 and 1967, on a longitudinal crack and a circumferential crack subjected to internal pressure and bending acting on the crack edges as depicted in Figure 4.8. The membrane “bulging factor” obtained by Folias for longitudinal and circumferential cracks were

$$\beta_{bulging}^{long} = 1 + \frac{5\pi\lambda^2}{64} \quad (4.17)$$

and

$$\beta_{bulging}^{circ} = 1 + \frac{\pi\lambda^2}{64} \quad (4.18)$$

, respectively; where λ is the shell curvature parameter defined as

$$\lambda = \sqrt[4]{12(1-\nu^2)} \frac{a}{\sqrt{Rt}} \quad (4.19)$$

Both the reported formulas are, however, limited for $\lambda < 1$ (i.e. for short cracks length and/or high shell radiuses) due to the approximation employed by Folias to resolve the complicated singular equations involved in the problem 27. It can be highlighted as the bulging factor for *circumferential cracks is one fifth of the bulging factor for longitudinal cracks* under the same loading conditions. Therefore, the equations (4.17) and (4.18) indicate that the bulging effect for circumferential cracks can be considered less critical than longitudinal cracks in terms of DT design. In fact, the effect of the circumferential crack bulging is commonly disregarded in practice.

This theoretical work was further developed in a brief time period by Copley and Summers [22] and successively by Erdogan et.al [20][21], between the 1968 and 1973, extending the analytical solutions up to $\lambda \cong 10$. In Figure 4.12 are reported the membrane (β_m), bending (β_b) and the total ($\beta_m + \beta_b$) bulging factor a function of λ for a longitudinal crack. The most important results obtained from these analyses were the direct expression of the local crack tip stress as a function of the curvature parameter λ , highlighting the strong coupling between the membrane and bending stresses. It is important to note that in all these theoretical essays the effect of the longitudinal stress σ_x is not considered, because in the linear shallow-shell theory the effect of this stress can only be superimposed at the infinity in the final solution. Therefore the results in Figure 4.12, should be intended to be valid only for an infinite cylinders without ending caps, i.e. for $\chi=0$.

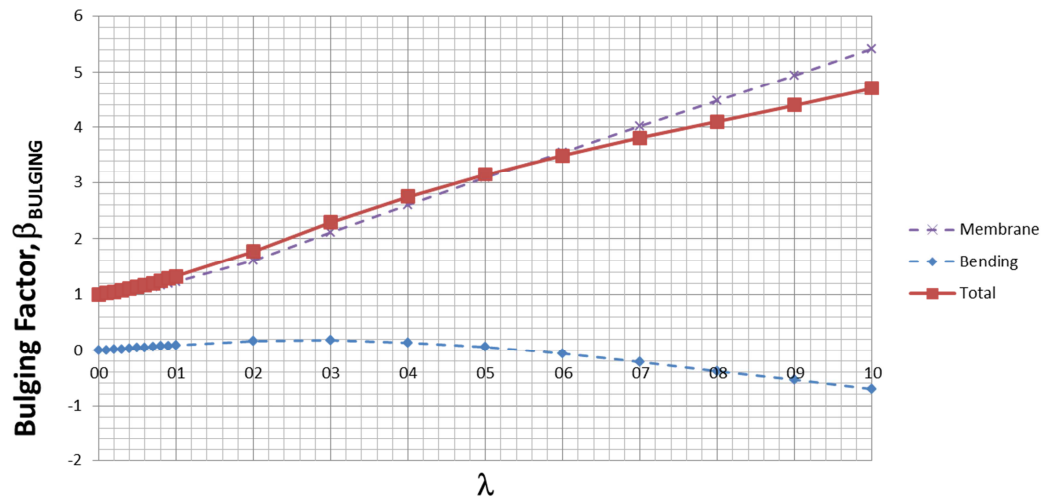


Figure 4.12. Membrane and bending bulging factor, Ref. [21][22].

Despite its importance to understand the bulging phenomenon, the theoretical approach was moved in the background spending, on the other hand, many efforts for the finite element modelling of bulging phenomenon in pressurized fuselages. A non-linear methodology was carried out by Riks [23] to calculate the strain energy release rate for a cracked cylinder subjected to the boiler stresses (i.e. $\chi = 0.5$, see chapt. 2). His analysis pointed out the non-linear behaviour of the out-of-plane displacement at the centre of the crack (w_0 , see Figure 4.9) with the applied internal pressure, founding that both $\beta_{bulging}$ and w_0 decrease increasing the pressure, as sketched in Figure 4.13. Another important aspect highlighted by Riks was that the non-linear FEM results were significantly smaller than linear ones. Similar observations were made by Ansell [24] who also computes the bending component of the SIF concluding that it could be neglected since is much smaller than the membrane stress components of the SIF.

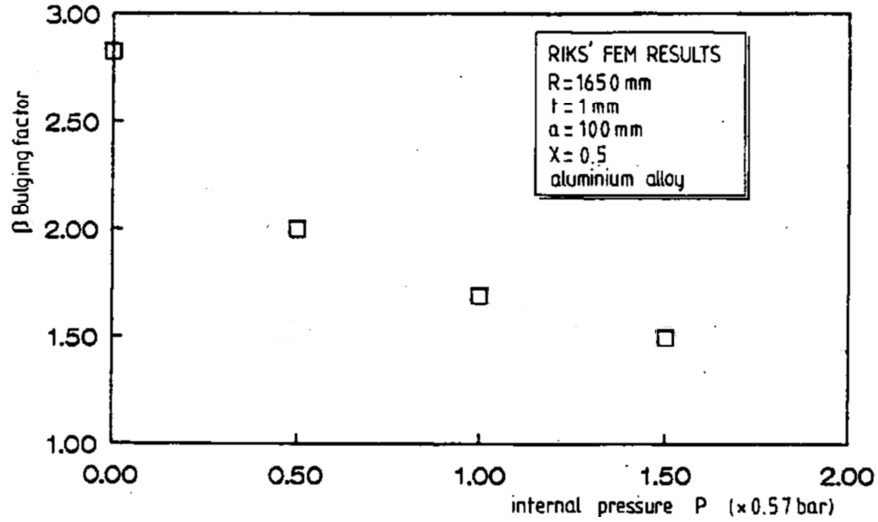


Figure 4.13. Effect of the pressure on the crack bulging factor.

On the basis of the finite element analysis done by Riks [23] and Ansell [24], Chen [25] proposed a semi-empirical formulation for longitudinal cracks propagating in unstiffened cylinders calibrated also by an experimental campaign made on both unstiffened pressurized cylinders and curved panels under a biaxial-stress ratio of $\chi=0$ and $\chi=0.24$.

Using an energy balance method, Chen expressed the $\beta_{bulging}$ as a function of the increment of the out-of-plane deformation (at the centre of the crack) dw_0 due to the crack extension da .

$$\beta_{bulging}^{long} = \sqrt{1 + \frac{5}{3} \frac{E t a}{p \pi R^2} \frac{dw_0}{da}} \quad (4.20)$$

Fitting experimental and FEM results, Chen derived the following equation for dw_0/da :

$$\frac{dw_0}{da} = \frac{0.316}{\sqrt{1 + 18\chi}} \tanh\left(0.06 \frac{R}{t} \sqrt{\frac{p a}{E t}}\right) \quad (4.21)$$

Finally, substituting the (4.21) into the (4.20)

$$\beta_{bulging}^{long} = \sqrt{1 + \frac{5}{3} \frac{E t a}{p \pi R^2} \frac{0.316}{\sqrt{1 + 18\chi}} \tanh\left(0.06 \frac{R}{t} \sqrt{\frac{p a}{E t}}\right)} \quad (4.22)$$

founding that $\beta_{bulging}$ is strongly affected by the biaxial stress ratio χ in non-linear way. The above equation agrees well with the Swift-Kuhn for wide-body geometries like the DC-10, as shown in Figure 4.14. This is because the (4.22) is often used instead of the (4.16), being more general and physically correct.

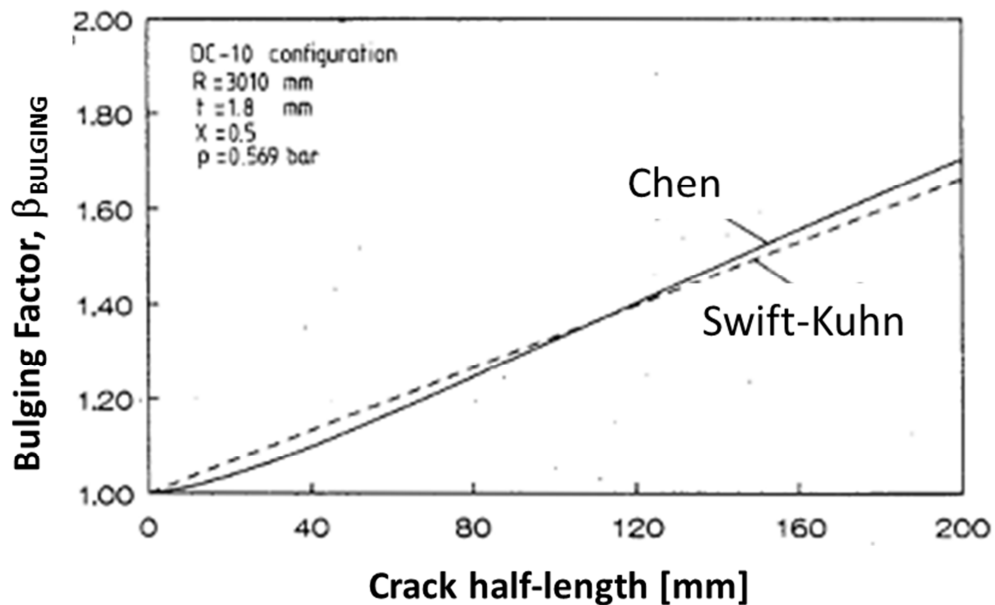


Figure 4.14. Comparison between Chen and Swift-Kuhn formula. Ref. [25].

Chen concludes that LEFM theories cannot be useful in practice because the bulging factor is driven by huge nonlinear effects, and so can be studied only by means of experiments or non-linear FE modelling.

It should be noted that, in spite of the usual interpretation of the experimental and numerical data, there is an arguments against the direct correlation between the so-called bulging effect and the crack bulging out-of-plane deformation: Increasing the pressure the bulging correction factor decrease, whereas the out-of-plane displacement increase (as reported in [25] and sketched in Figure 4.15).

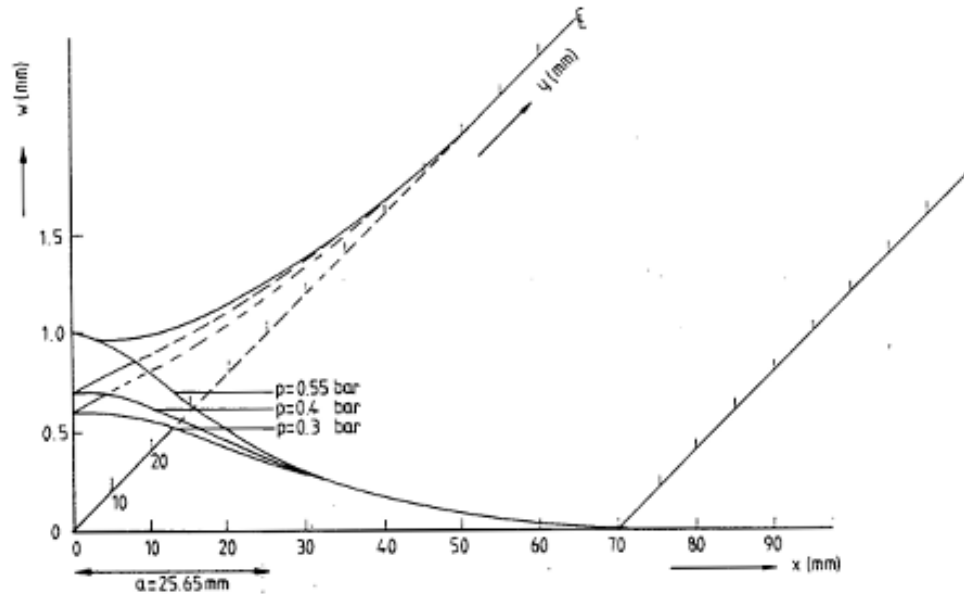


Figure 4.15. Effect of the pressure on the skin out-of-plane displacement at the crack centre (w_0).

Starting from the first argument, is not clear to this author why if both w_0 and dw_0/da , which should drive the bugling effect, are increasing function of the pressure p whereas the bulging factor itself decreases with the pressure. This point can be cleared looking at the extensive parametrical FEM analysis conducted by Young *et.al.* [26] on unstiffened pressurized cylinders. In that work the effect of $\beta_{bulging}$ is related to the unique parameter λ/η , where

$$\eta = \sqrt{\frac{\sigma_{hoop} R}{E t} \left(\sqrt[4]{12 \cdot (1 - \nu^2)} \right)} \quad (4.23)$$

Recalling that σ_{hoop} is the far field circumferential stress deriving by the pressurization (pR/t). η drives the non-linear behaviour of $\beta_{bulging}$ with σ_{hoop} , which Chen attributes directly to the pressure p . Although Young completely agrees with the statements on the very limited capability of the LFM approach to catch the bulging phenomenon, he pointed out insistently the evidence of the strong coupling between membrane and bending stresses as already evidenced in the theoretical essay by Folias, Copley and Erdogan.

Moreover, he found that the Chen's formula is in good agreement with his numerical results only when the bulging effect is dominated by the membrane stresses, found to be for $\eta > 2$. Comparing the theoretical results in Figure 4.12 with the (4.22) for $\eta \cong 2$ and $\chi = 0$ a surprisingly correspondence is found as depicted in Figure 4.16. Obviously for different (higher) values of η differences arise, but it is evident due the non-linearity of the problem. Being the linear solution valid only for small out-of-plane displacement, and together with the consideration made by Young using the η parameter, the out-of plane bulging could not be the cause of the aggravated SIF but just an evident effect. Recalling that the (4.22) derive from energetic consideration, the good agreement between the Chen's equation and the observations (FE models and experiments) can be justified considering the out-of-plane deformation as a good choice to measure the energy release rate. But as a drawback, could not be such a good choice to understand the real phenomena involved.

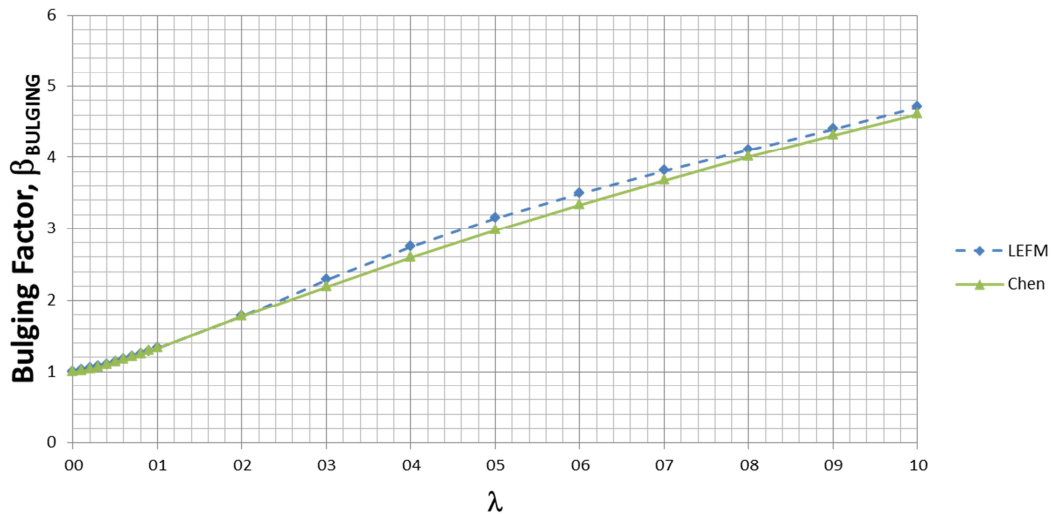


Figure 4.16. Comparison between LEFM bulging factor and Chen's formula, $\chi=0$ and $\eta \cong 2$.

Moreover, this demonstrates that even though LEFM approach is limited it could be very useful to investigate the bulging mechanism, helping to get insight the physics of the phenomenon. Further investigations are thus suggested by this author in order to see if it is possible to include the non-linear effects due to the circumferential and longitudinal loads, maybe adopting the non-linear shallow shell theory.

References

- [1] S.R. Joshi and J. Schewchuk. *Fatigue crack propagation in a biaxial-stress field*, Experimental Mechanics, Vol. 10, (12),pp. 529-533, 1970.
- [2] H. Wilson and D. J. White. *Cruciform specimens for biaxial fatigue tests: an investigation using finite element analysis and photo-elastic coating techniques*, Journal of Strain Analysis, Vol. 6, (7), pp. 27-37, 1971.
- [3] J. J. Kibler and R. Roberts. *The effect of biaxial stresses on fatigue and fracture*, Transactions of the ASME Journal of Engineering for Industry, Vol 70, pp. 727-734, 1970.
- [4] N. J. Adams. *Some comments on the effect of biaxial stress on fatigue crack growth and fracture*, Engineering Fracture Mechanics, Vol. 3, pp. 983-991, 1973.
- [5] O. Keiji, O. Kiyosugu, O. Yoshiji. *Fatigue crack growth under biaxial loading*, International Journal of Fracture, Vol. 10, pp. 609-610, 1974.
- [6] E. J. Beck. *Fatigue flaw growth behavior in stiffened and unstiffened panels' loaded in biaxial tension*. NASA CR-128904, 1973.
- [7] T. Swift. *The effects of fastener flexibility and stiffener geometry on the stress intensity in stiffened cracked sheet*, Proceedings of the International Conference of Fracture Mechanics, pp. 389-404, 1974.
- [8] M.M. Ratwani and D.P. Wilhem, *Influence of the biaxial loading on analysis of cracked stiffened panels*, Engineering Fracture Mechanics, Vol. 11, pp. 585-593, 1979.
- [9] G. Dowrick and D.J. Cartwright. *Biaxial stress effects in a reinforced cracked sheet*, International Journal of Strain Analysis, Vol. 19, pp. 61-69, 1984.
- [10] T. Swift. *Fracture Analysis of stiffened structures*, Damage Tolerance of Metallic Structures: analysis Methods and Applications, ASTM STP 842, pp 69-107, 1984.
- [11] T. Swift. *The application of fracture mechanics in the development of the DC-10 fuselage*, In *Fracture Mechanics of Aircraft Structures*, AGARD-AG-176, H.Liebowitz, Ed. AGARD Advisory Group for Aerospace Research and Development, pp 226- 287, 1974.
- [12] T. Swift and D.Y. Wang. *Damage Tolerant Design – Analysis Methods and Test Verification of Fuselage Structures*, Air force Conference on Fatigue and Fracture of Aircraft Structures and Materials, AFFDL-TR-70-144, 1969.

- [13] R.W. Peters and P. Kuhn. *Bursting Strength of Unstiffened Pressure Cylinders with Slits*, NACA TN-3993, 1957.
- [14] R.B. Anderson and T.L. Sullivan. *Fracture Mechanics of Through-Cracked Cylindrical Pressure Vessels*, NASA TN D-3252, 1966
- [15] P. Kuhn. *Notch Effects on Fatigue and Static Strength*, Presented at the Symposium on Aeronautical Fatigue Sponsored by the International Committee on Aeronautical Fatigue (ICAF) and the Structures and Materials Panel of the Advisory Group for Aeronautical Research and Development (AGARD), 1963.
- [16] Shallow shell
- [17] E.S. Folias. *An axial crack in a pressurized cylindrical shell*, International Journal of Fracture Mechanics, Vol. 1 , pp. 104-113, 1965.
- [18] E.S. Folias. *A Circumferential Crack in a Pressurized Cylindrical Shell*, International Journal of Fracture Mechanics, Vol. 1 , pp. 1-22, 1967.
- [19] E.S. Folias. *A Finite Line Crack in a Pressurized Spherical Shell*, International Journal of Fracture Mechanics, Vol. 1, pp. 20-46, 1965.
- [20] F. Erdogan and J.J. Kibler. *Cylindrical and Spherical Shells with Cracks*, International Journal of Fracture Mechanics, Vol. 5, pp. 229-237, 1969.
- [21] F. Erdogan. *Crack problems in cylindrical and spherical shells*, NASA CR-145066, 1976.
- [22] L.G. Copley and J.L. Sanders Jr. *A longitudinal Crack in a Cylindrical Shell under Internal Pressure*, International Journal of Fracture mechanics, Vol. 5, (2), 1969.
- [23] E. Riks. *Bulging Cracks in Pressurized Fuselages: A Numerical Study*, NLR MP 87058 U, 1987.
- [24] H. Ansell. *Bulging of Cracked Pressurized Aircraft Structure*, Technical Licentiate Dissertation, Department of Mechanical Engineering, Linkoping Institute of Technology, Linkoping, Sweden, 1988.
- [25] D. Chen. *Bulging of Fatigue Cracks in a Pressurized Aircraft Fuselage*, TU-Delft Report LR-647, 1990
- [26] R.D. Young, C.A. Rose, J.H. Starnes Jr. *Nonlinear Bulging Factors for Longitudinal and Circumferential Cracks in Cylindrical Shells subjected to Combined Loads*, AIAA-2000-1514, 2000.

5. CONCLUSIONS

Different arrangements of stiffened panels typical of aeronautical constructions were analysed and reported in this paper to highlight the parameters which drive their DT performances.

The choice of the fastening system plays an important role on the behaviour of a stiffened panel subjected to fatigue loads. Mechanically fastened and, in particular, adhesively bonded stiffeners confirmed to be very effective as crack retarders, whereas integral stiffeners “as is” should not be used where the F&DT requirements are critical.

A significant improvement of the DT capabilities of a structure can be achieved by bonding additional doublers between the main stiffeners. Doublers with higher aspect ratio w_d/t_d provide lower crack growth rates, and higher fatigue propagation life, than thick and narrow reinforcements at the same cross-sectional area. High static and fatigue strength materials, like titanium alloys, should be preferred as doubler materials instead of aluminium alloys.

The adoption of additional bonded reinforcements could reduce the operative costs by allowing less burdensome inspections or by reducing the structural weight. In order to assess correctly the DT properties of bonded reinforcements, the likely presence of adhesive debonding must be considered carefully because the adhesive failure reduces drastically the effectiveness of a bonded stiffener.

Moreover, the crack-bridging model implemented provided an effective and reliable tool for the prediction of the Fatigue Crack Propagation (FCP) of cracks growing through the skin above the adhesively bonded stringers of stiffened panels of typical fuselage configurations.

As a consequence, the long FCP period under the bonded stringers, completely neglected in the current sizing of the bonded stiffened panels due to the limits of the adopted methods, could be fully exploited. The employment of the crack-bridging model permits to optimize the Damage Tolerance properties of the bonded stiffened panels, providing significant benefits in terms of reliability, maintenance costs and weights.

And last but not least, the phenomenon of crack bulging, on which much has been already written, seems to be still not well understood in the light of the consistency of the results of LEFM. Further investigations should be required to verify the possibility to extend the current theoretical treatments in order to include non-linear phenomena related to the load of pressurization.